

Sensor and Simulation Notes

Note 254

August 1978

Source Excitation of an Open,  
Parallel-Plate Waveguide, Numerical Results

V. Krichevsky  
University of Illinois at Urbana-Champaign  
Urbana, Illinois 61801

CLEARED  
FOR PUBLIC RELEASE  
AFRL/DEOB-PA  
29 JUL 98

Abstract

In this work we investigate numerically the problem of the source excitation of an open, parallel-plate waveguide. The following assumptions are made for the source current 1) the current is oriented in the y-direction, 2) it is located at  $x = 0$ , 3) there is no variation in the y-direction, 4) and the current has  $\exp(i\beta z)$  behavior along the longitudinal z-direction. We provide graphical output for the EM-field components as functions of a longitudinal propagation constant and transverse coordinates and then discuss these results.

Acknowledgement

The author is thankful to Professor R. Mittra for discussion of the problem and for the helpful suggestions during the course of this work. The financial support of AFOSR Grant 76-3066B is gratefully acknowledged.

AFRL/DE 98-557

## I. INTRODUCTION

In the previous report [1], we derived analytical expressions for the source excitation of an open parallel-plate waveguide. However, these formulas were very complicated, and it became necessary to evaluate them numerically. The purpose of this report is to present the numerical results. The computer program contained in Appendix A was written and used to obtain the field distribution as a function of the longitudinal propagation constant and the transverse coordinates. The numerical outputs are presented in graphical forms. The Cyber 175 at the University of Illinois was used for all of the numerical studies.

The organization of the report is as follows: Section II contains a statement of the problem and the basic formulation. Section III presents the real and imaginary parts and the amplitude of the component field distribution as functions of several parameters in graphical form and a detailed discussion of the numerical results. Finally, Section IV is the conclusion.

## II. STATEMENT OF THE PROBLEM AND BASIC FORMULATION

In this section the fields due to a vertical current located inside an open, finite waveguide are investigated. The geometry of the problem considered is shown in Figure 1. This structure consists of two perfectly conducting plates with separation  $2H$  located in a homogeneous and isotropic medium. A Cartesian coordinate system with its  $y$ -axis normal to the plates is erected. Both plates are infinite in the  $z$ -direction and finite in the  $x$ -direction with length  $2L$  as shown in Figure 1. All figures appear at the end of Chapter II. The current is oriented in the  $y$ -direction and is defined as

$$J = \hat{y}\delta(x) \exp(i\beta z) \quad , \quad (1)$$

where  $\beta$  is the propagation constant in the  $z$ -direction, and  $\delta(x)$  is the delta function. In [1] using the vector-potential approach and the Wiener-Hopf technique, we obtained a solution for the problem at hand in a general form for any parameters with one restriction:  $kL$  must be much greater than 1, i.e.,

$$kL \gg 1 \quad , \quad (2)$$

where

$$k = \sqrt{\omega^2 \epsilon \mu - \beta^2} \quad (3)$$

and  $\epsilon$ ,  $\mu$  are the homogeneous media parameters. Using the solution which was obtained in [1], we will perform a numerical calculation for the case:

$$W = \frac{H}{L} = 0.16670 \quad , \quad (4)$$

$$\frac{L}{\lambda_0} = 5 \quad , \quad (5)$$

where

$$\lambda_0 = \frac{2\pi}{\omega\sqrt{\epsilon\mu}} \quad (6)$$

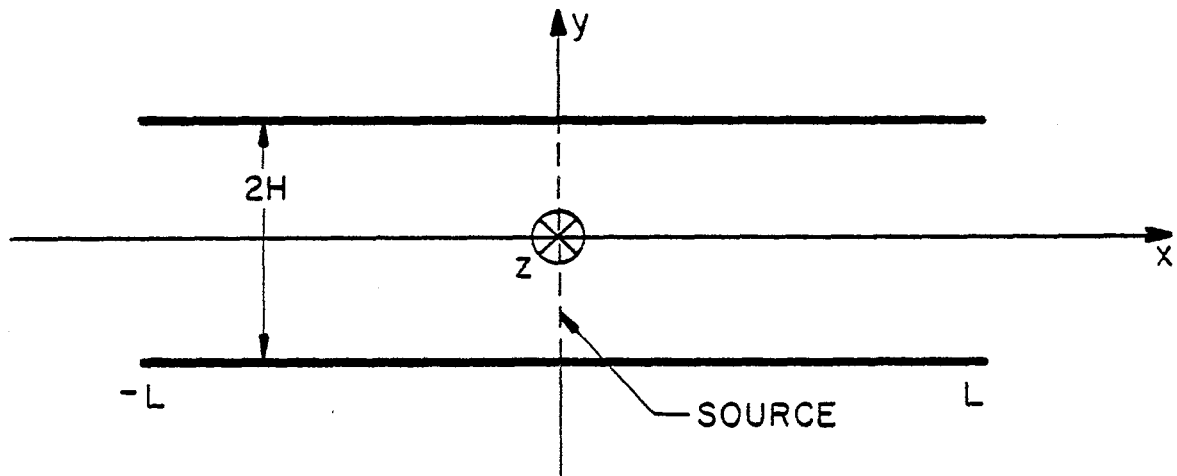


Figure 1. Geometry of the problem of source excitation of a parallel-plate waveguide.

is the free-space wave length. Because of the limitations of Equations (2), (3), and (5) we calculated numerical results for

$$0 < \tilde{\beta} < 0.93 \quad , \quad (7)$$

where  $\tilde{\beta}$  is the normalized propagation constant  $\tilde{\beta} = \frac{\beta}{\omega\sqrt{\epsilon\mu}}$ . It can be readily proved from Equations (3), (4), and (5) that if  $\tilde{\beta}$  is in the region  $[\tilde{\beta}_0, 0.93]$ , where

$$\tilde{\beta}_0 = 0.80008997 \quad , \quad (8)$$

then only the first mode can propagate in the x-direction; therefore, the electromagnetic field has only three components  $[E_y, H_x, H_z]$ . When  $\tilde{\beta}$  intersects the point  $\tilde{\beta}_0$  and goes to zero, the second mode begins to propagate, and the EM-field consists of five components  $[E_x, E_y, E_z, H_x, H_z]$ . Rewriting the field solution from [1] for the case, when no more than two modes can propagate, we arrive at the EM field:

$$\bar{E}'(x,y,z) = \bar{E}(x,y) \cdot \exp(i\beta z) \quad (9)$$

$$\bar{H}'(x,y,z) = \bar{H}(x,y) \cdot \exp(i\beta z) \quad (10)$$

$$\bar{E}(x,y) = \hat{x}E_x + \hat{y}E_y + \hat{z}E_z \quad (11)$$

$$\bar{H}(x,y) = \hat{x}H_x + \hat{z}H_z \quad (12)$$

$$E_y = \sqrt{\frac{\mu}{\epsilon}} \cdot \frac{0.1 \cdot \theta}{w} \cdot F_2 \sin\left(\frac{\pi}{Hy}\right) \sin\left(\theta \cdot \frac{x}{L}\right) \quad (13)$$

$$E_x = \sqrt{\frac{\mu}{\epsilon}} \cdot 10\pi \left\{ F_1 \cos\left(a \cdot \frac{x}{L}\right) + \left(1 - \frac{0.01}{w^2}\right) \cdot F_2 \cos\left(\frac{\pi}{Hy}\right) \cos\left(\theta \cdot \frac{x}{L}\right) - \frac{1}{2a} \exp\left(-a\left|\frac{x}{L}\right|\right) \right\} \quad (14)$$

$$E_z = -i \sqrt{\frac{\mu}{\epsilon}} \cdot \frac{\beta}{\omega\sqrt{\epsilon\mu}} \cdot \frac{\pi}{w} F_2 \sin\left(\frac{\pi y}{H}\right) \cos\left(\theta \cdot \frac{x}{L}\right) \quad , \quad (15)$$

$$H_x = -\mu \frac{\beta}{\omega\sqrt{\epsilon\mu}} \cdot 10\pi \left\{ F_1 \cos\left(\frac{\alpha x}{L}\right) + F_2 \cos\left(\pi \cdot \frac{y}{H}\right) \cdot \cos\left(\theta \cdot \frac{x}{L}\right) - \frac{1}{2a} \exp\left(ia\left|\frac{x}{L}\right|\right) \right\}, \quad (16)$$

$$H_z = i\mu a F_1 \sin\left(\frac{\alpha x}{L}\right) + i\theta F_2 \cos\left(\pi \frac{y}{H}\right) \sin\left(\theta \cdot \frac{x}{L}\right) - 0.5 \cdot \exp\left(ia\left|\frac{x}{L}\right|\right) \cdot \frac{x}{|x|}, \quad (17)$$

where

$$F_1 = \frac{[M_{1+}(k)]^2 \exp(i2a)}{(1 + T_1)a} \cdot \left\{ 1 + \frac{2b[M_{1+}(\alpha_1)]^2 \exp(i2\frac{a}{b}\alpha_1)}{\theta} \right\}, \quad (18)$$

$$F_2 = \frac{2bM_{1+}(k)M_{1+}(\alpha_1) \exp\left[ia\left(1 + \frac{\alpha_1}{b}\right)\right]}{a \cdot Q}, \quad (19)$$

$$Q = (1 + T_1)\alpha_1 \cdot \left\{ \frac{[M_{1+}(\alpha_1)]^2 \exp(i2\frac{a}{b}\alpha_1)}{2\alpha_1} \left[ \frac{4T_1b}{1 + T_1} - \frac{(\alpha_1 + b)^2}{\alpha_1} \right] - 1 \right\}, \quad (20)$$

$$M_{1+}(k) = (\alpha_1 + b) \cdot \exp\left\{ i \left[ b(2-C + \ln\left(\frac{2}{b}\right) + i\frac{\pi}{2}) - \frac{\pi}{2} + \sum_{n=2}^{\infty} \left( \frac{b}{n} - \arcsin \frac{b}{n} \right) \right] \right\}, \quad (21)$$

$$M_{1+}(\alpha_1) = \sqrt{2} \cdot \alpha_1 \cdot \frac{1 - i\alpha_1}{b} \exp\left\{ i \left[ \alpha_1(2-C + \ln\left(\frac{2}{b}\right) + i\frac{\pi}{2}) + \sum_{n=2}^{\infty} \left( \frac{\alpha_1}{n} - \arcsin \frac{\alpha_1}{\sqrt{n^2 - 1}} \right) \right] \right\}, \quad (22)$$

$$\alpha_1 = \sqrt{b^2 - 1}, \quad (23)$$

$$a = kL = 10\pi \sqrt{1 - \left| \frac{\beta}{\omega\sqrt{\epsilon\mu}} \right|^2}, \quad (24)$$

$$b = a \cdot \frac{W}{\pi}, \quad (25)$$

$$\theta = \frac{\pi\alpha_1}{W}, \quad (26)$$

$$T_1 = [M_{1+}(k)]^2 \exp(i2a) \left[ 1 + \frac{b\sqrt{\pi}}{\sqrt{a}} \exp\left(-i\frac{\pi}{4}\right) \right] \quad (27)$$

It should be mentioned that we investigated the lossless medium case; therefore, in the region  $\tilde{\beta}_0 < \tilde{\beta} < 0.93$ , the propagation constant for the second mode has only an imaginary part. Because we neglect terms which decrease exponentially, our results for the above mentioned region of  $\tilde{\beta}$  reduce to:

$$1) E_x = E_z = 0 \quad \text{and}$$

2) more simple expressions for the other three components of the field.

We apply numerical analysis only over the regions  $0 \leq y < H$ ,  $0 < x < L$ .

For the remainder of the waveguide, one can obtain results using the correlations:

$$\begin{aligned} E_x(x,y) &= -E_x(-x,y) ; E_x(x,y) = -E_x(x,-y) \\ E_y(x,y) &= E_y(-x,y) ; E_y(x,y) = E_y(x,-y) \\ E_z(x,y) &= E_z(-x,y) ; E_z(x,y) = -E_z(x,-y) \\ H_x(x,y) &= H_x(-x,y) ; H_x(x,y) = H_x(x,-y) \\ H_z(x,y) &= -H_z(-x,y) ; H_z(x,y) = H_z(x,-y) \end{aligned} \quad (28)$$

It is interesting to note that  $E_x$ ,  $H_z$  are continuous and that  $E_y$ ,  $E_z$ ,  $H_x$  are discontinuous when  $\tilde{\beta}$  crosses  $\tilde{\beta}_0$  (or more exactly: they are exponentially decreasing). It is also of interest to determine the character of the behavior of the x-component of Poynting's vector. As one can easily see from the previous expressions for the EM fields, the x-component of Poynting's vector for the second mode is proportional to  $\alpha_1$  and goes to zero when  $\tilde{\beta} \rightarrow \tilde{\beta}_0$ . From this, one finds that the energy flow in the x-direction is continuous when  $\tilde{\beta}$  intersects the point  $\tilde{\beta}_0$ .

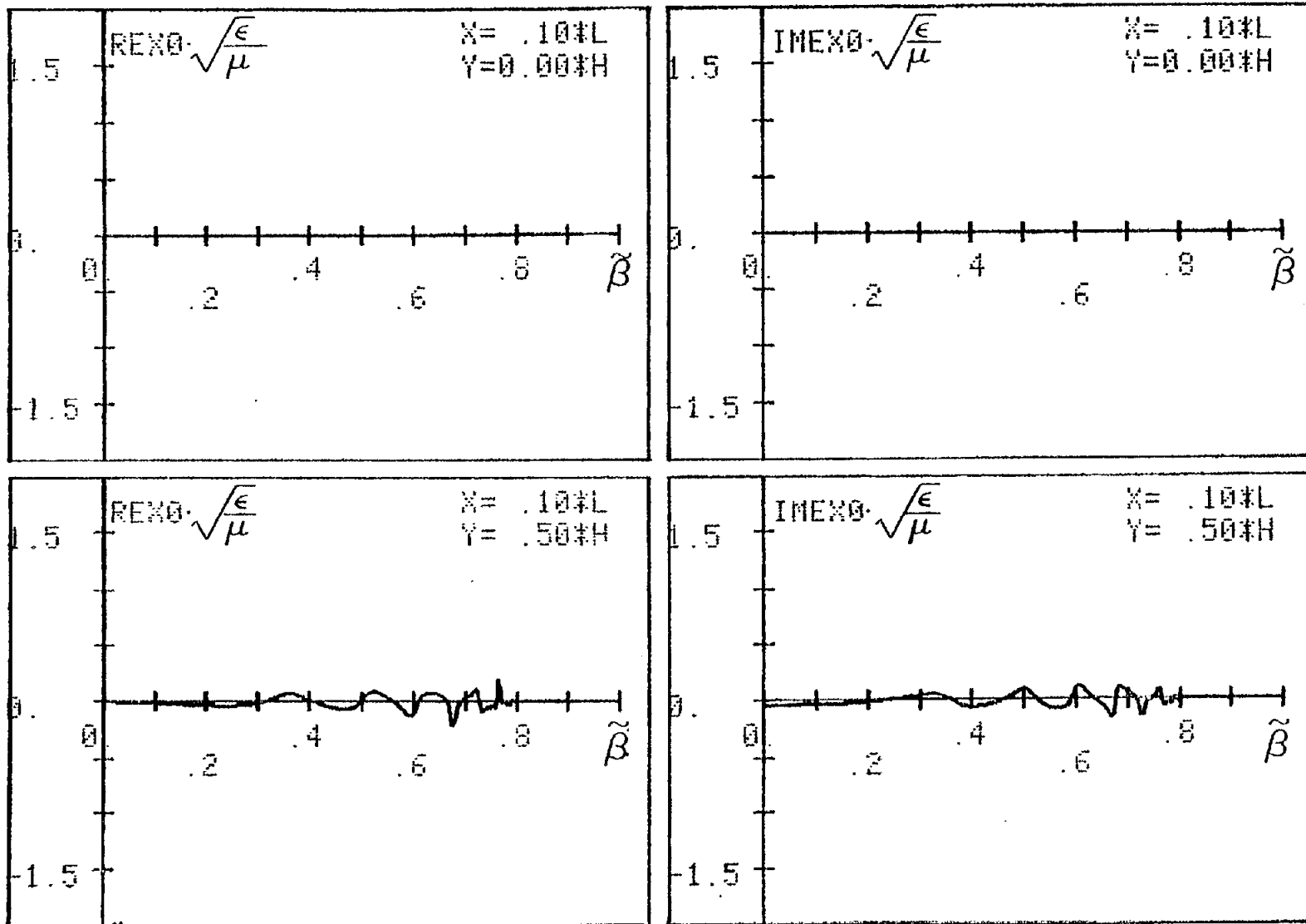


Figure 2. The real and imaginary parts of an x-component of the electric field as functions of a longitudinal propagation constant for points of view:  $\frac{X}{L} = 0.1$ ;  $\frac{Y}{H} = 0.0, 0.5$ .

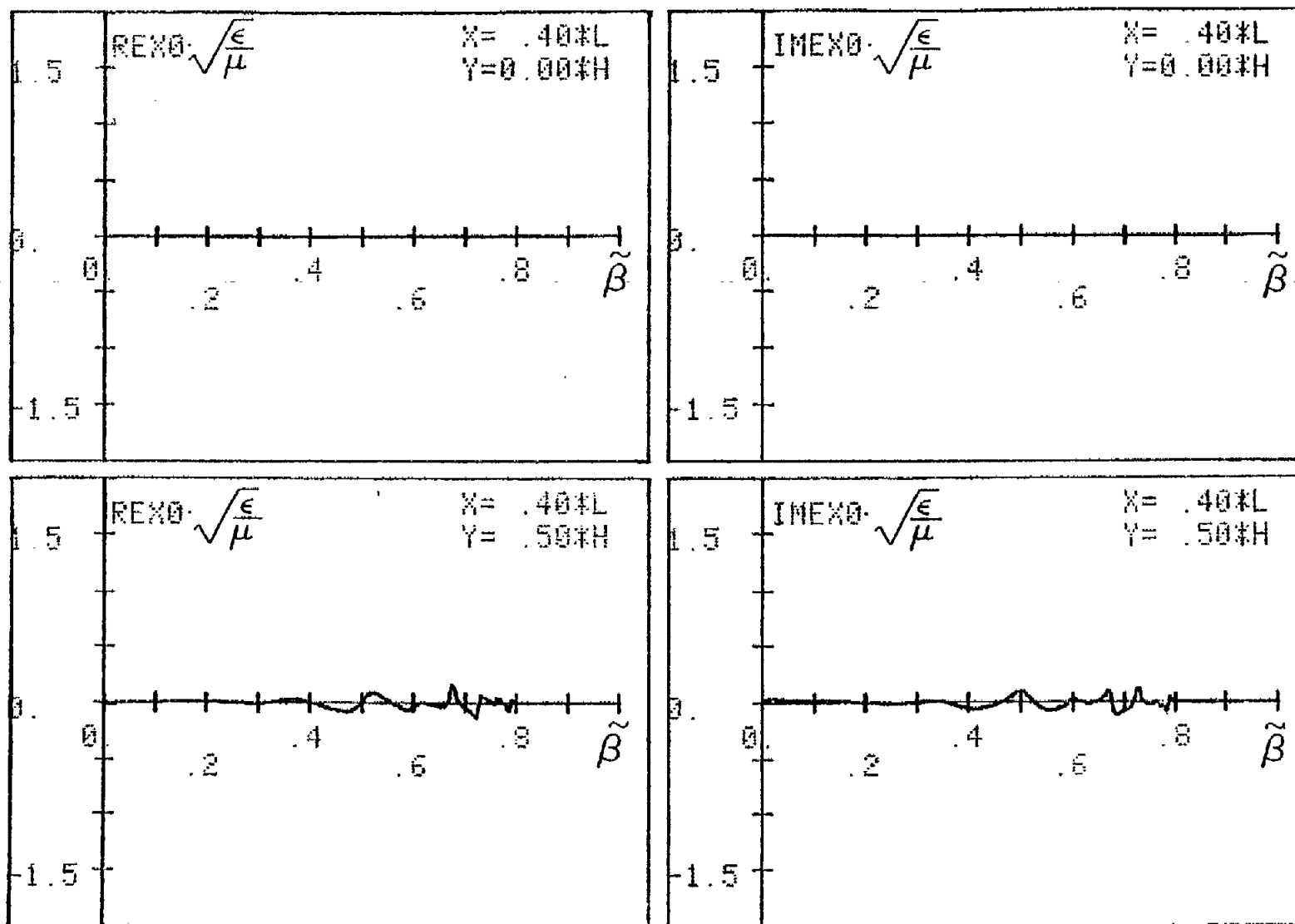


Figure 3. The real and imaginary parts of an x-component of the electric field as functions of a longitudinal propagation constant for points of view:  $\frac{X}{L} = 0.4$ ;  $\frac{Y}{H} = 0.0, 0.5$ .

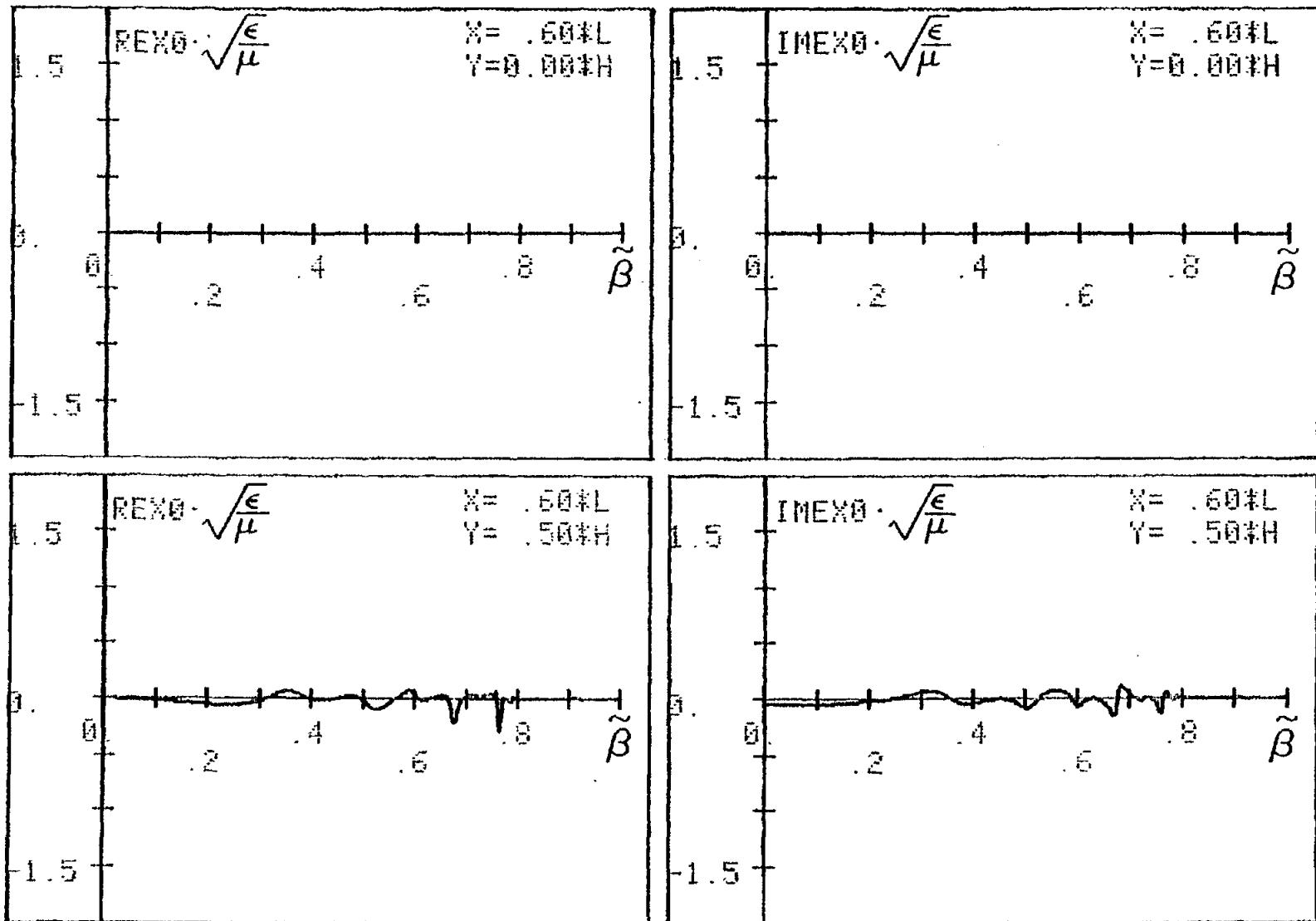


Figure 4. The real and imaginary parts of an x-component of the electric field as functions of a longitudinal propagation constant for points of view:  $\frac{X}{L} = 0.6$ ;  $\frac{Y}{H} = 0.0, 0.5$ .

390

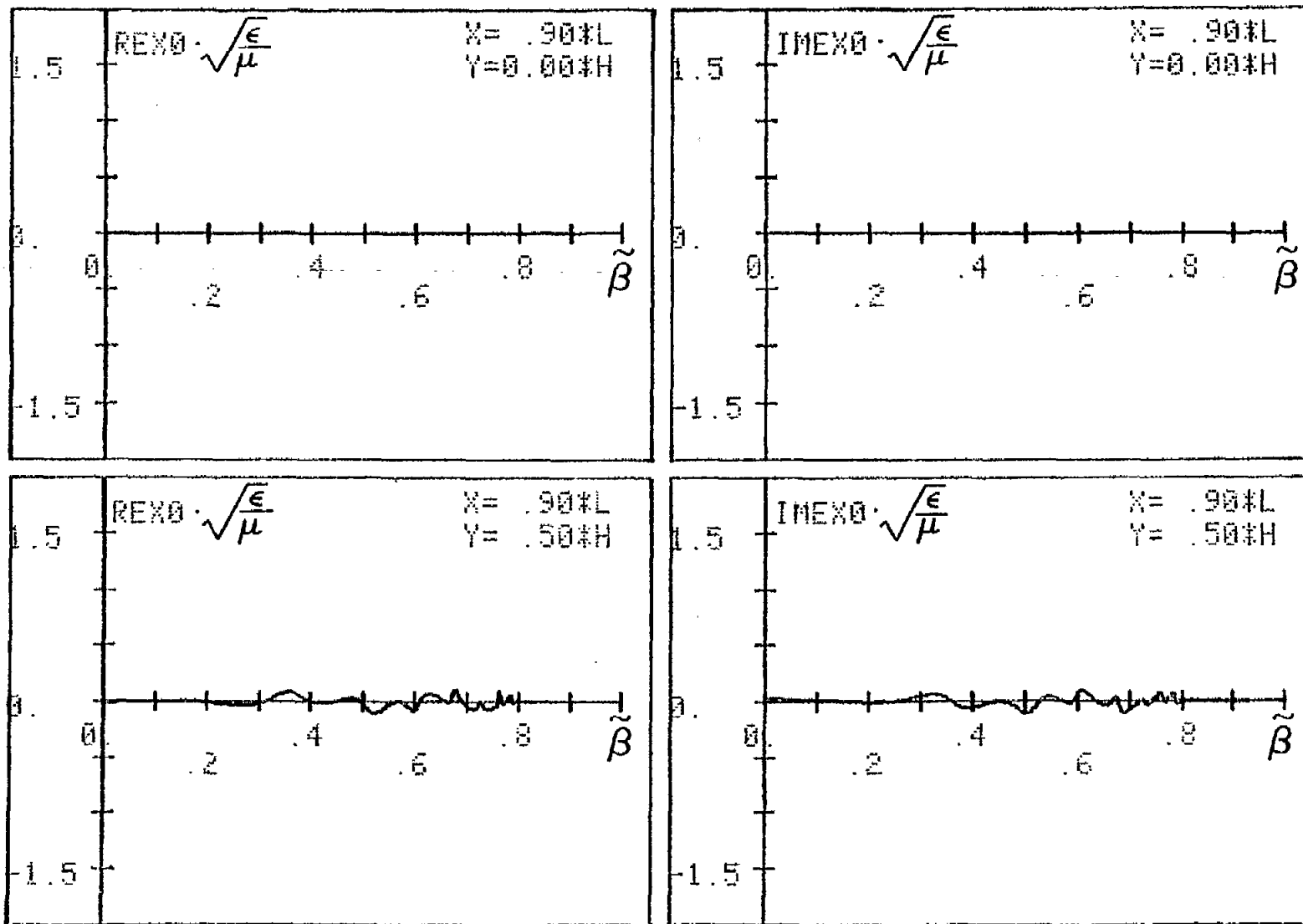


Figure 5. The real and imaginary parts of an x-component of the electric field as functions of a longitudinal propagation constant for points of view:  $\frac{X}{L} = 0.9$ ;  $\frac{Y}{H} = 0.0, 0.5$ .

391

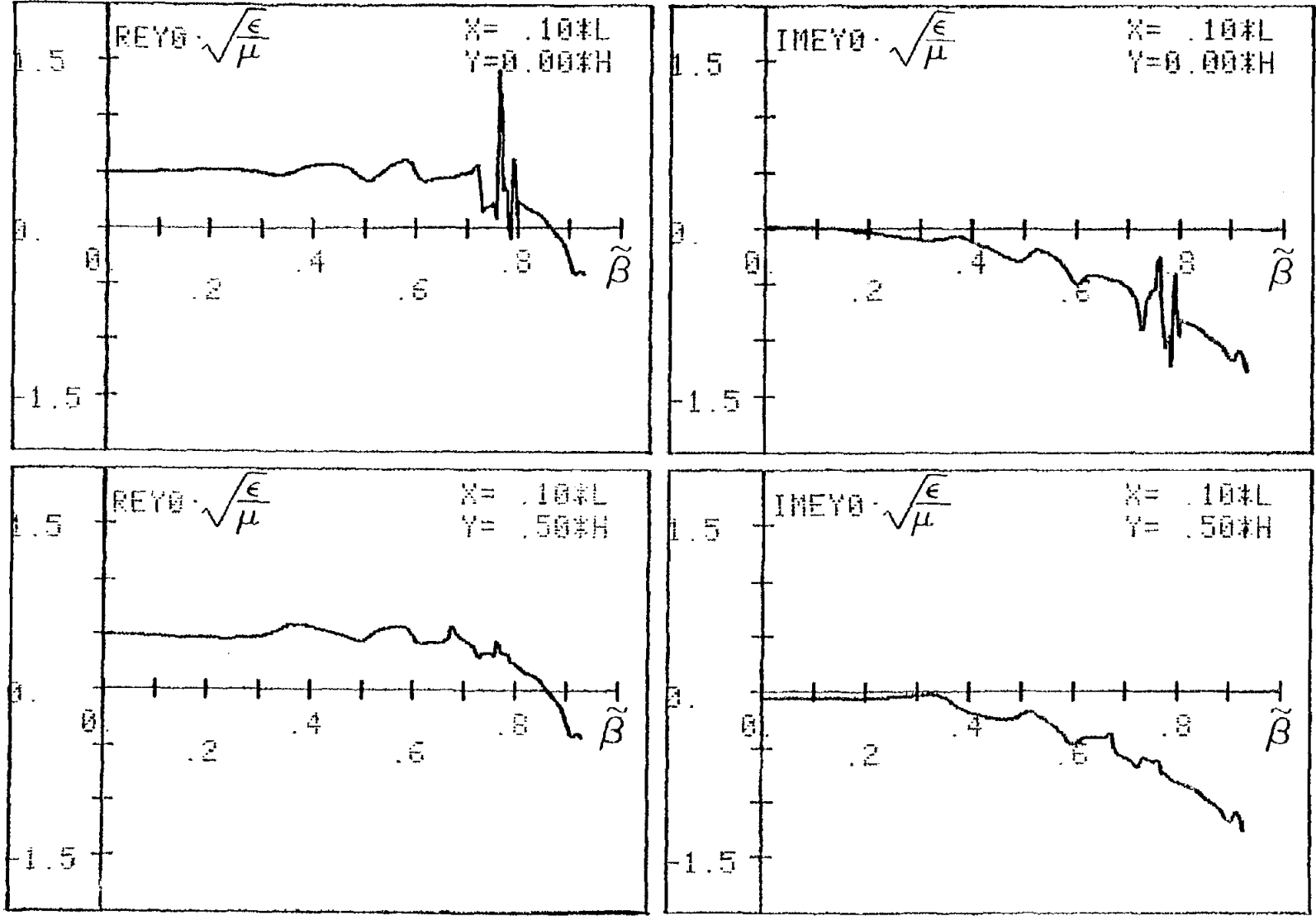


Figure 6. The real and imaginary parts of a y-component of the electric field as functions of a longitudinal propagation constant for points of view:  $\frac{X}{L} = 0.1$ ;  $\frac{Y}{H} = 0.0, 0.5$ .

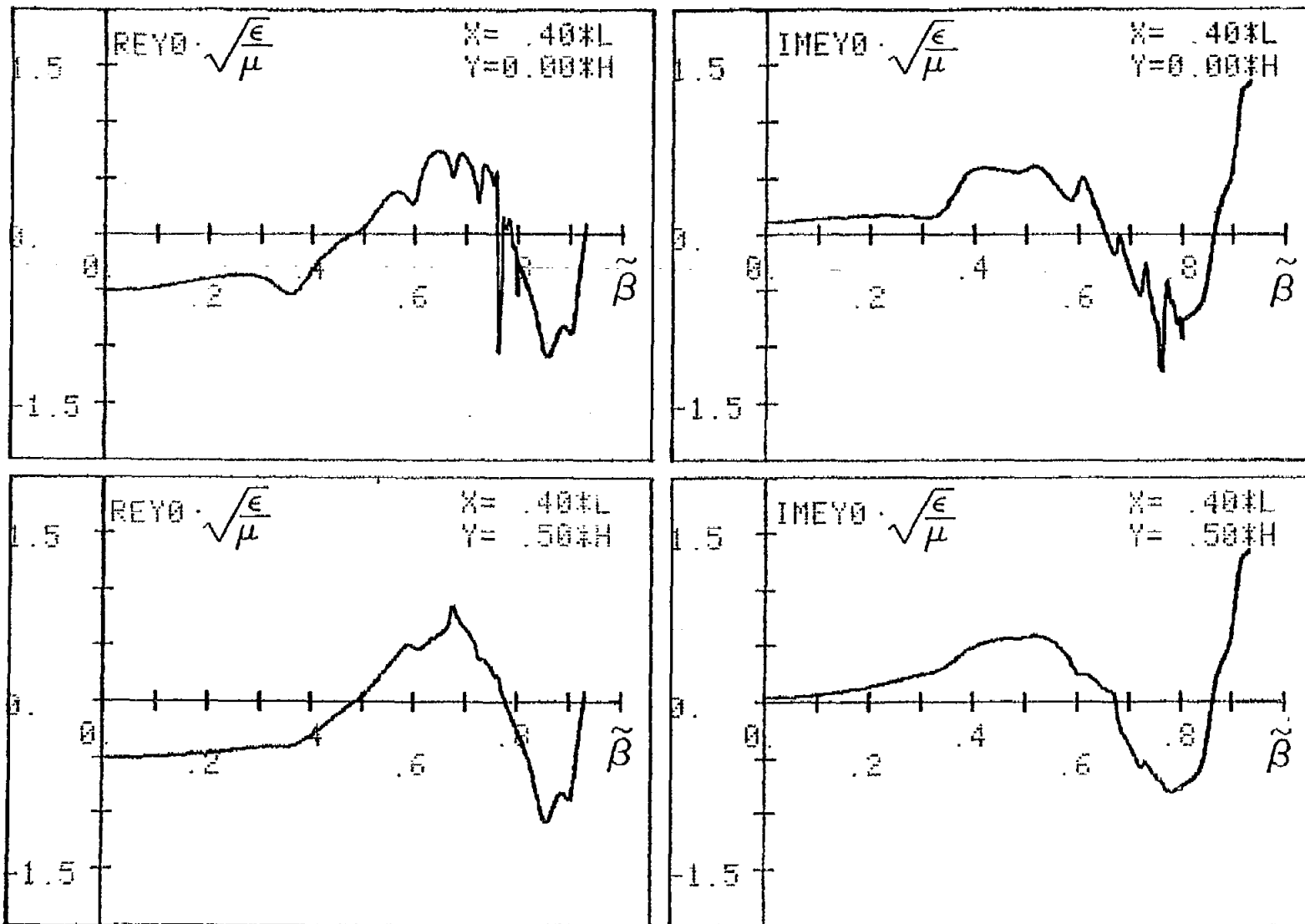


Figure 7. The real and imaginary parts of a y-component of the electric field as functions of a longitudinal propagation constant for points of view:  $\frac{x}{L} = 0.4$ ;  $\frac{y}{H} = 0.0, 0.5$ .

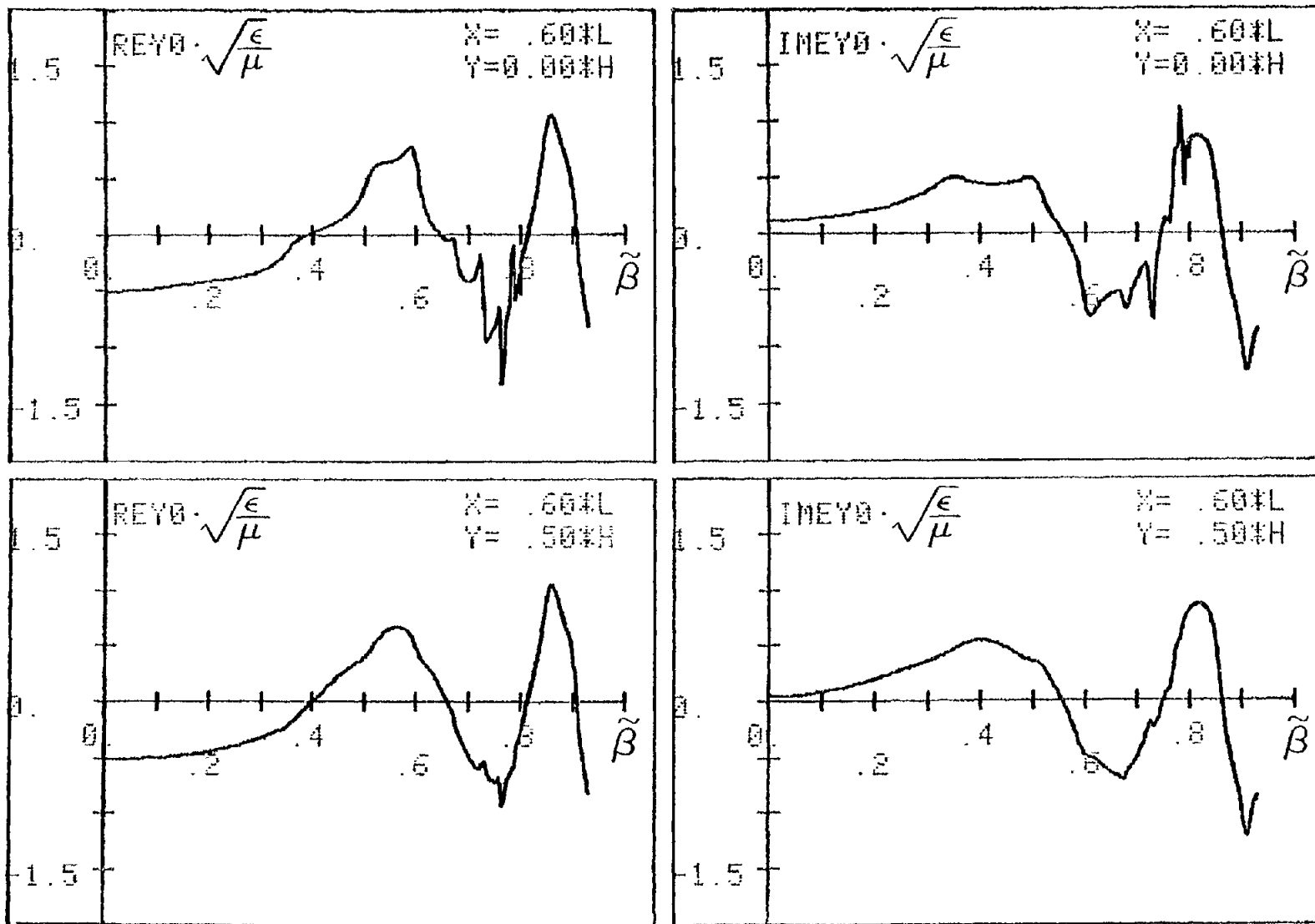


Figure 8. The real and imaginary parts of a y-component of the electric field as functions of a longitudinal propagation constant for points of view:  $\frac{X}{L} = 0.6$ ;  $\frac{Y}{H} = 0.0, 0.5$ .

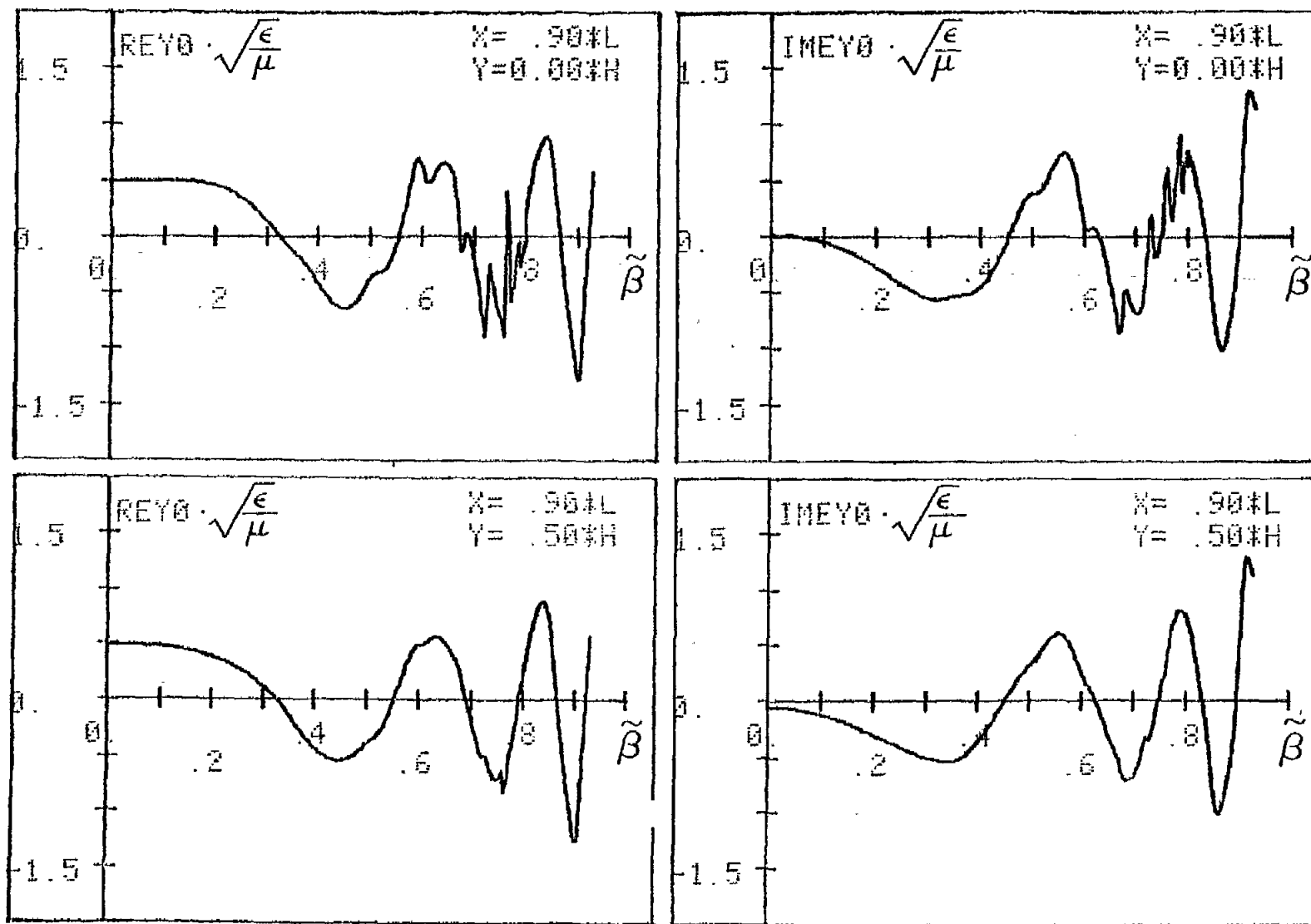


Figure 9. The real and imaginary parts of a y-component of the electric field as functions of a longitudinal propagation constant for points of view:  $\frac{X}{L} = 0.9$ ;  $\frac{Y}{H} = 0.0, 0.5$ .

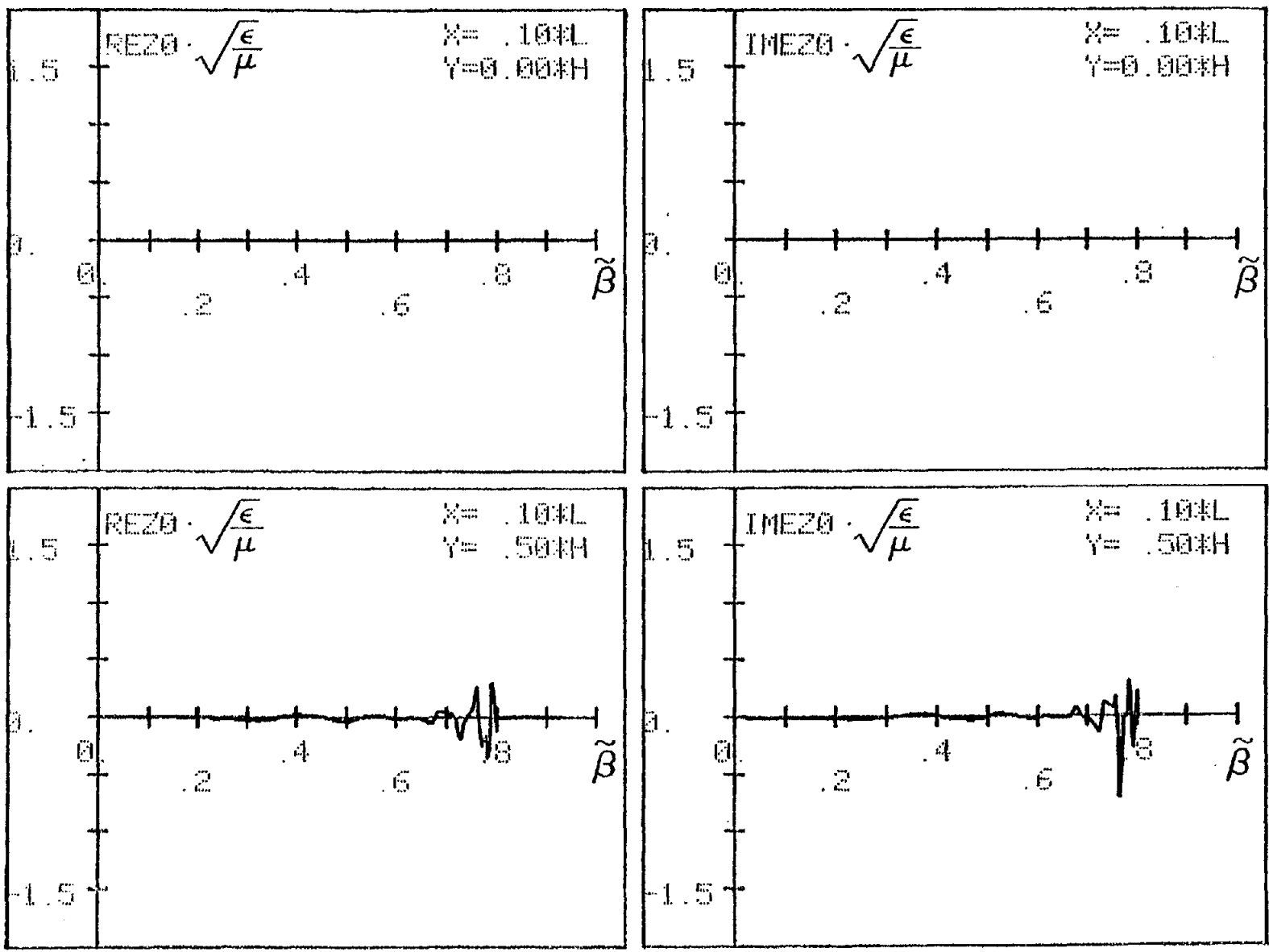


Figure 10. The real and imaginary parts of a z-component of the electric field as functions of a longitudinal propagation constant for points of view:  $\frac{x}{L} = 0.1$ ;  $\frac{y}{H} = 0.0, 0.5$ .

396

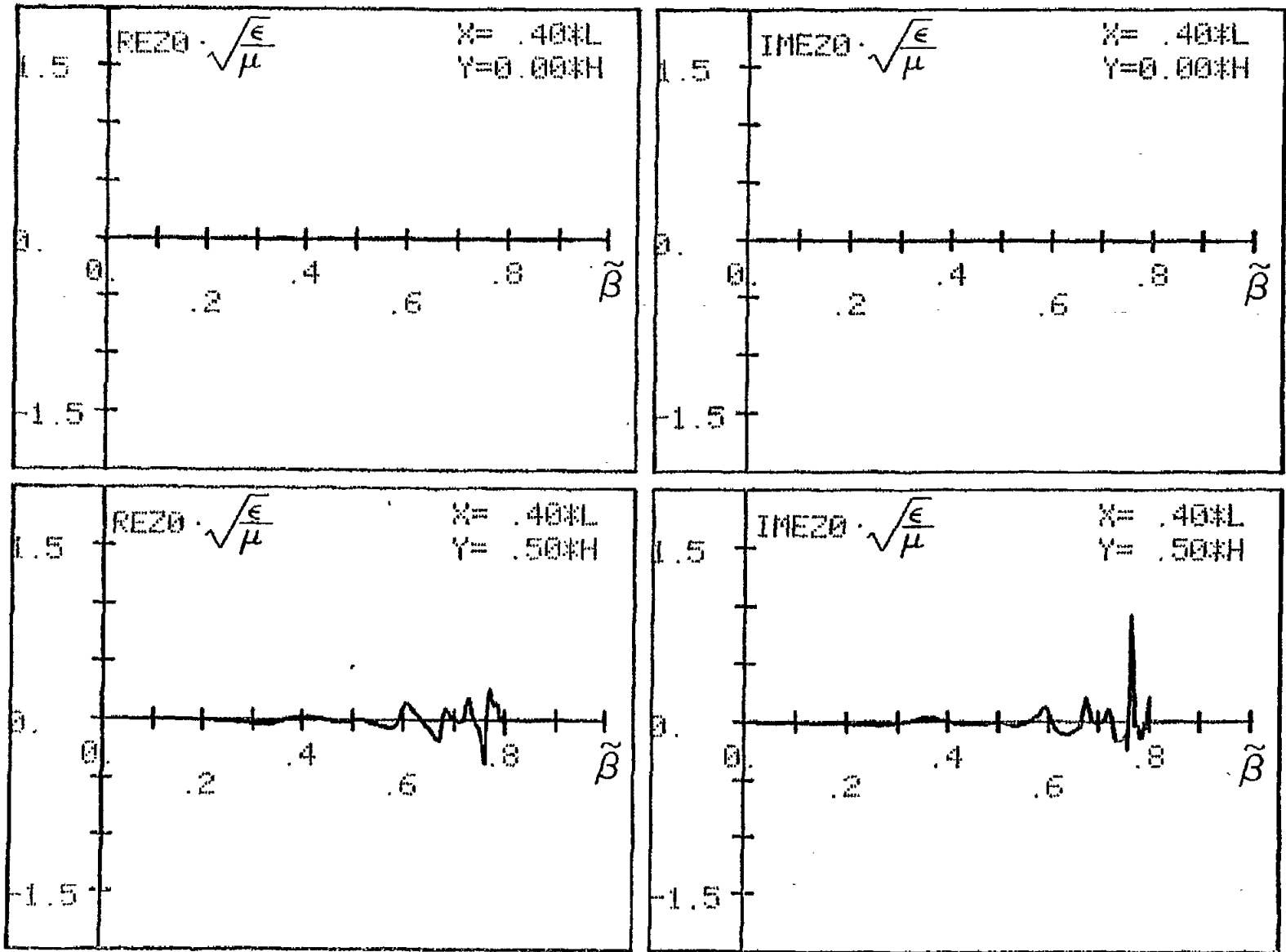


Figure 11. The real and imaginary parts of a z-component of the electric field as functions of a longitudinal propagation constant for points of view:  $\frac{x}{L} = 0.4$ ;  $\frac{y}{H} = 0.0, 0.5$ .

397

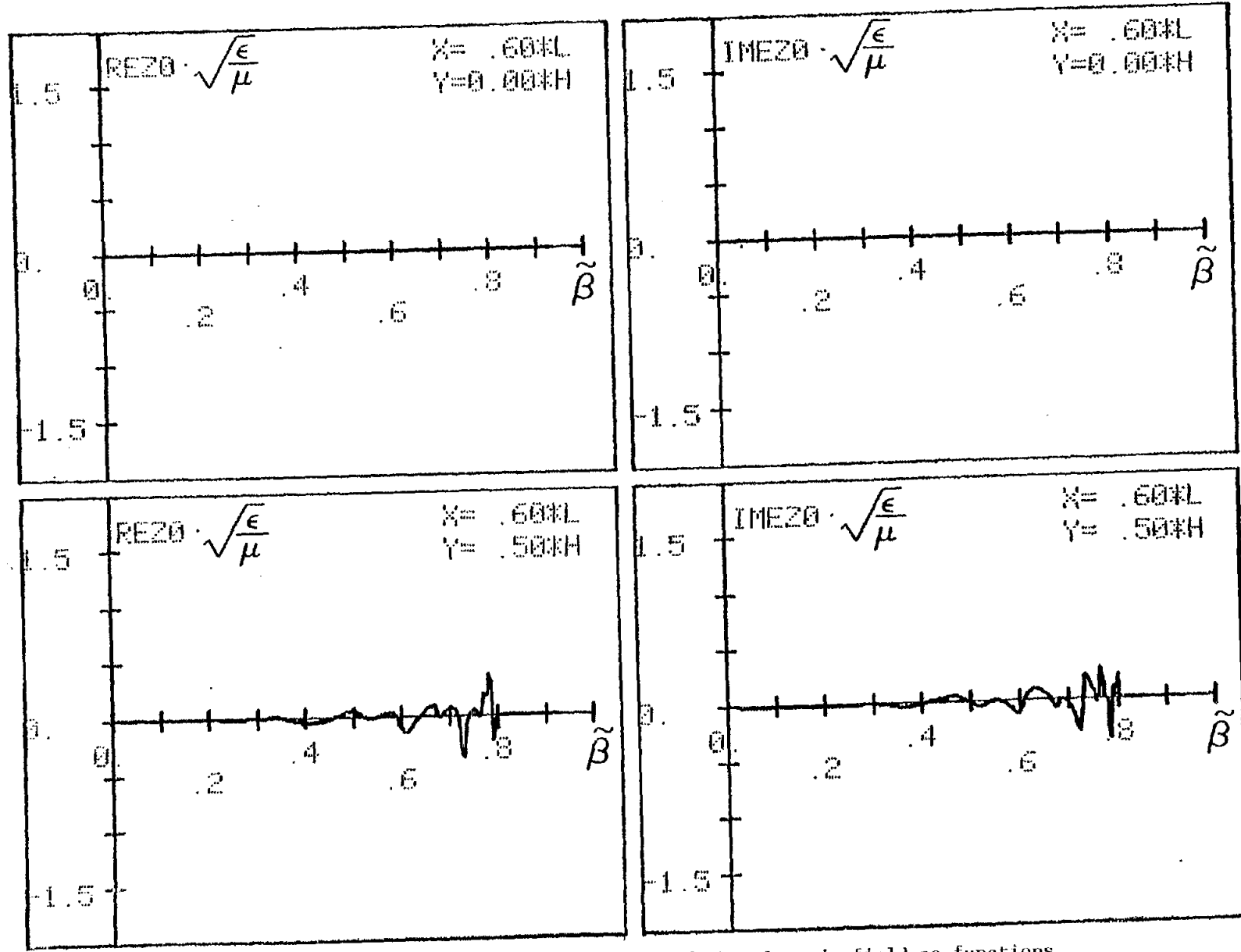
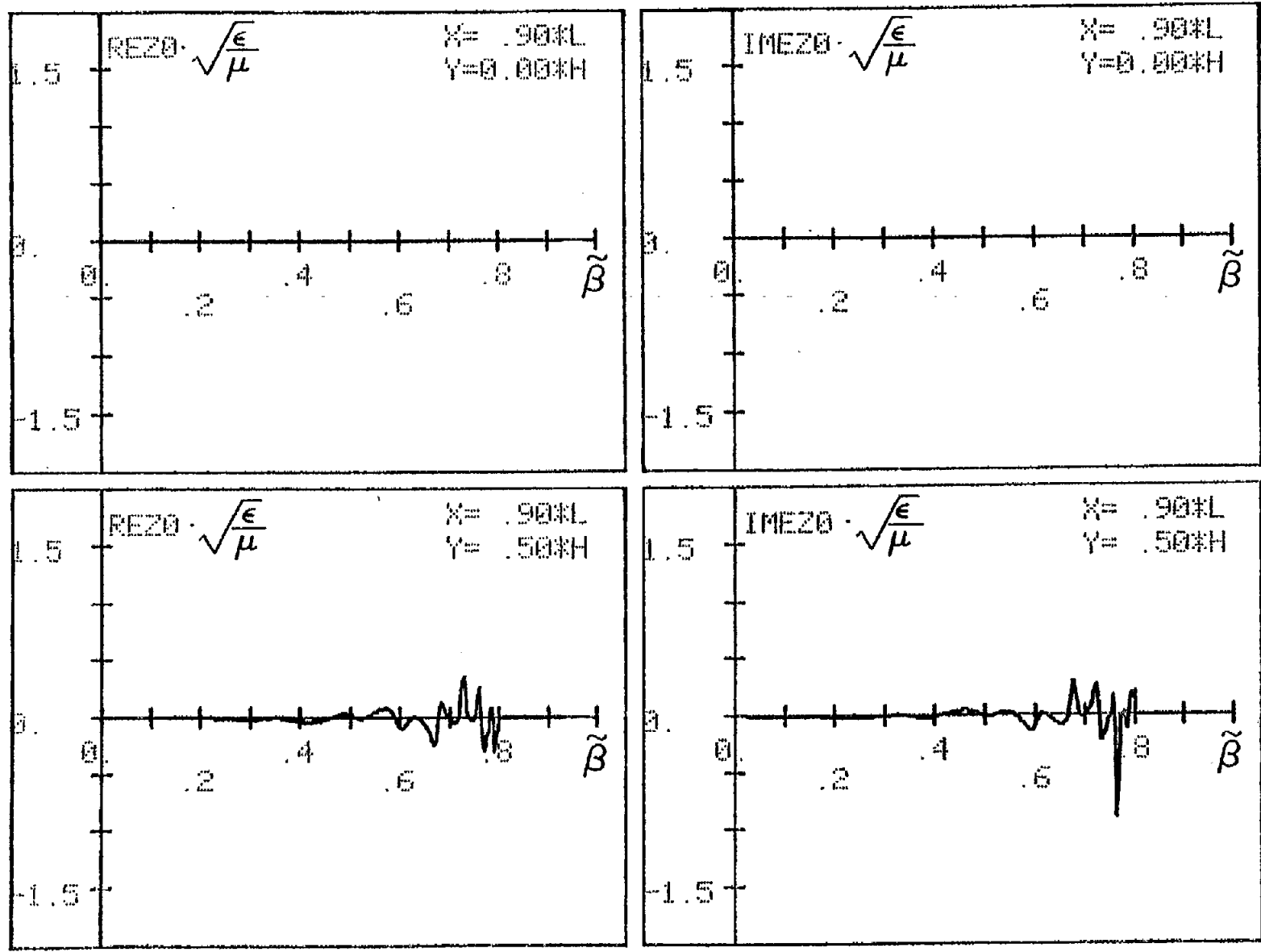


Figure 12. The real and imaginary parts of a z-component of the electric field as functions of a longitudinal propagation constant for points of view:  $\frac{x}{L} = 0.6$ ;  $\frac{y}{H} = 0.0, 0.5$ .



398

Figure 13. The real and imaginary parts of a z-component of the electric field as functions of a longitudinal propagation constant for points of view:  $\frac{X}{L} = 0.9$ ;  $\frac{Y}{H} = 0.0, 0.5$ .

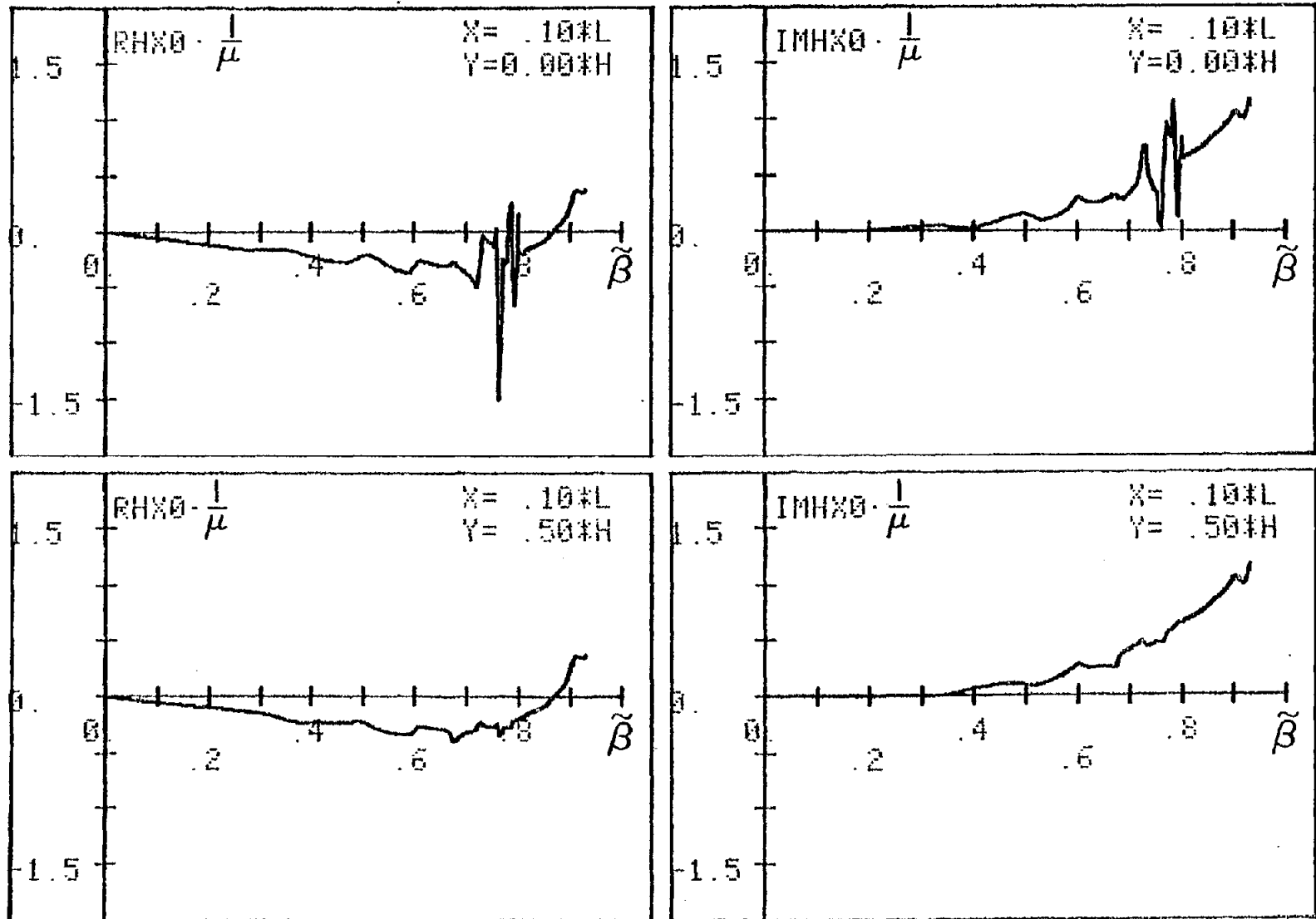


Figure 14. The real and imaginary parts of an x-component of the magnetic field as functions of a longitudinal propagation constant for points of view:  $\frac{X}{L} = 0.1$ ;  $\frac{Y}{H} = 0.0, 0.5$ .

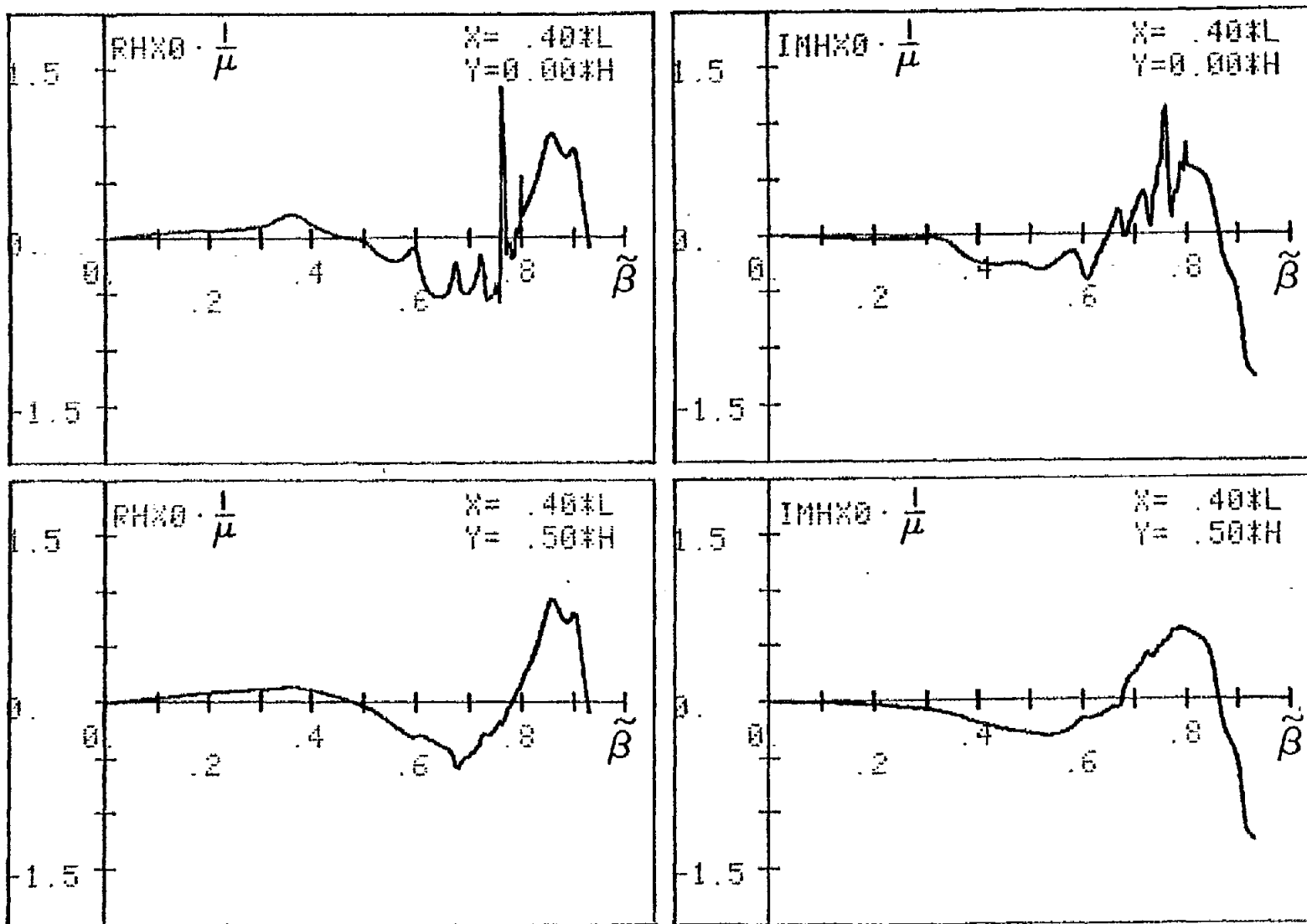


Figure 15. The real and imaginary parts of an x-component of the magnetic field as functions of a longitudinal propagation constant for points of view:  $\frac{x}{L} = 0.4$ ;  $\frac{y}{H} = 0.0, 0.5$ .

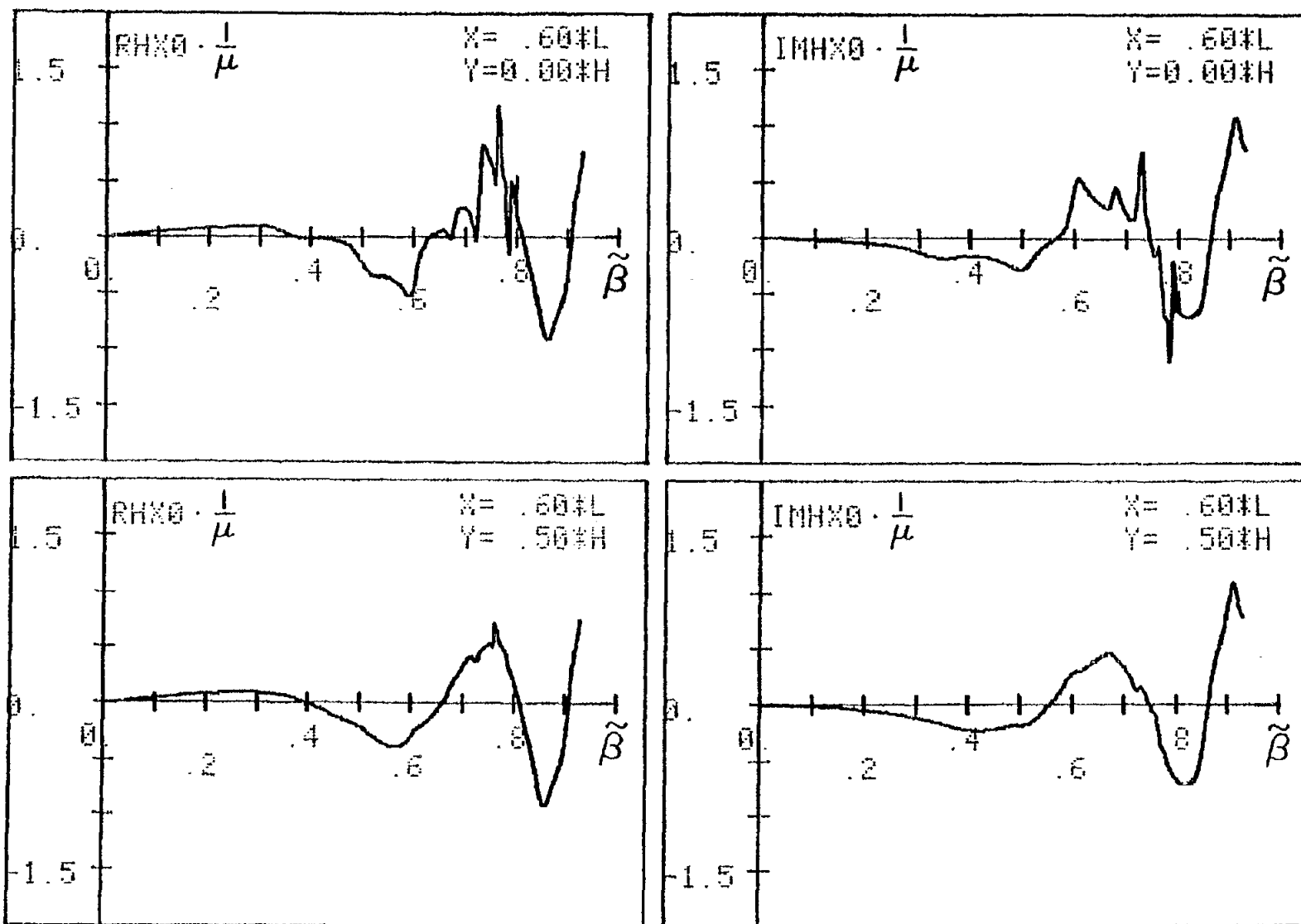
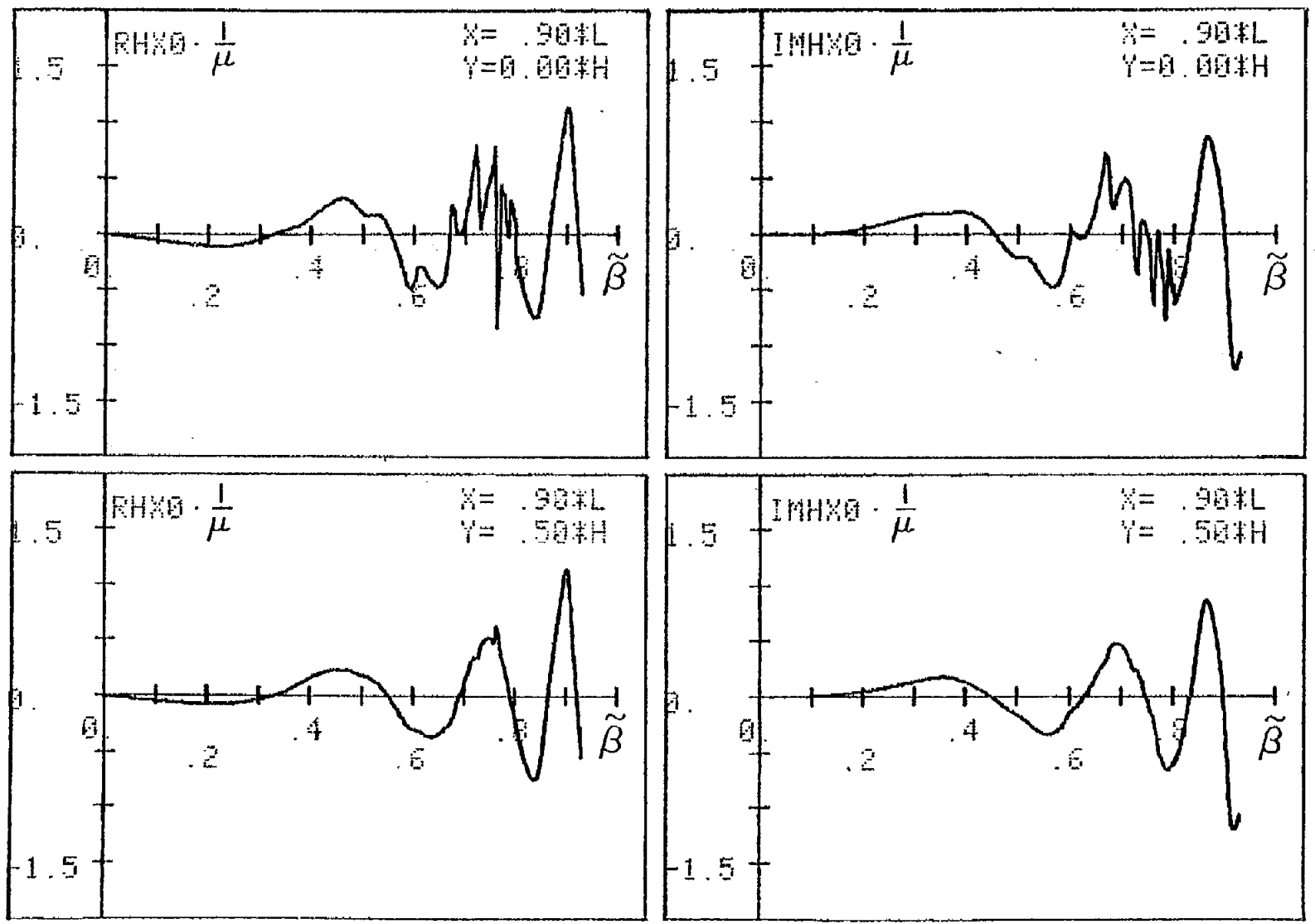


Figure 16. The real and imaginary parts of an x-component of the magnetic field as functions of a longitudinal propagation constant for points of view:  $\frac{X}{L} = 0.6$ ;  $\frac{Y}{H} = 0.0, 0.5$ .



402

Figure 17. The real and imaginary parts of an x-component of the magnetic field as functions of a longitudinal propagation constant for points of view:  $\frac{X}{L} = 0.9$ ;  $\frac{Y}{H} = 0.0, 0.5$ .

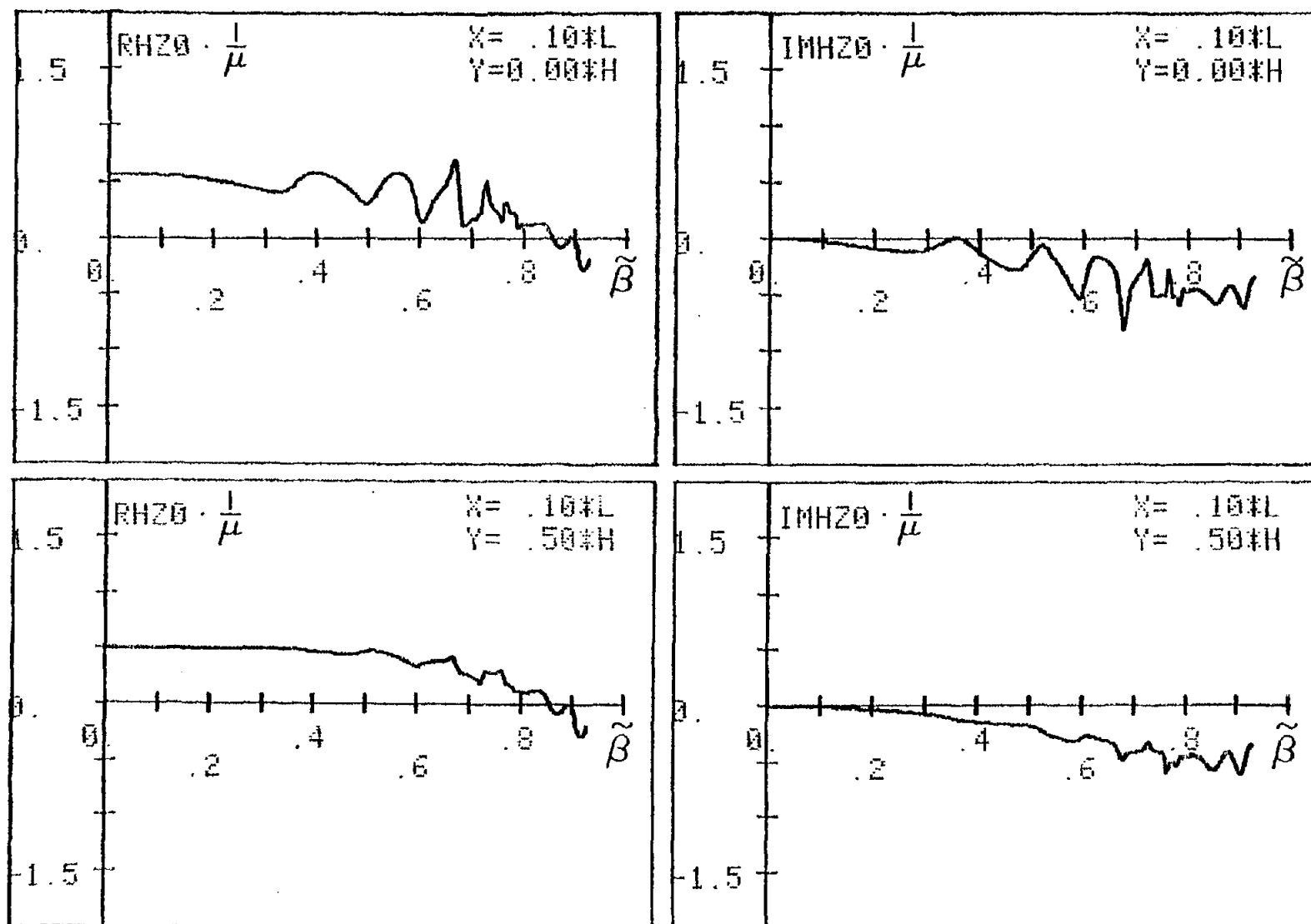


Figure 18. The real and imaginary parts of a z-component of the magnetic field as functions of a longitudinal propagation constant for points of view:  $\frac{X}{L} = 0.1$ ;  $\frac{Y}{H} = 0.0, 0.5$ .

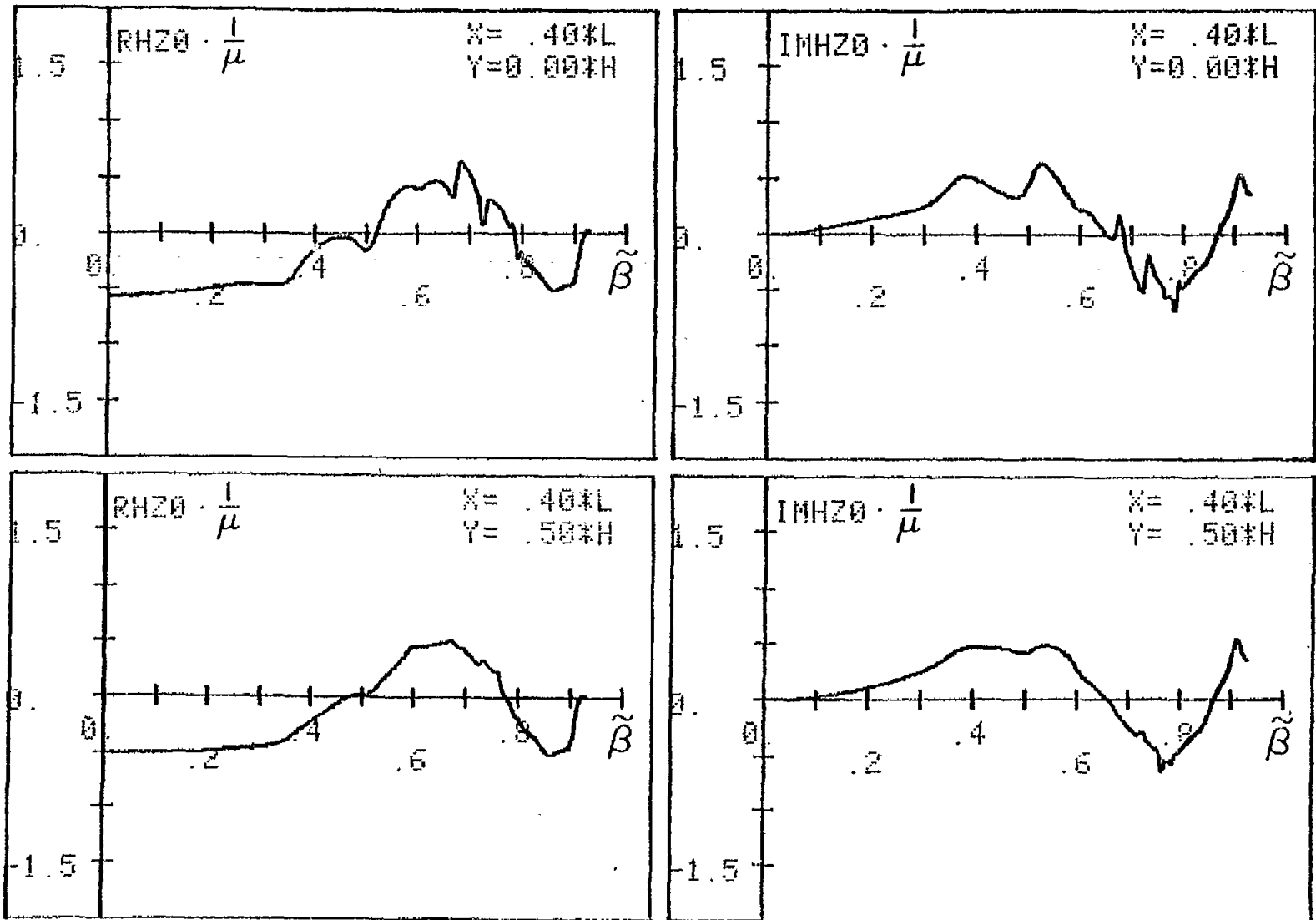


Figure 19. The real and imaginary parts of a z-component of the magnetic field as functions of a longitudinal propagation constant for points of view:  $\frac{X}{L} = 0.4$ ;  $\frac{Y}{H} = 0.0, 0.5$ .

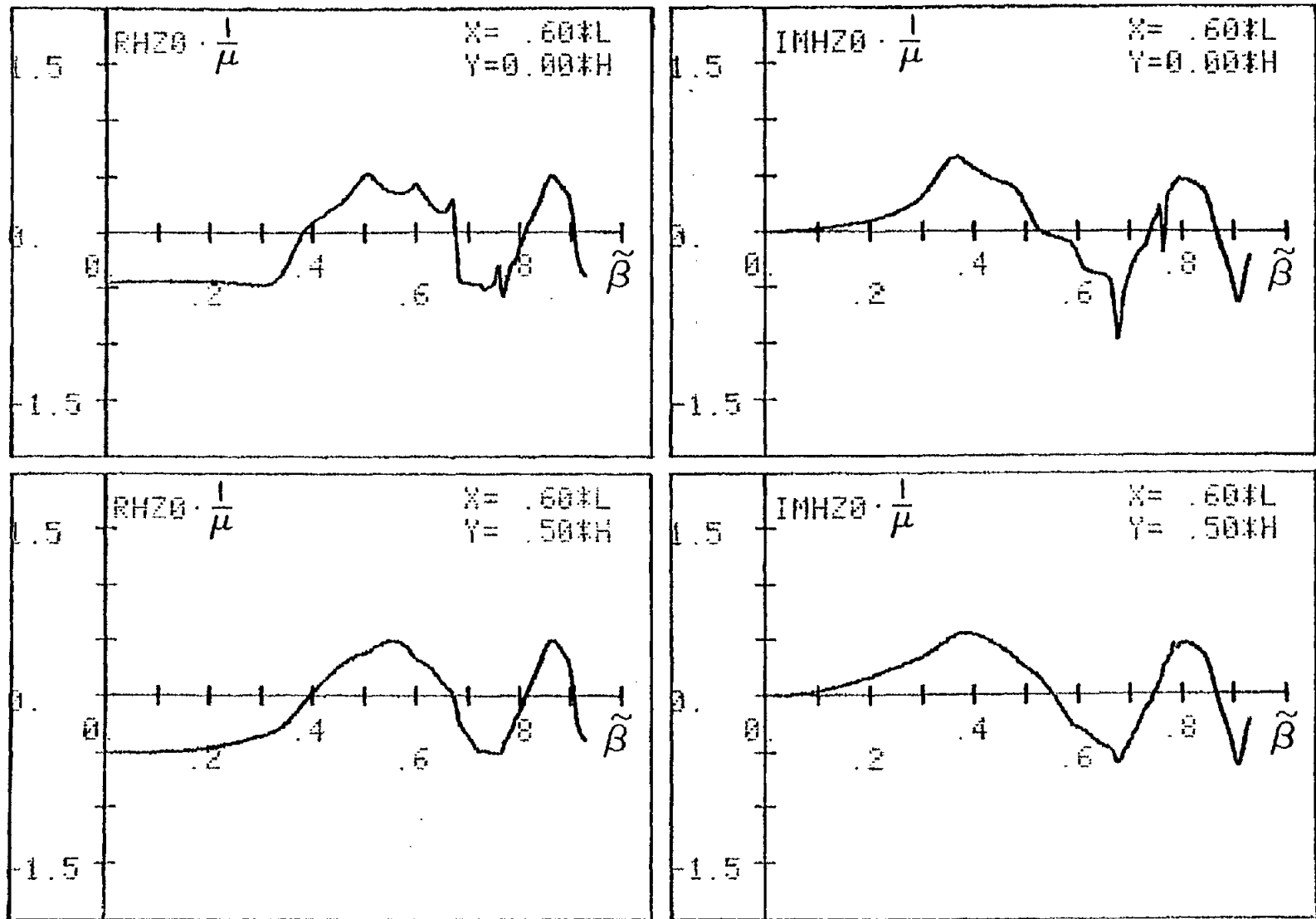


Figure 20. The real and imaginary parts of a z-component of the magnetic field as functions of a longitudinal propagation constant for points of view:  $\frac{X}{L} = 0.6$ ;  $\frac{Y}{H} = 0.0, 0.5$ .

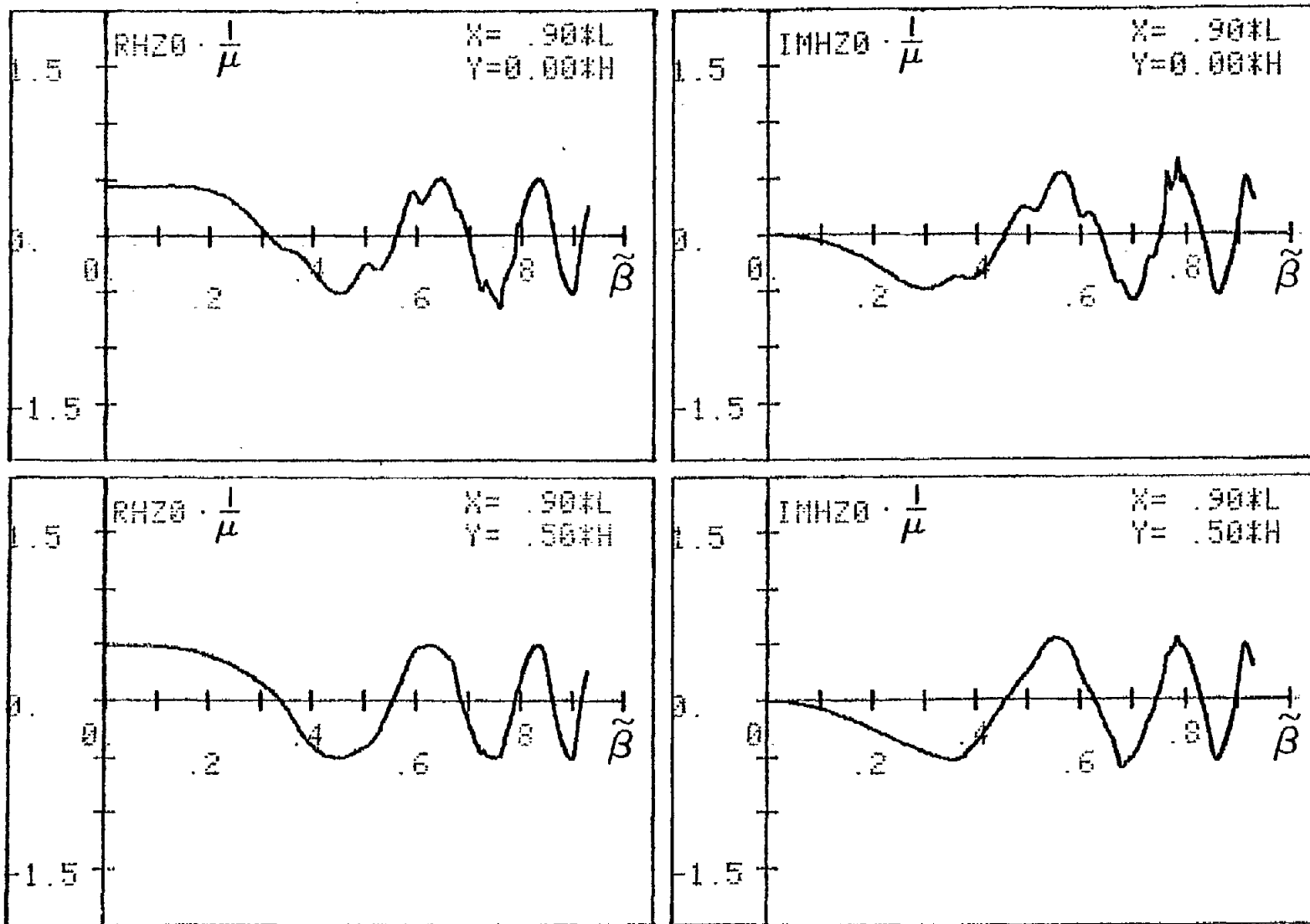


Figure 21. The real and imaginary parts of a z-component of the magnetic field as functions of a longitudinal propagation constant for points of view:  $\frac{X}{L} = 0.9$ ;  $\frac{Y}{H} = 0.0, 0.5$ .

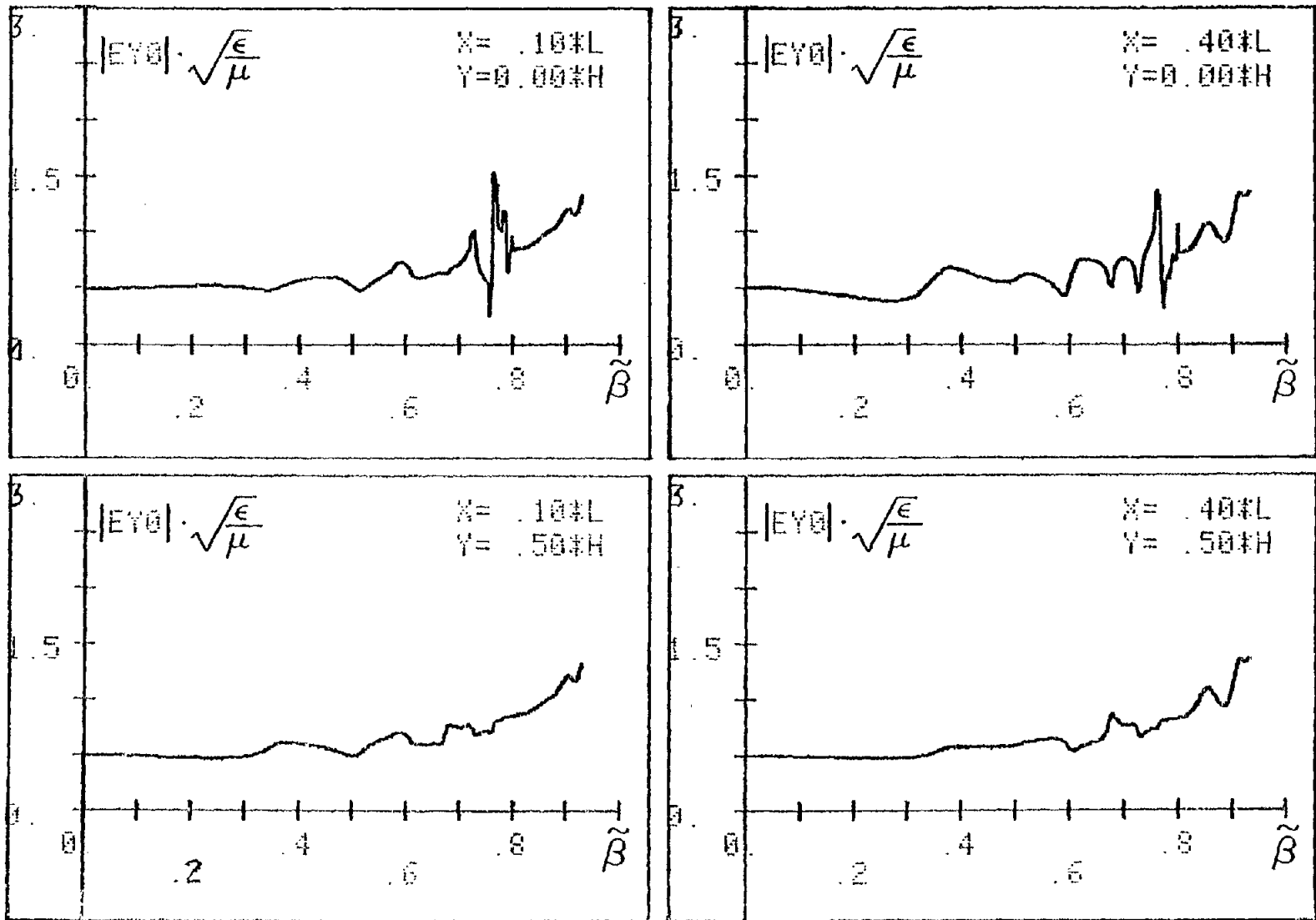


Figure 22. The module of a y-component of the electric field as a function of a longitudinal propagation constant for points of view:  $\frac{x}{L} = 0.1, 0.4$ ;  $\frac{y}{H} = 0.0, 0.5$ .

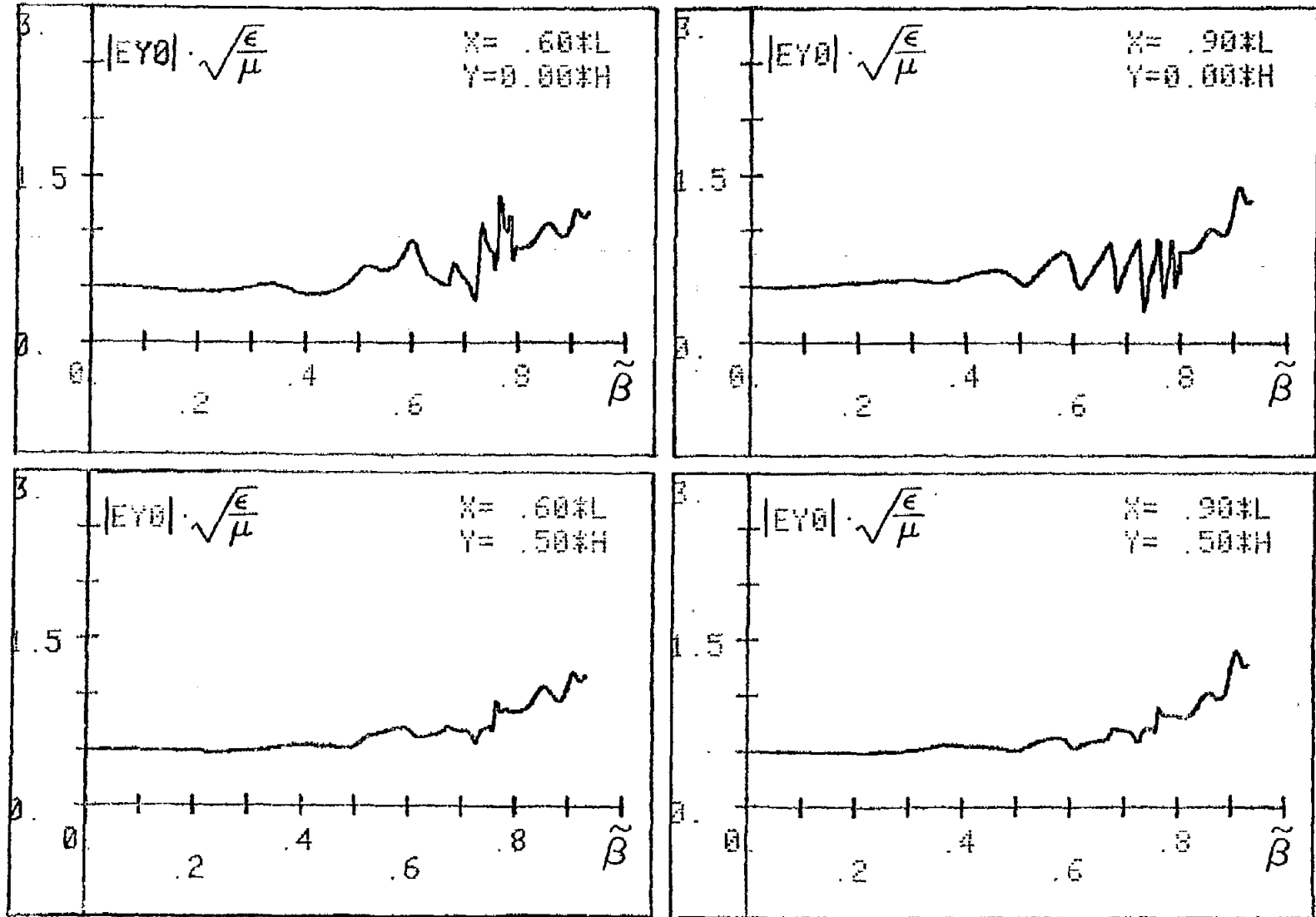


Figure 23. The modulus of a y-component of the electric field as a function of a longitudinal propagation constant for points of view:  $\frac{X}{L} = 0.6, 0.9$ ;  $\frac{Y}{H} = 0.0, 0.5$ .

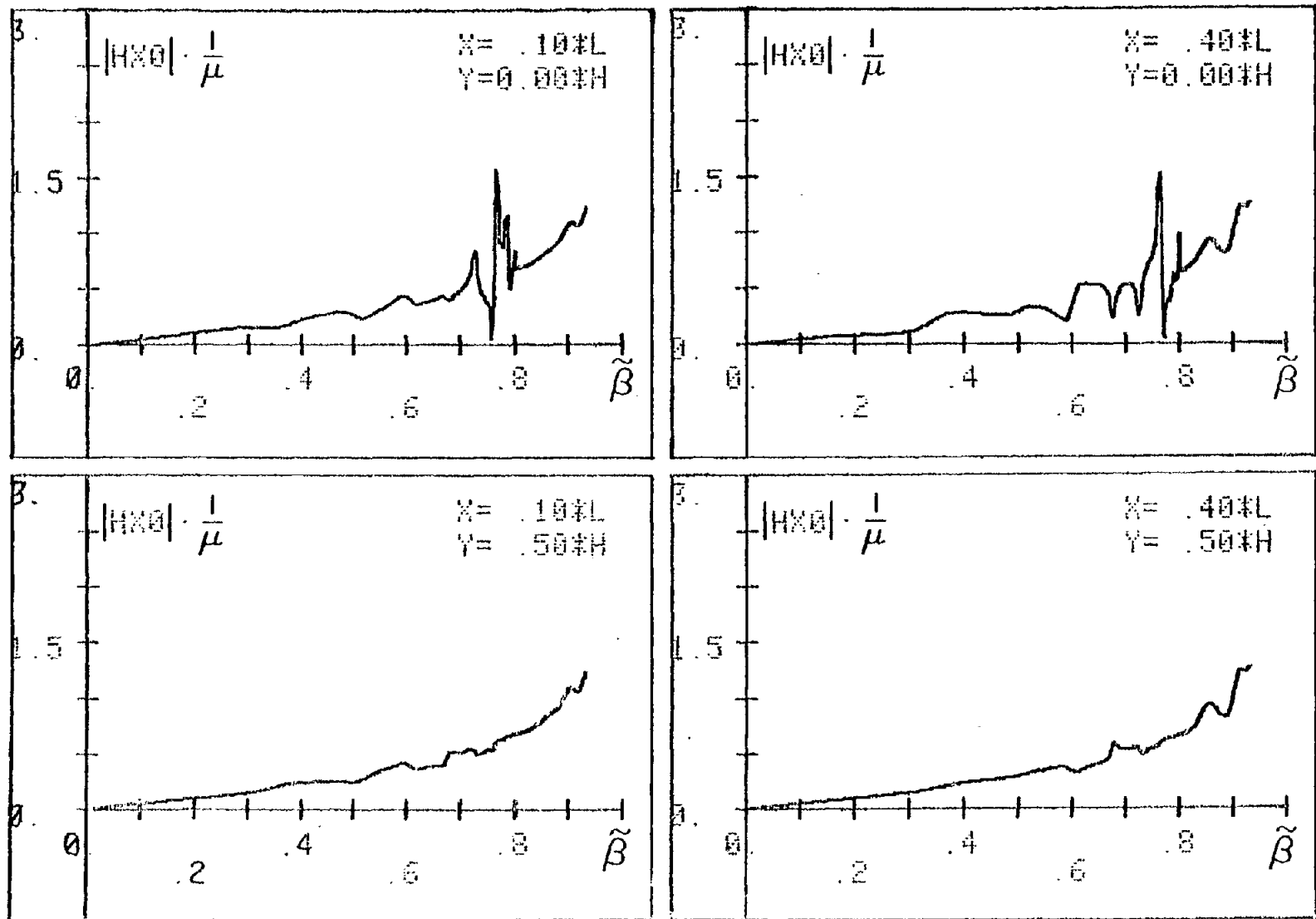
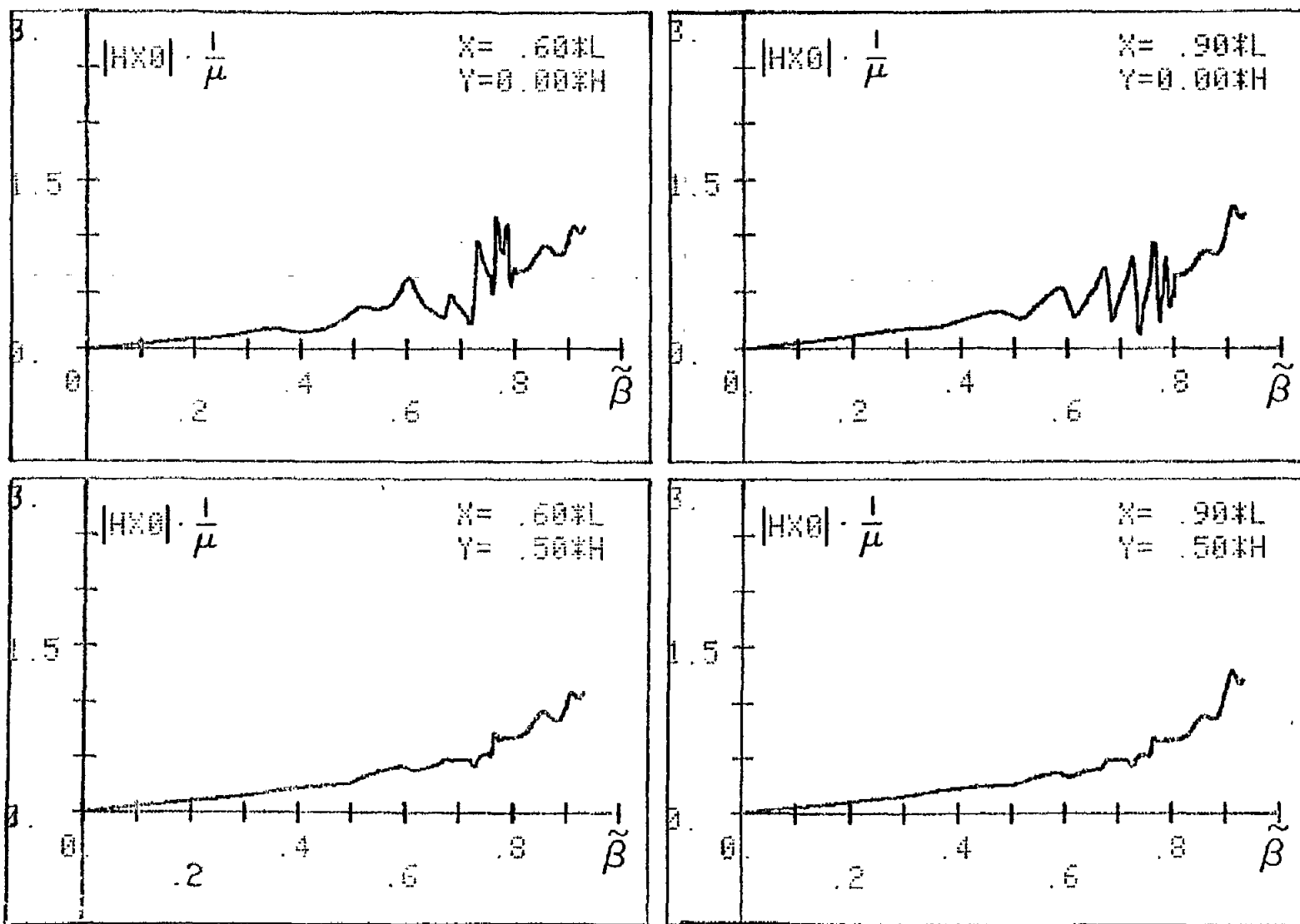


Figure 24. The module of an x-component of the magnetic field as a function of a longitudinal propagation constant for points of view:  $\frac{X}{L} = 0.1, 0.4$ ;  $\frac{Y}{H} = 0.0, 0.5$ .



410

Figure 25. The module of an x-component of the magnetic field as a function of a longitudinal propagation constant for points of view:  $\frac{X}{L} = 0.6, 0.9$ ;  $\frac{Y}{H} = 0.0, 0.5$ .

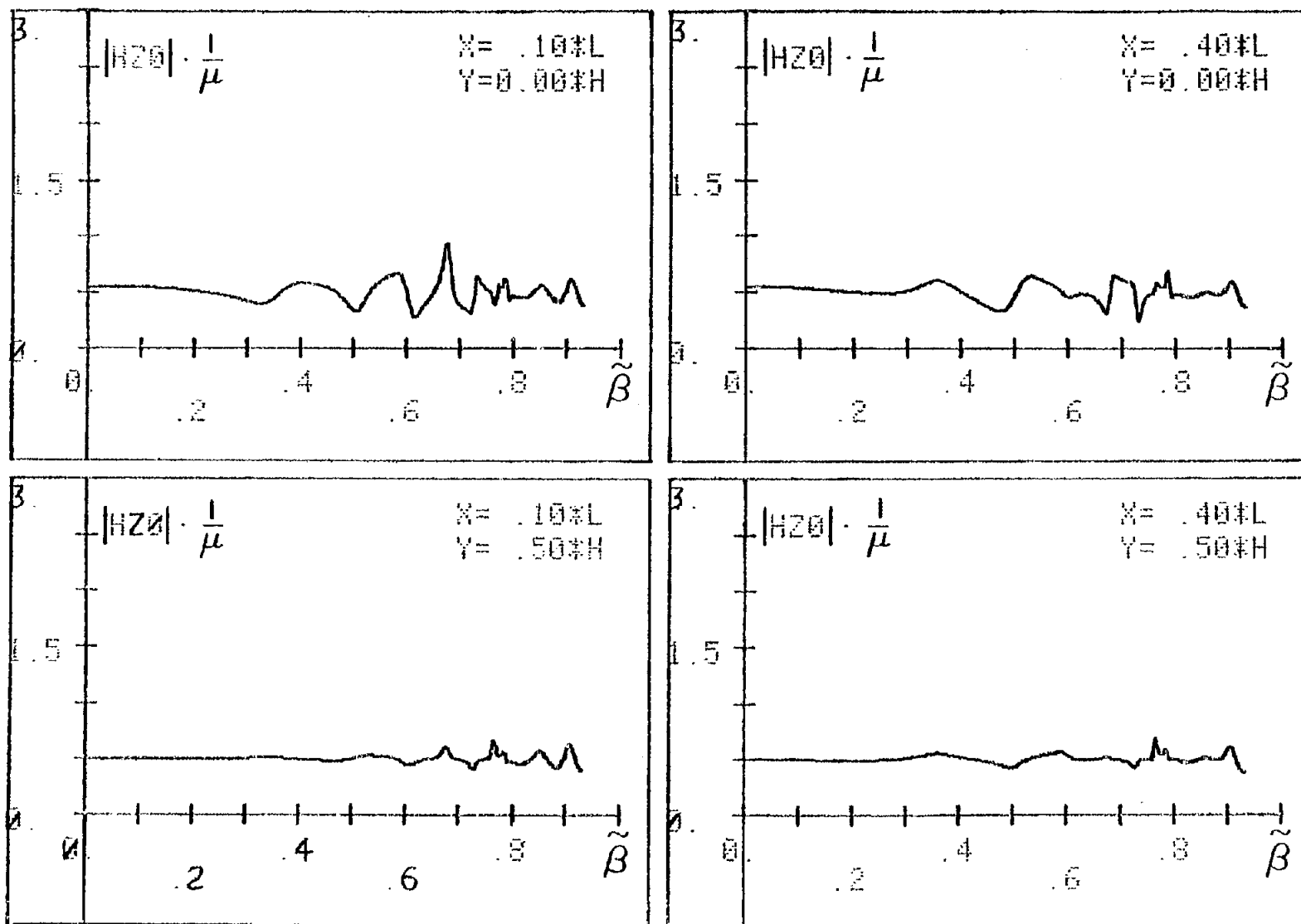


Figure 26. The module of a z-component of the magnetic field as a function of a longitudinal propagation constant for points of view:  $\frac{X}{L} = 0.1, 0.4$ ;  $\frac{Y}{H} = 0.0, 0.5$ .

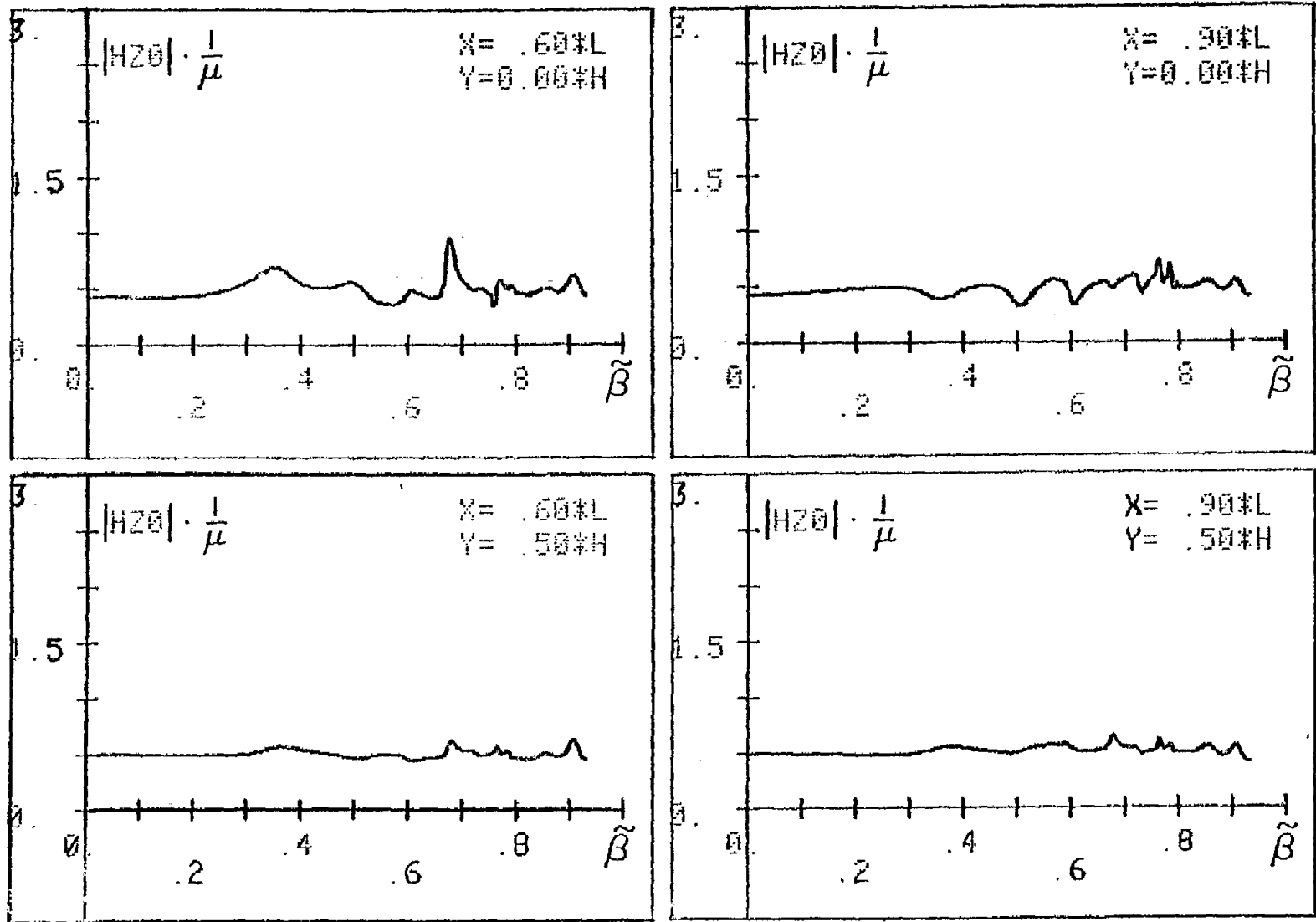


Figure 27. The module of a z-component of the magnetic field as a function of a longitudinal propagation constant for points of view:  $\frac{X}{L} = 0.6, 0.9$ ;  $\frac{Y}{H} = 0.0, 0.5$ .

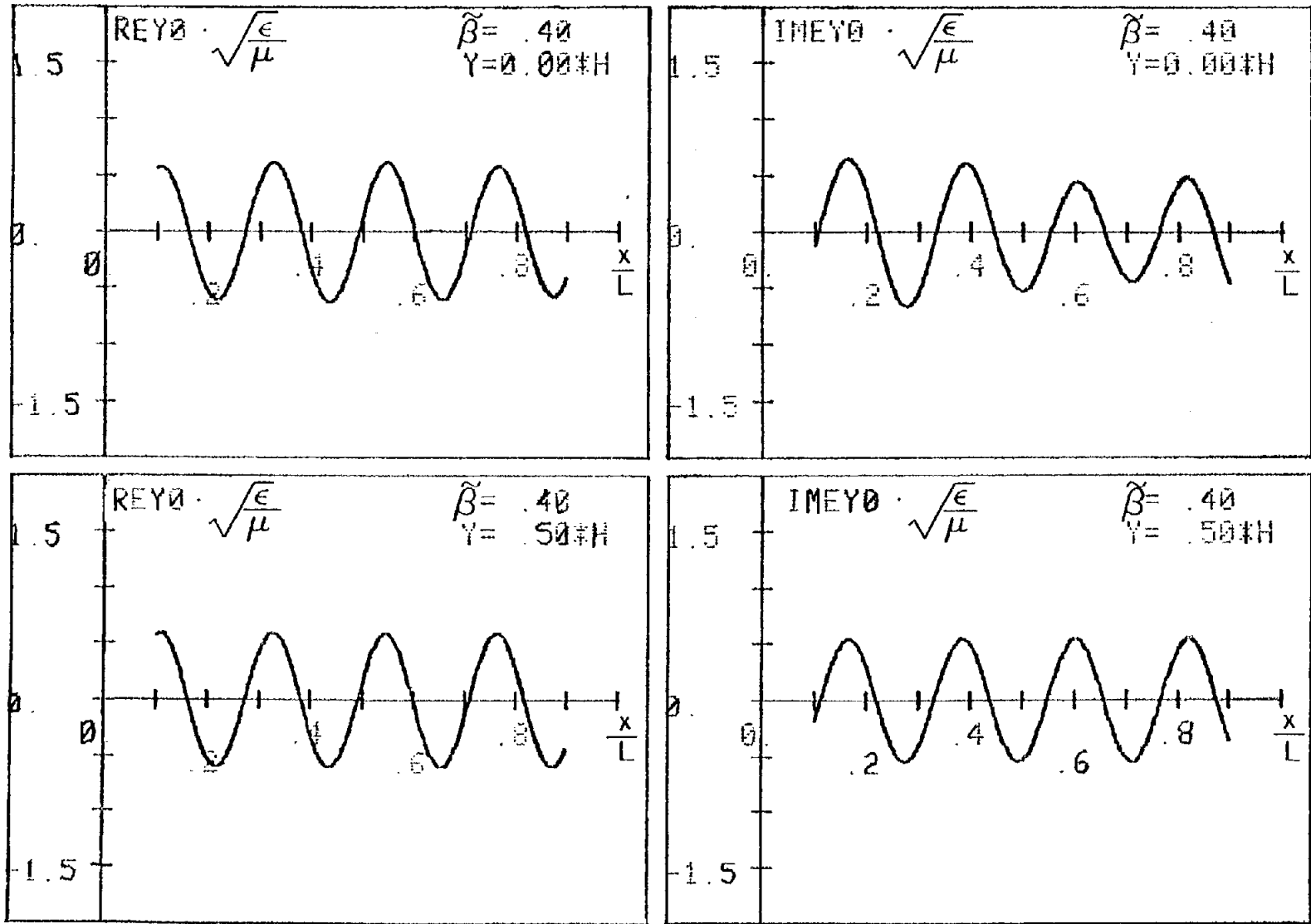


Figure 28. The real and imaginary parts of a  $y$ -component of the electric field as functions of an  $x$ -coordinate for  $\tilde{\beta} = 0.4$ ;  $\frac{Y}{H} = 0.0, 0.5$ .

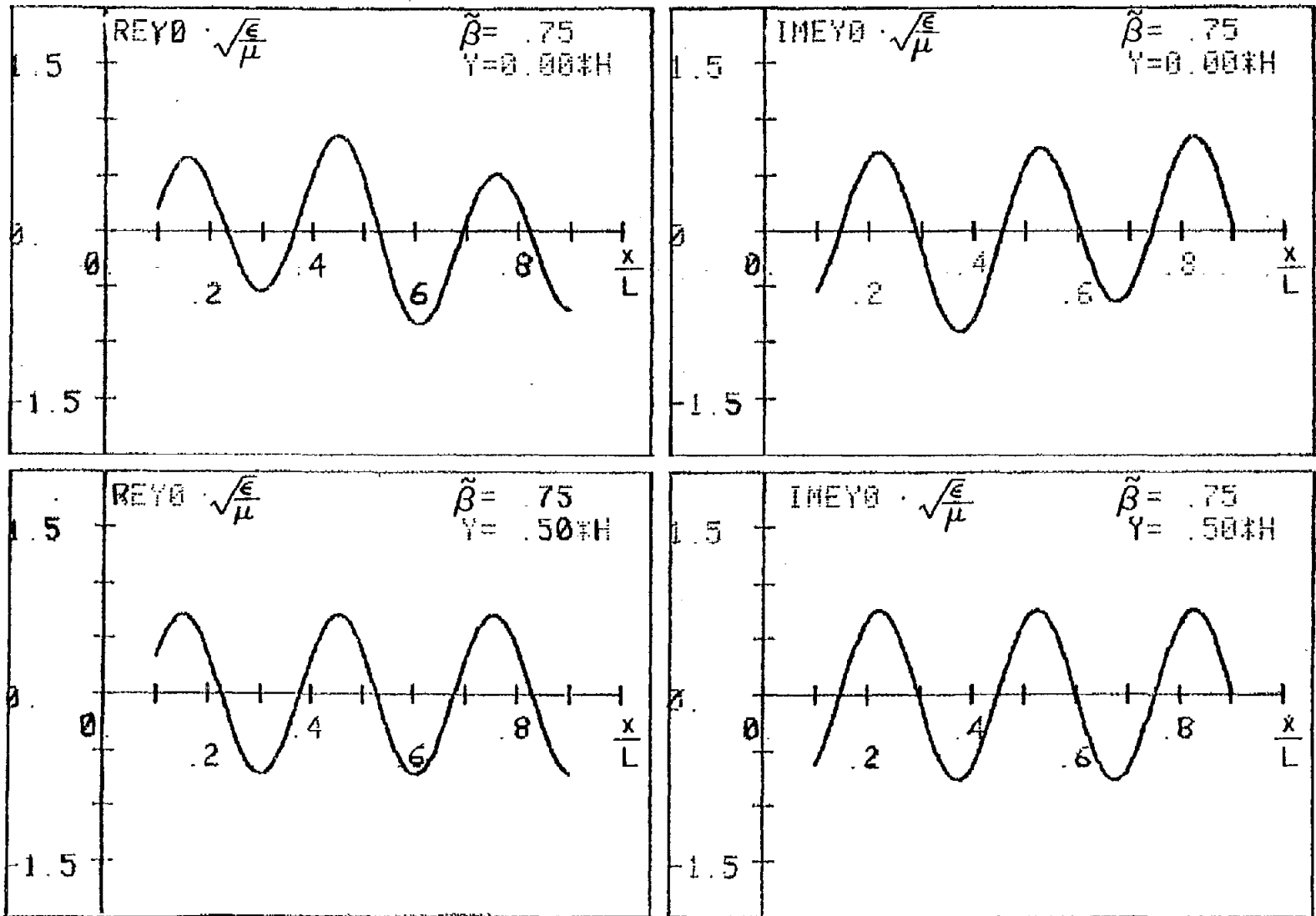


Figure 29. The real and imaginary parts of a  $y$ -component of the electric field as functions of an  $x$ -coordinate for  $\tilde{\beta} = 0.75$ ;  $\frac{Y}{H} = 0.0, 0.5$ .

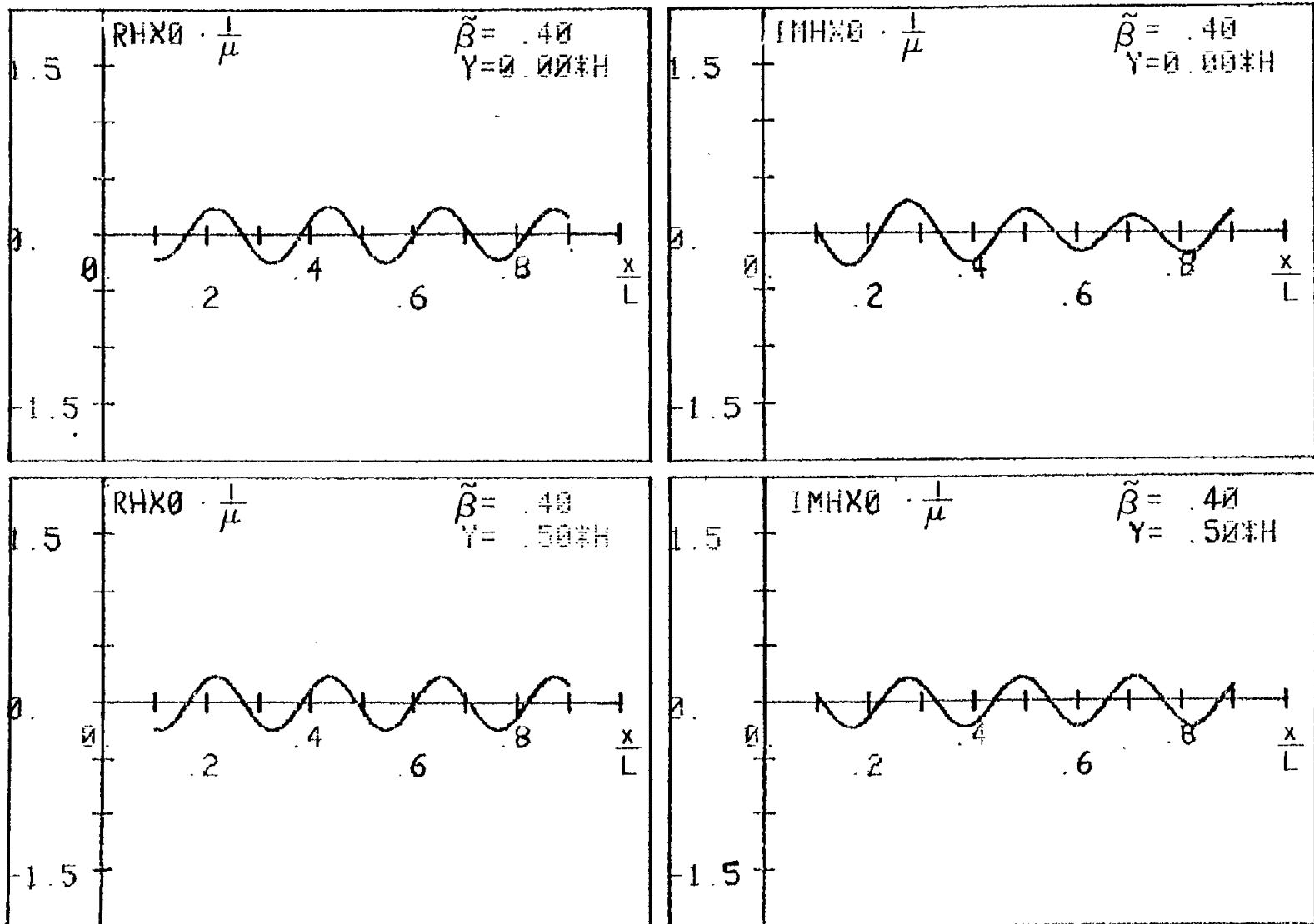


Figure 30. The real and imaginary parts of an  $x$ -component of the magnetic field as functions of an  $x$ -coordinate for  $\tilde{\beta} = 0.4$ ;  $\frac{Y}{H} = 0.0, 0.5$ .

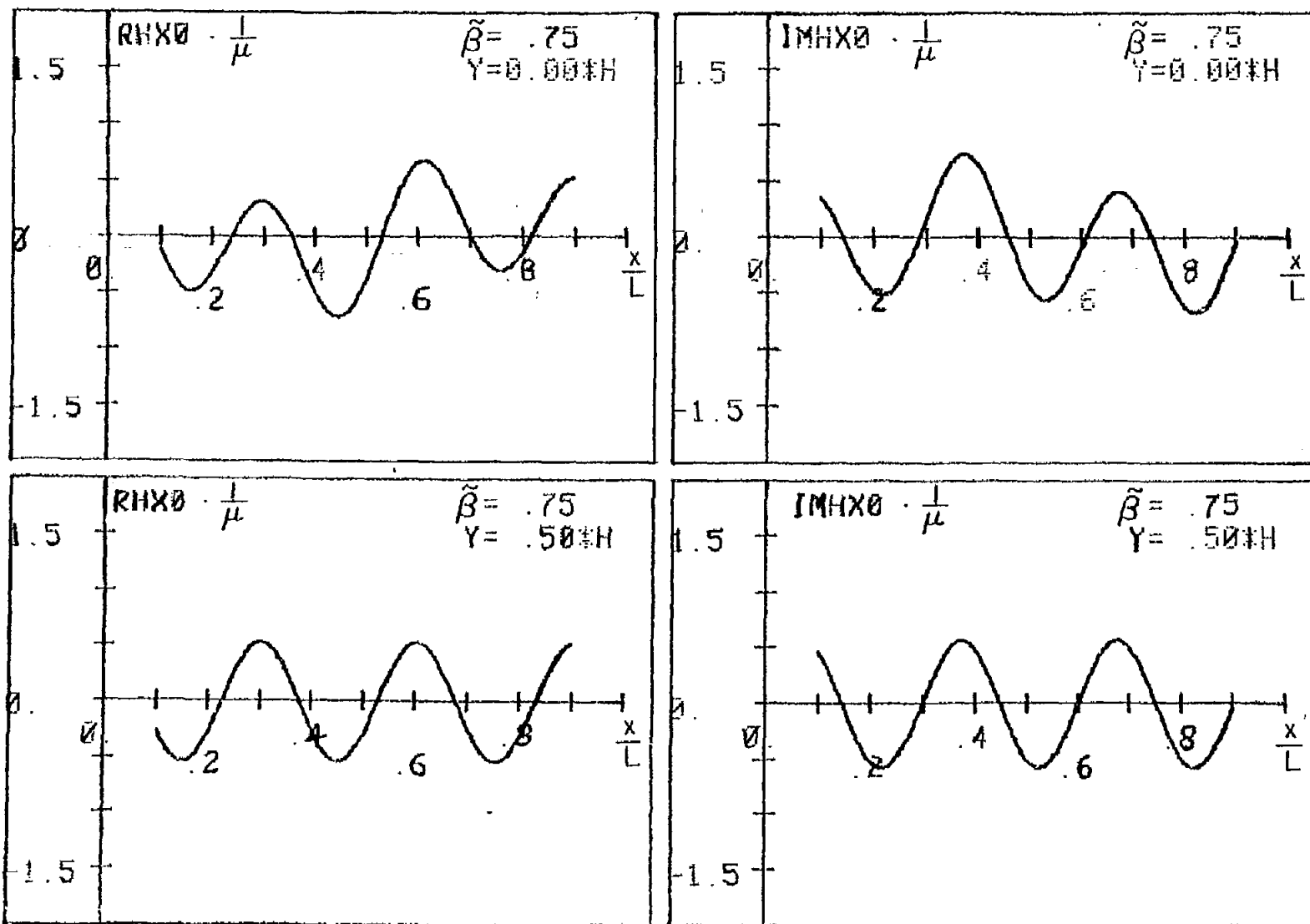


Figure 31. The real and imaginary parts of an  $x$ -component of the magnetic field as functions of an  $x$ -coordinate for  $\tilde{\beta} = 0.75$ ;  $\frac{Y}{H} = 0.0, 0.5$ .

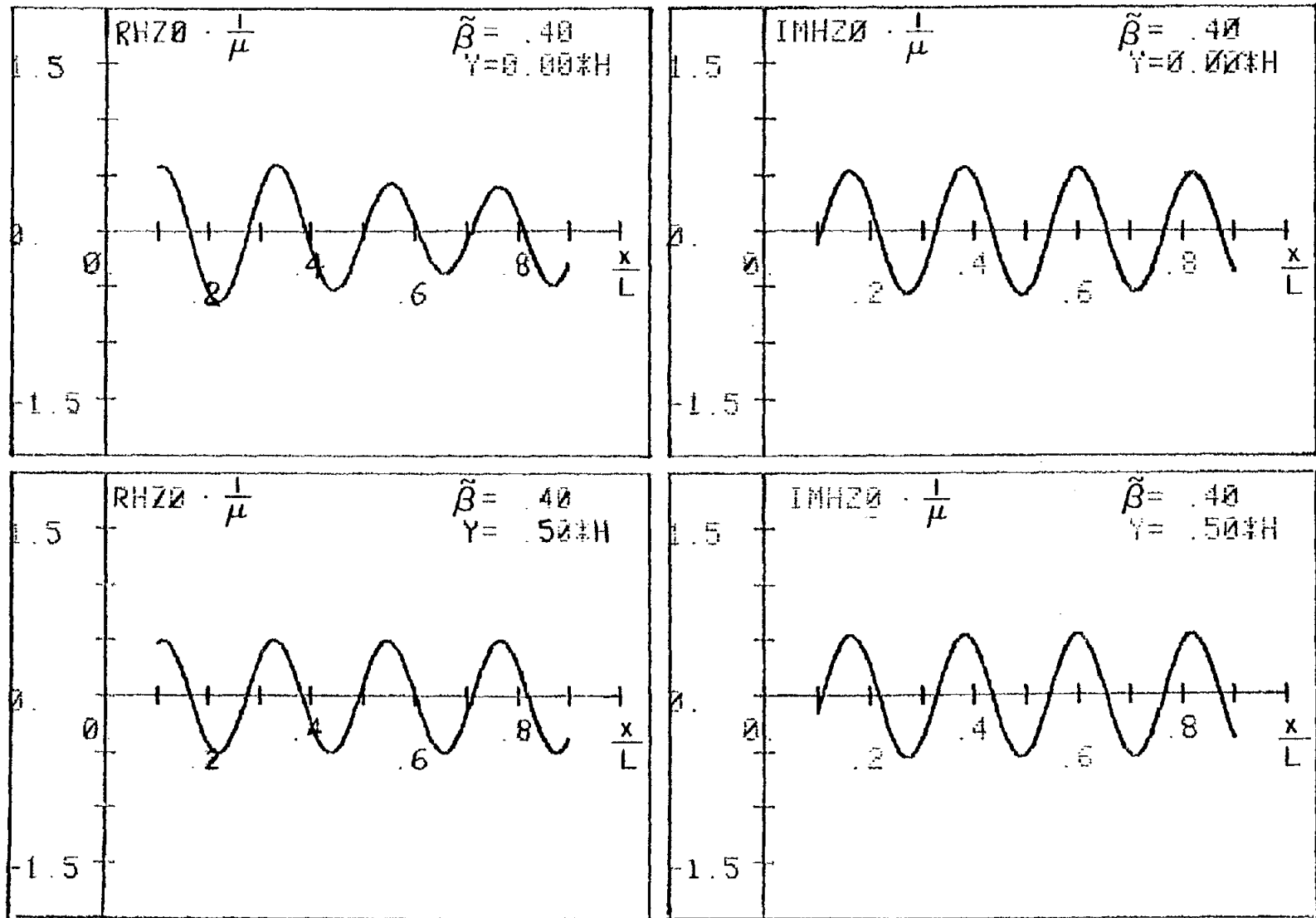


Figure 32. The real and imaginary parts of a  $z$ -component of the magnetic field as functions of an  $x$ -coordinate for  $\tilde{\beta} = 0.4$ ;  $\frac{Y}{H} = 0.0, 0.5$ .

418

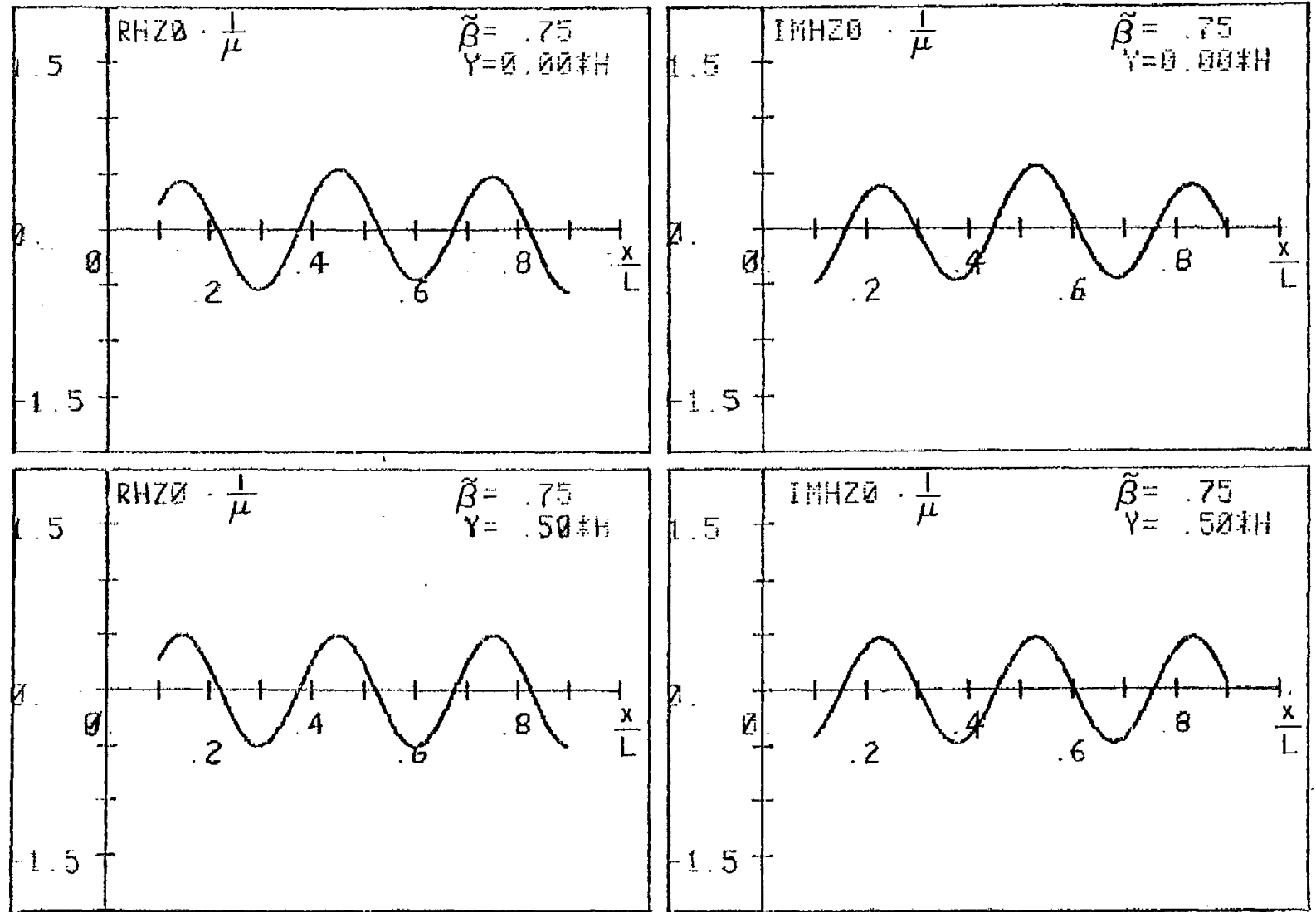


Figure 13. The real and imaginary parts of a  $y$ -component of the magnetic field as functions of an  $x$ -coordinate for  $\tilde{\beta} = 0.75$ ;  $\frac{\gamma}{H} = 0.0, 0.5$ .

### III. NUMERICAL STUDY OF THE PROBLEM

Because the analytical expressions derived in the second section are rather complicated and difficult to analyze, we numerically evaluated the solutions using a digital computer. The results are presented in this section in graphical form. This section consists of two parts: in the first we discuss the field components as functions of the longitudinal propagation constant; in the second - as functions of the transverse coordinates.

#### A. Real and Imaginary Parts and Amplitudes of the Field Components As Functions of the Longitudinal Propagation Constant

The graphics that are supplied in this section were plotted with a step for  $\tilde{\beta}$  equal to 0.005. The point,  $\tilde{\beta} = 0.80009$ , also was used. The figures were plotted using 188 points. The output for the real and imaginary parts and the amplitudes of all five field components for eight observation points:  $\frac{X}{L} = 0.1, 0.4, 0.6, 0.9$  and  $\frac{Y}{H} = 0.0, 0.5$  are presented. From the figures it is observed that  $E_y, H_x, H_z$  are dominant components. In Figures 6-9 the real and imaginary parts of  $E_y$  are given. By comparing these results, one can observe for points  $\frac{Y}{H} = 0.0$  and  $\frac{Y}{H} = 0.5$  that the  $E_y, H_x, H_z$  - field behaviors as functions of  $\tilde{\beta}$  are more complicated in the middle of the waveguide. This is hardly surprising in view of the largest contribution of the second mode for the above-mentioned components for  $\frac{Y}{H} = 0.0$ . When the point of observation approaches  $\frac{Y}{H} = 0.5$ , the contribution of the second mode for those components decreases and has a limiting value equal to zero. In Figures 6-9, 14-17, 22-25 we observe the step changing for the  $E_y, H_x$  components at  $\tilde{\beta} = \tilde{\beta}_0$ . The

second mode is responsible for this misbehavior. When  $\frac{y}{H} \rightarrow 0.5$ , the contribution of that step decreases, and for  $\frac{y}{H} = 0.5$ , it equals zero. One can observe that the curves are smooth at  $\tilde{\beta} = \tilde{\beta}_0$ . It should be mentioned that:

(a) The discontinuous behavior is observed because we have neglected the exponentially decreasing terms;

(b) In a lossy medium, the rate of decrease would be less. The  $H_z$ -component (see Figures 18-21, 26) doesn't have the step behavior because the contribution of the second mode is proportional to  $\alpha_1$ , which goes to 0, when  $\tilde{\beta} \rightarrow \tilde{\beta}_0$ . The other two components,  $E_x$  and  $E_z$ , are equal to zero on the x-axis and have their largest contribution for  $\frac{y}{H} = 0.5$  (see Figures 2-5, 10-13).  $E_x$  is smooth and  $E_z$  exhibits the step behavior at  $\tilde{\beta}_0$ . The figures demonstrate that the complexity of the curves occurs approximately in the region  $0.7 < \tilde{\beta} < 0.8$ , where we observe a sharp peak, which is due to the resonance. In the region  $0 < \tilde{\beta} < 0.5$  the figures demonstrate the very smooth character of the curves.

#### B. Real and Imaginary Parts of the Field Components as Functions of Transverse Coordinates

In this section we present the real and imaginary parts of the dominant field components  $E_y$ ,  $H_x$ ,  $H_z$  as functions of the x-coordinate for two values of  $\frac{y}{H} = 0.0; 0.5$  and two values of  $\tilde{\beta} = 0.4; 0.75$ . The graphic output, shown in Figures 28-33, was obtained using the results of calculations for 81 points of  $\frac{x}{L}$  in the region  $[0.1, 0.9]$  (step = 0.010). All the graphs have very smooth characteristics. For  $\tilde{\beta} = 0.75$  they have slightly more complicated form than for  $\tilde{\beta} = 0.4$ . As mentioned in the

previous section, for  $\frac{y}{H} = 0.5$  the contribution of the second mode equals zero. We see that the amplitudes of the curves are constant for the entire region of view. For the  $\frac{y}{H} = 0.0$ , the field components are sums of the contributions of two modes. One can observe that the amplitudes of the curves are changing along the x-direction.

## IV. CONCLUSIONS

In this report the problem of a source excitation of an open parallel-plate waveguide was developed. Extensive numerical results for the field components in the waveguide as functions of several parameters of the waveguide and propagation constant were supplied.

## V. REFERENCES

- [1] V. Krichevsky and R. Mittra, "Source excitation of an open parallel-plate waveguide," Sensor and Simulation Note 253, October 1977.

## VI. APPENDIX A

## SOURCE EXCITATION OF AN OPEN, PARALLEL-PLATE WAVEGUIDE PROGRAM

A complete program for source excitation of an open, parallel-plate waveguide program is presented. The computer program provides three-dimensional data-storage for the real and imaginary parts of five components of the EM field. Data were obtained for  $\frac{x}{L}$  between 0.1 - 0.9 with step 0.1;  $\frac{y}{H}$  between 0.0 - 0.9 with step 0.1; and  $\beta$  - propagation constant between 0.0 - 0.93 with step 0.005 plus ( $\cdot$ ) 0.80009. These data were used to plot EM field components as functions of the propagation constant. The program can be readily modified to obtain data for plotting the EM-field component as a function of the x-coordinate.

```

PROGRAM AFIELD(INPUT,OUTPUT,TAPES,TAPE1=INPUT)
  COMPLEX BRK,BBAL,TI,F1,F2,EXO,EYO,EZO,HXO,HZO,CONST,AA,BB
  DIMENSION XX(9),YY(10),BETAB(188),REXO(10,9,188),AMEXO(10,9,188),
  #REYO(10,9,188),AMEYO(10,9,188),REZO(10,9,188),AMEZO(10,9,188),
  #RHXO(10,9,188),AMHXO(10,9,188),RHZO(10,9,188),AMHZO(10,9,188)
  READ(1,2)W,YBRI,YBRS,YBRF,XBRI,XBRS,XBRF
  2 FORMAT(F7.5,6(F7.3))
  M=1000
  PI=3.141592654
  CONST=CMPLX(0.,1.)
  CON=2.11593152
  BETAB(1)=0.
  DO 70 I=1,160
    BETAB(I+1)=BETAB(I)+0.005
  70 CONTINUE
    BETAB(162)=0.80009
    BETAB(163)=0.805
    DO 75 I=1,25
      BETAB(I+163)=BETAB(I+162)+0.005
  75 CONTINUE
    DO 98 N=1,161
      BETA=BETAB(N)
      K=N
      A=10.*PI*SQRT(1.-BETA**2)
      B=A*KW/PI
      ALFA1=SQRT(B**2-1.)
      DD=PI*KALFA1/W
      CALL BE1(A,B,BBK,PI,M,CON,ALFA1)
      CALL BE2(A,B,BBAL,PI,M,CON,ALFA1)
      CALL TE1(A,B,TI,BBK,PI)
      CALL F12(A,B,TI,ALFA1,BBK,BBAL,F1,F2)
      X=XBRI
      J=1
    30 Y=YBRI
      I=1
    20 EXO=(PI*KALFA1/(10.*W**2))*F2*SIN(PI*KY)*SIN(DD*KX)
      EYO=10.*PI*(F1*DCOS(A*KX)+(1.-(1./100.*W**2)))*F2*DCOS(PI*KY)*
      #COS(DD*KX)-CEXP(CMPLX(0.,A*KX))/(2.*A))
      EZO=-CONST*BETA*(PI/W)*F2*SIN(PI*Y)*DCOS(DD*KX)
      HXO=-BETA*10.*PI*(F1*DCOS(A*KX)+F2*DCOS(PI*Y)*DCOS(DD*KX)-(1./2.*A))*
      #CEXP(CMPLX(0.,A*KX))
      HZO=CONST*K*F1*SIN(A*KX)+CONST*DD*F2*DCOS(PI*Y)*SIN(DD*KX)-
      #0.5*CEXP(CMPLX(0.,A*KX))
      REXO(I,J,K)=REAL(EXO)
      AMEXO(I,J,K)=AIMAG(EXO)
      REYO(I,J,K)=REAL(EYO)

```

```

AMEYO(I,J,K)=AIMAG(EYO)
REZO(I,J,K)=REAL(EZO)
AMEZO(I,J,K)=AIMAG(EZO)
RHXO(I,J,K)=REAL(HXO)
AMHXO(I,J,K)=AIMAG(HXO)
RHZO(I,J,K)=REAL(HZO)
AMHZO(I,J,K)=AIMAG(HZO)
Y=Y+YBRS
I=I+1
IF(Y.LE.YBRF) GO TO 20
X=X+XBRS
J=J+1
IF(X.LE.XBRF) GO TO 30
98 CONTINUE
DO 99 L=162,188
BETA=BETAB(L)
K=L
A=10.*PI*SQRT(1.-BETA**2)
X=XBRI
J=1
B=A*W/PI
CALL BE(A,B,BB,PI,M)
X=XBRI
17 AA=CEXP(CMPLX(0.,A*X))
EYO=-0.5*(AA-BB*COS(A*X))/SQRT(1.-BETA**2)
HXO=-BETA*EYO
HZO=0.5*(-SIGN(1.,X)*AA+CONST*BB*SIN(A*X))
DO 18 I=1,10
REXO(I,J,K)=0.
AMEXO(I,J,K)=0.
REZO(I,J,K)=0.
AMEZO(I,J,K)=0.
REYO(I,J,K)=REAL(EYO)
AMEYO(I,J,K)=AIMAG(EYO)
RHXO(I,J,K)=REAL(HXO)
AMHXO(I,J,K)=AIMAG(HXO)
RHZO(I,J,K)=REAL(HZO)
18 AMHZO(I,J,K)=AIMAG(HZO)
X=X+XBRS
J=J+1
IF(X.LE.XBRF) GO TO 17
99 CONTINUE
WRITE(3,101) REXO,AMEXO,REYO,AMEYO,REZO,AMEZO,RHXO,AMHXO,RHZO,AM
$HZO
101 FORMAT(10F8.5)
DY=0.1
DX=0.1
YY(1)=0.
DO 50 I=1,9
YY(I+1)=YY(I)+DY
50 CONTINUE

```

```

      XX(I)=0.1
      DO 60 I=1,S
      XX(I+1)=XX(I)+DX
60 CONTINUE
      WRITE(3,101) YY,XX,BETAB
      STOP
      END
      SUBROUTINE BE1(A,B,BK,PI,M,CON,ALFA1)
      COMPLEX F,BK
      AM1=0,
      DO 10 I=2,M
      AM1=AM1+B/I-ASIN(B/I)
10 CONTINUE
      F=CEXP(CMPLX(-BK*PI/2.,BK*(CON-ALOG(B)))-PI/2.+A+AM1))
      BK=(ALFA1+B)*F
      RETURN
      END
      SUBROUTINE BE2(A,B,BBAL,PI,M,CON,ALFA1)
      COMPLEX F,BBAL,D
      AM1=0,
      DO 10 I=2,M
      AM1=AM1+ALFA1/I-ASIN(ALFA1/SQRT(I**2-1.))
10 CONTINUE
      F=CEXP(CMPLX(-ALFA1*PI/2.,ALFA1*(CON-ALOG(B))+AM1+ALFA1*A/B))
      D=CMPLX(1.,-ALFA1)
      BBAL=F*D*SQRT(2.)*ALFA1/B
      RETURN
      END
      SUBROUTINE TE1(A,B,T1,BK,PI)
      COMPLEX T1,BK,D1
      D=B*SQRT(PI)/SQRT(A*2.)
      D1=CMPLX(1.+D,-D)
      T1=BK**2*D1
      RETURN
      END
      SUBROUTINE F12(A,B,T1,ALFA1,BK,BBAL,F1,F2)
      COMPLEX T1,BK,BBAL,F1,F2,D1
      D1=ALFA1*(1.+T1)*(BBAL**2*(4.*T1*B/(1.+T1))-(ALFA1+B)**2/ALFA1)/
      *(2.*ALFA1)-1.)
      F1=(BK**2/((1.+T1)*A))*(1.+2.*B*BBAL**2/D1)
      F2=2.*B*BK*BBAL/(A*D1)
      RETURN
      END
      SUBROUTINE BE(A,B,BB,PI,M)
      COMPLEX T,F,BB
      CONST=1.115931515
      AM1=0,
      DO 10 I=1,M
      AM1=AM1+B/I-ASIN(B/I)
10 CONTINUE
      T=CEXP(CMPLX(-BK*PI*2.*(B*(CON-ALOG(B))+A+AM1)))
      F1=SQRT(PI)*B/SQRT(2.*A)
      F=CMPLX(1.+F1,-F1)
      BB=2.*T/(1.+T*F)
      RETURN
      END

```

VII. APPENDIX B  
 ADDITIONAL NUMERICAL RESULTS

In Section III of this report, we have calculated the electromagnetic fields as functions of  $\beta$ , the normalized propagation constant in the z-direction. The parameters chosen for the computation in the report were:

$$\frac{H}{L} = 0.16670, \quad \frac{L}{\lambda_0} = 5, \quad \text{where } \lambda_0 = \frac{2\pi}{\omega\sqrt{\epsilon\mu}} .$$

At the request of Dr. D. Giri of SAI\*, we have now derived additional numerical results for the following choice of parameters, which correspond to those of the experimental parallel-plate structure being investigated at Harvard.

$$L = 12.5 \text{ m}$$

$$H = 12.75 \text{ m}$$

$$f = 25 \text{ Mny } (\lambda_0 = 12\text{m})$$

$$\frac{H}{L} = 1.020 ; \quad \frac{L}{\lambda_0} = 1.041667$$

\*presently with LuTech, Inc., Berkeley, CA

The propagation constant in the x-direction can be written in the form:

$$\alpha_n = \frac{\pi}{H} \frac{kH}{\pi} - m^2 \quad 1/2, \quad m = 0, 1, 2, \dots$$

$$\text{where } k = k_0 \sqrt{1 - \beta^2}, \quad k_0 = \frac{2\pi}{\lambda_0}$$

$$kL \leq k_0 L = 2\pi \frac{L}{\lambda} = 6.544985.$$

The asymptotic analysis presented in this report was based on the assumption ( $kL \gg 1$ ). Consequently, great care should be exercised when the range of application of these formulas is extended below  $kL = 10$ .

It is not difficult to prove that in the range  $0 < \tilde{\beta} < 0.337916$ , only three modes are above cut-off in the x-direction. Furthermore, two modes are propagating in the range  $0.337916 < \tilde{\beta} < 0.882353$  and only one mode can propagate in the range  $\tilde{\beta} > 0.882353$ . The application of the formulas and computer programs developed in this report, though not the theory itself, is restricted to the range where two modes can propagate in the x-direction. For this reason, we develop the numerical results only for the region  $\tilde{\beta} \geq 0.34$ , and specifically for the range

$$0.34 \leq \tilde{\beta} \leq 0.9.$$

We would like to mention that it is possible to develop the necessary formulas and numerical results for the region  $0 < \tilde{\beta} < 0.34$  using the theory given in a previous report [1].

430

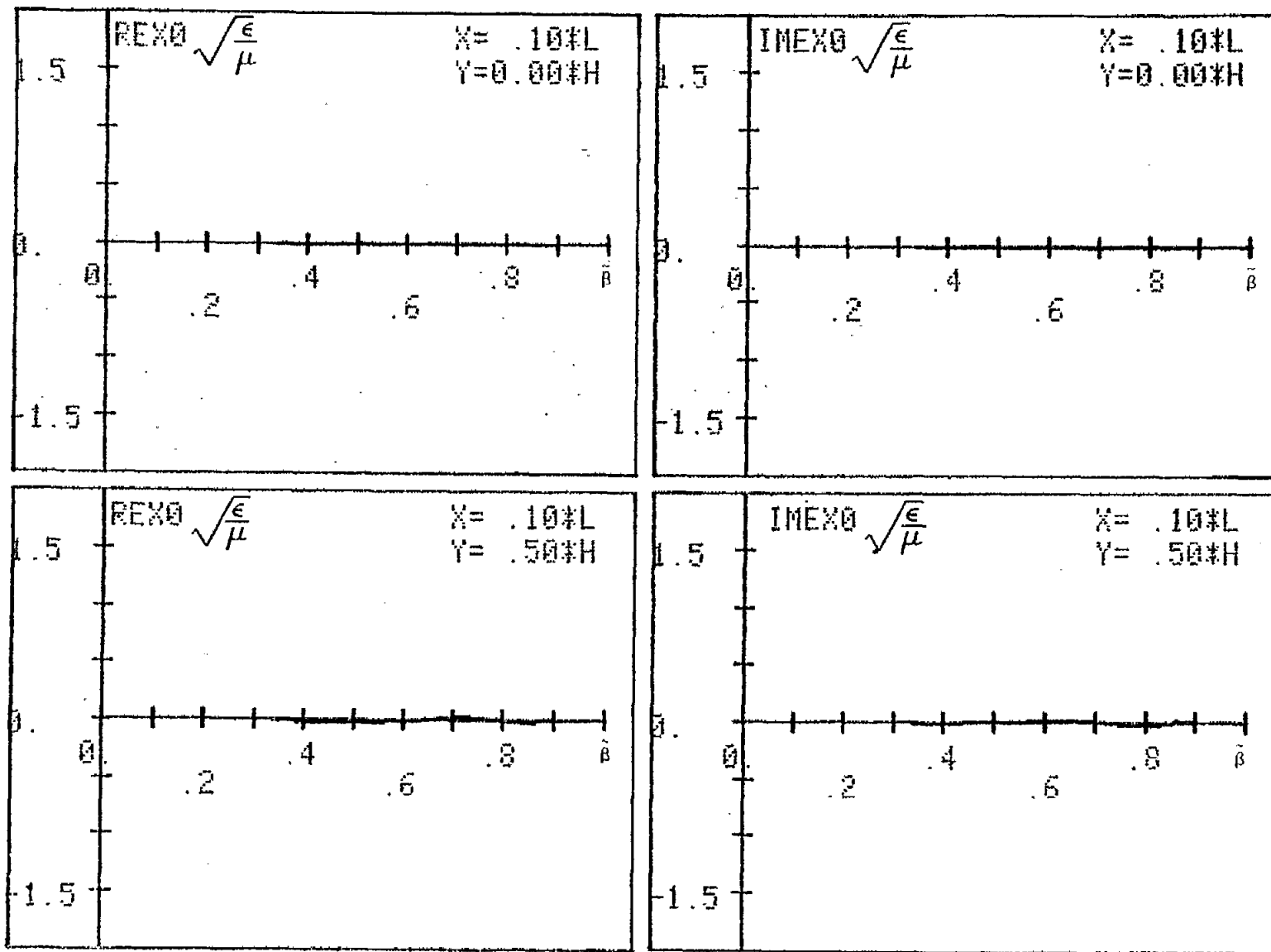


Figure 1. Real and imaginary parts of  $E$  as functions of  $\beta$  for parameters given in the lower half of Page 1. The  $x, y$  values of the observation point are shown in the inset.

431

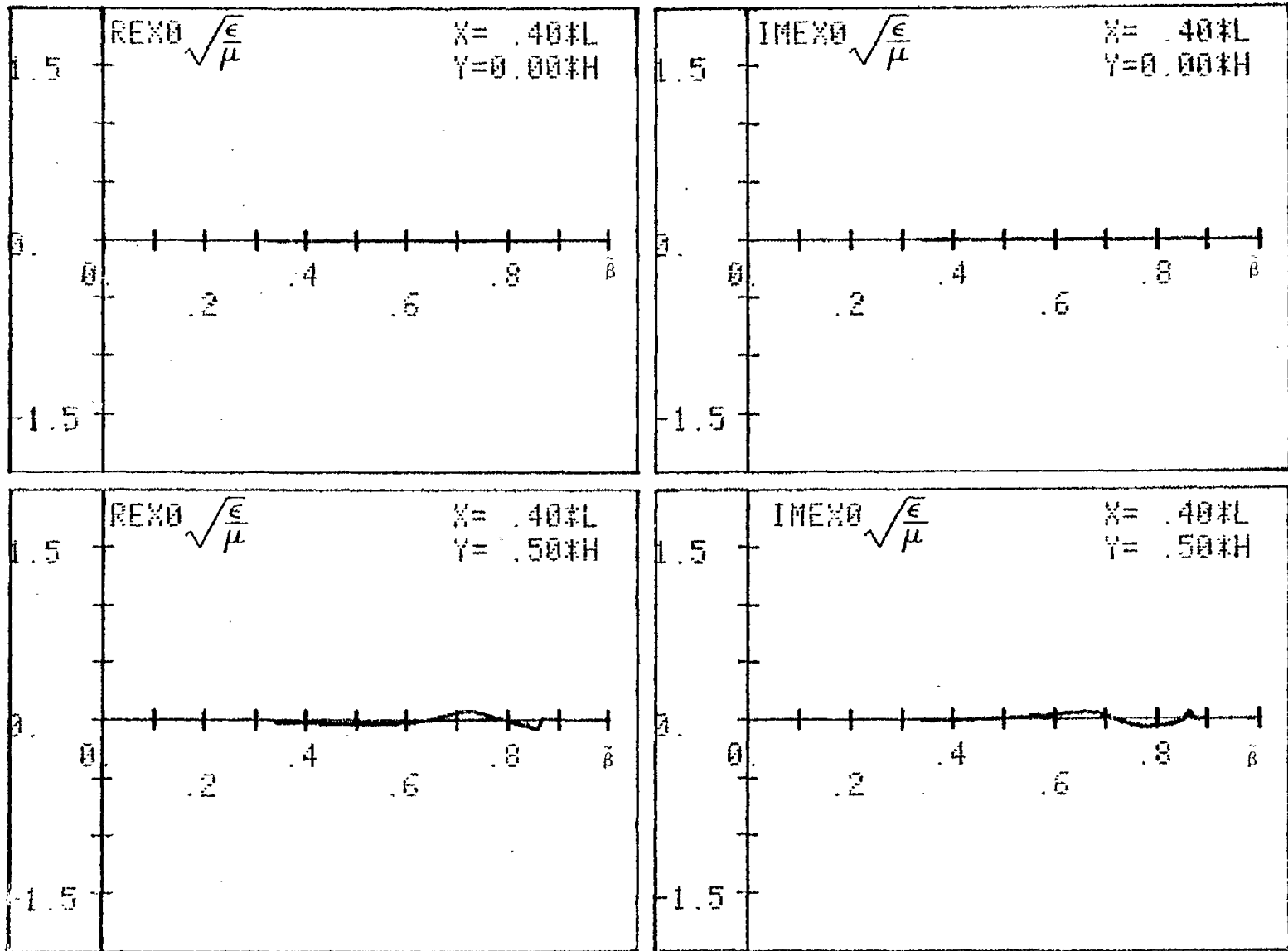
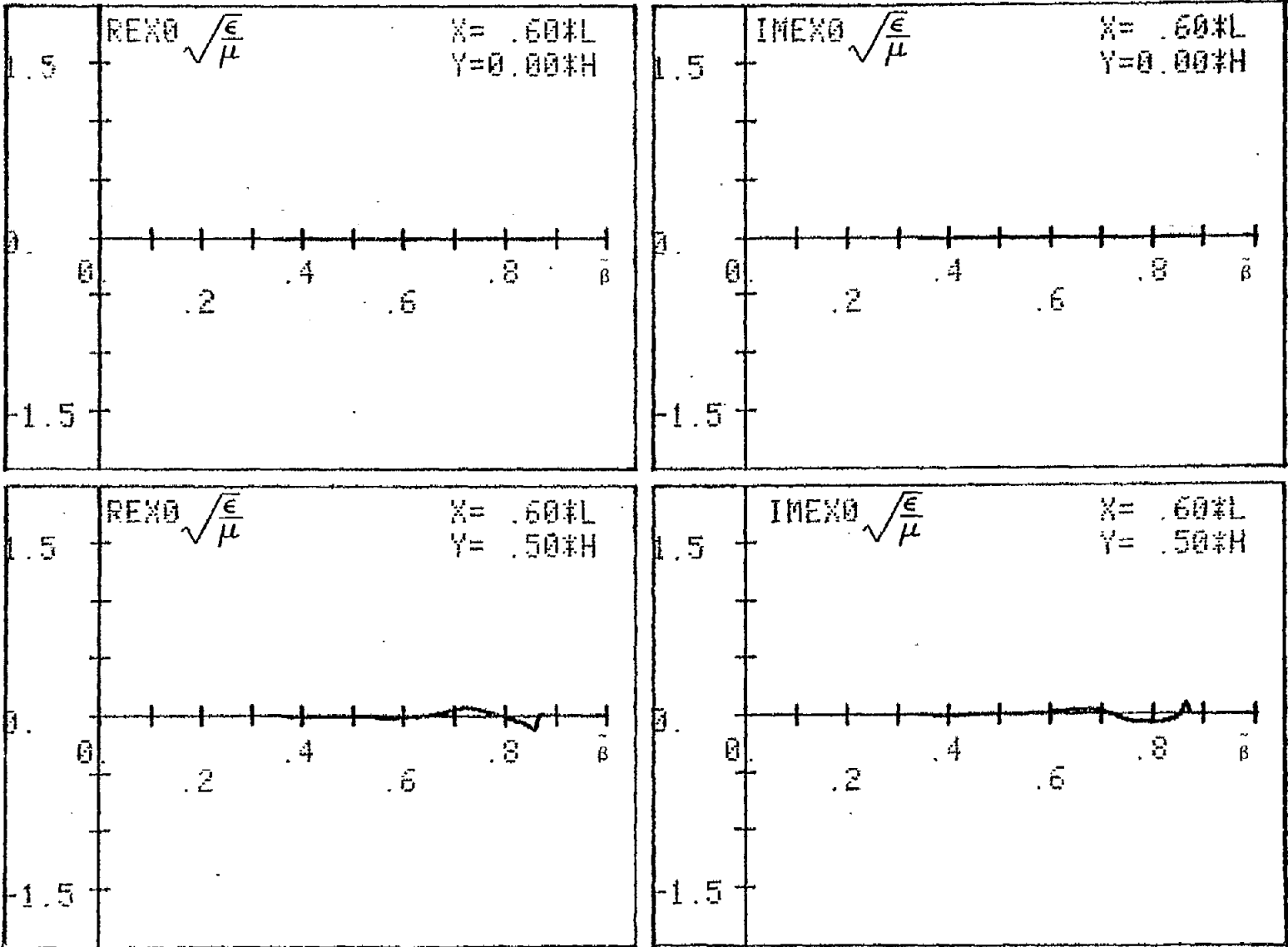


Figure 2. Real and imaginary parts of  $E$  as functions of  $\beta$  for parameters given in the lower half of Page 1. The  $x, y$  values of the observation point are shown in the inset.



432

Figure 3. Real and imaginary parts of  $E_x$  as functions of  $\beta$  for parameters given in the lower half of Page 1. The  $x, y$  values of the observation point are shown in the inset.

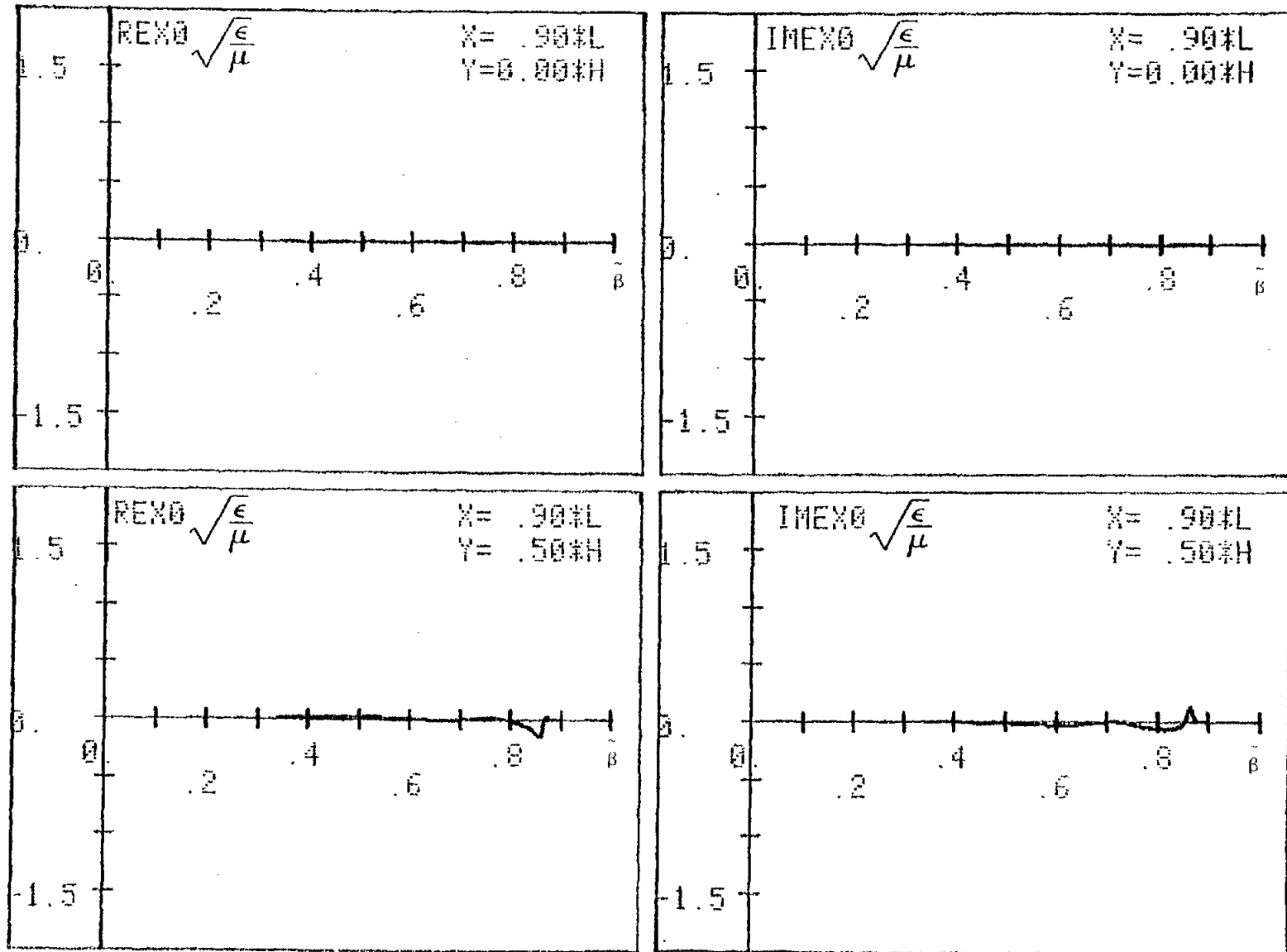
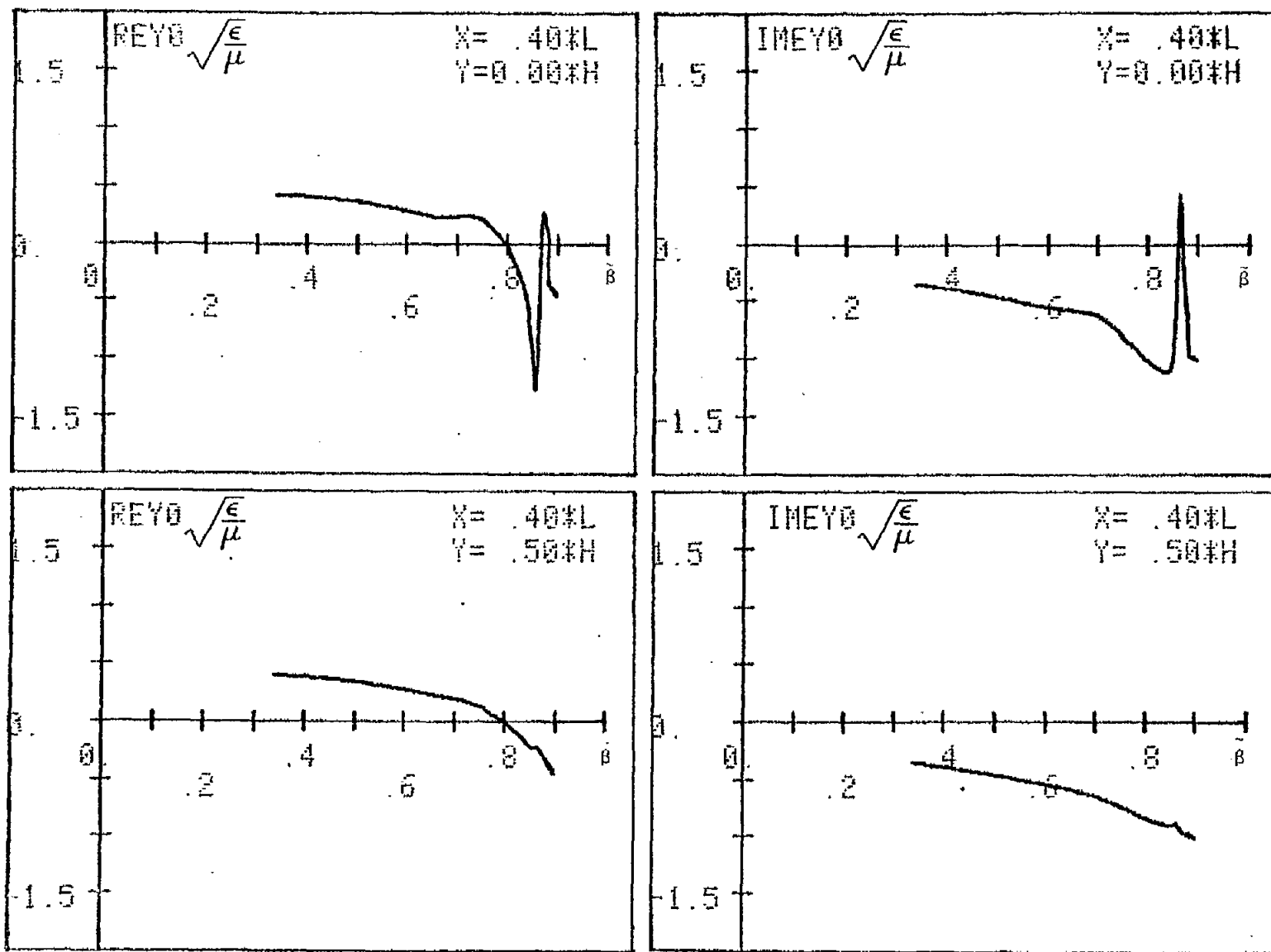


Figure 4. Real and Imaginary parts of  $E_x$  as functions of  $\bar{\beta}$  for parameters given in the lower half of Page 1. The x,y values of the observation point are shown in the inset.



434

Figure 6. Real and imaginary parts of  $E$  as functions of  $\beta$  for parameters given in the lower half of Page 1. The  $x, y$  values of the observation point are shown in the inset.

435

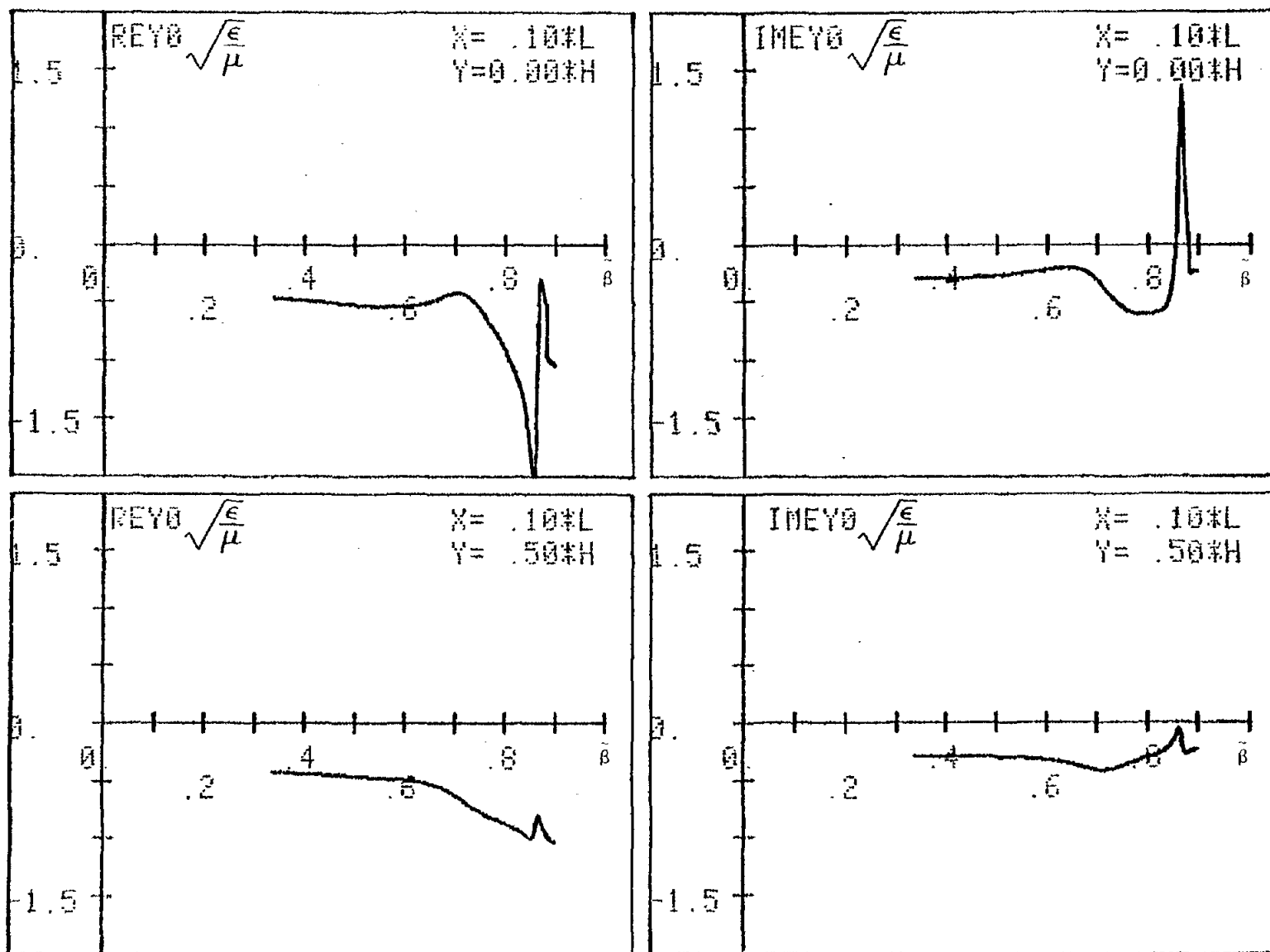


Figure 5. Real and imaginary parts of  $E_x$  as functions of  $\beta$  for parameters given in the lower half of Page 1. The  $x, y$  values of the observation point are shown in the inset.

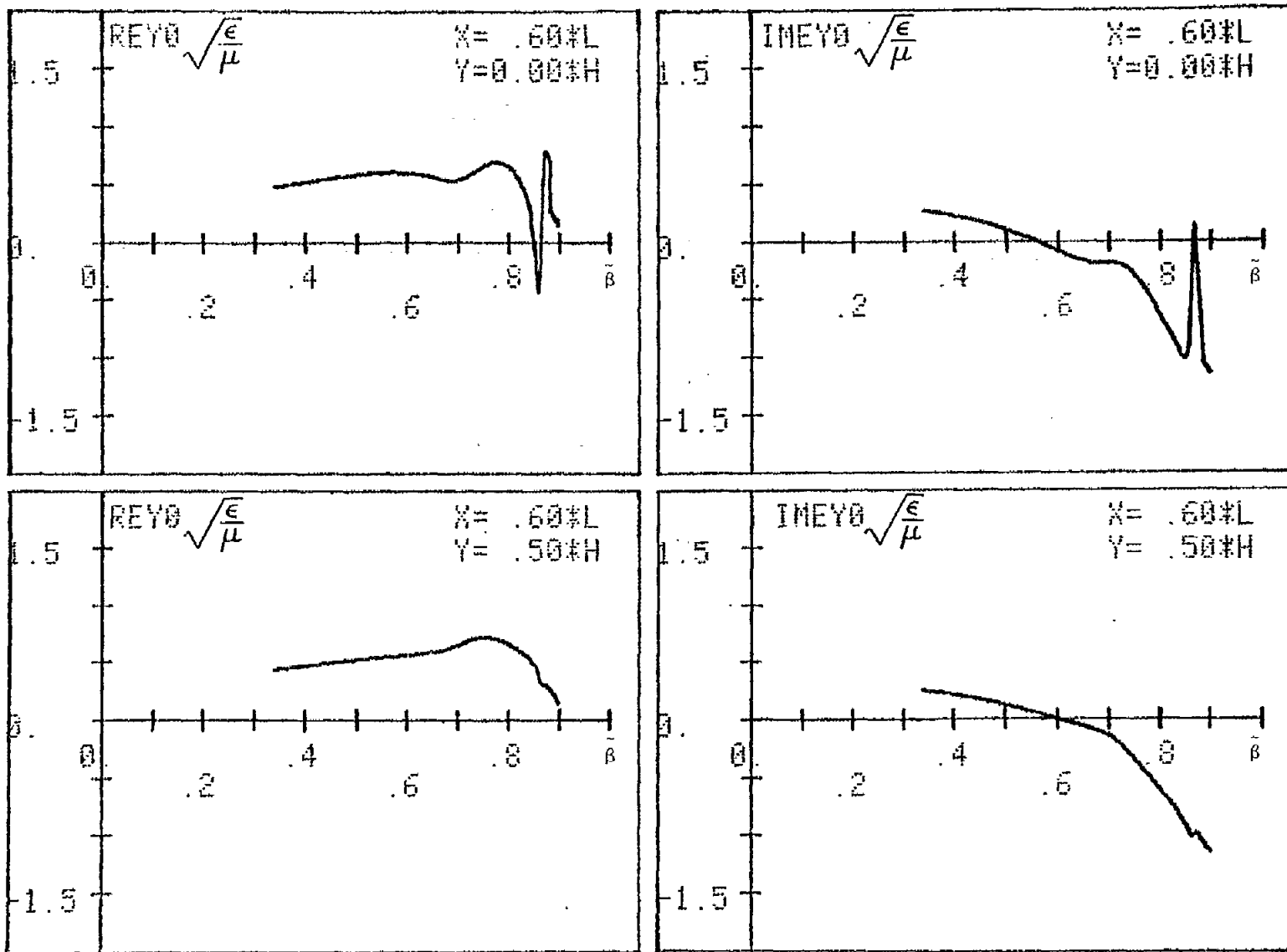


Figure 7. Real and imaginary parts of  $E_x$  as functions of  $\beta$  for parameters given in the lower half of Page 1. The  $x, y$  values of the observation point are shown in the inset.

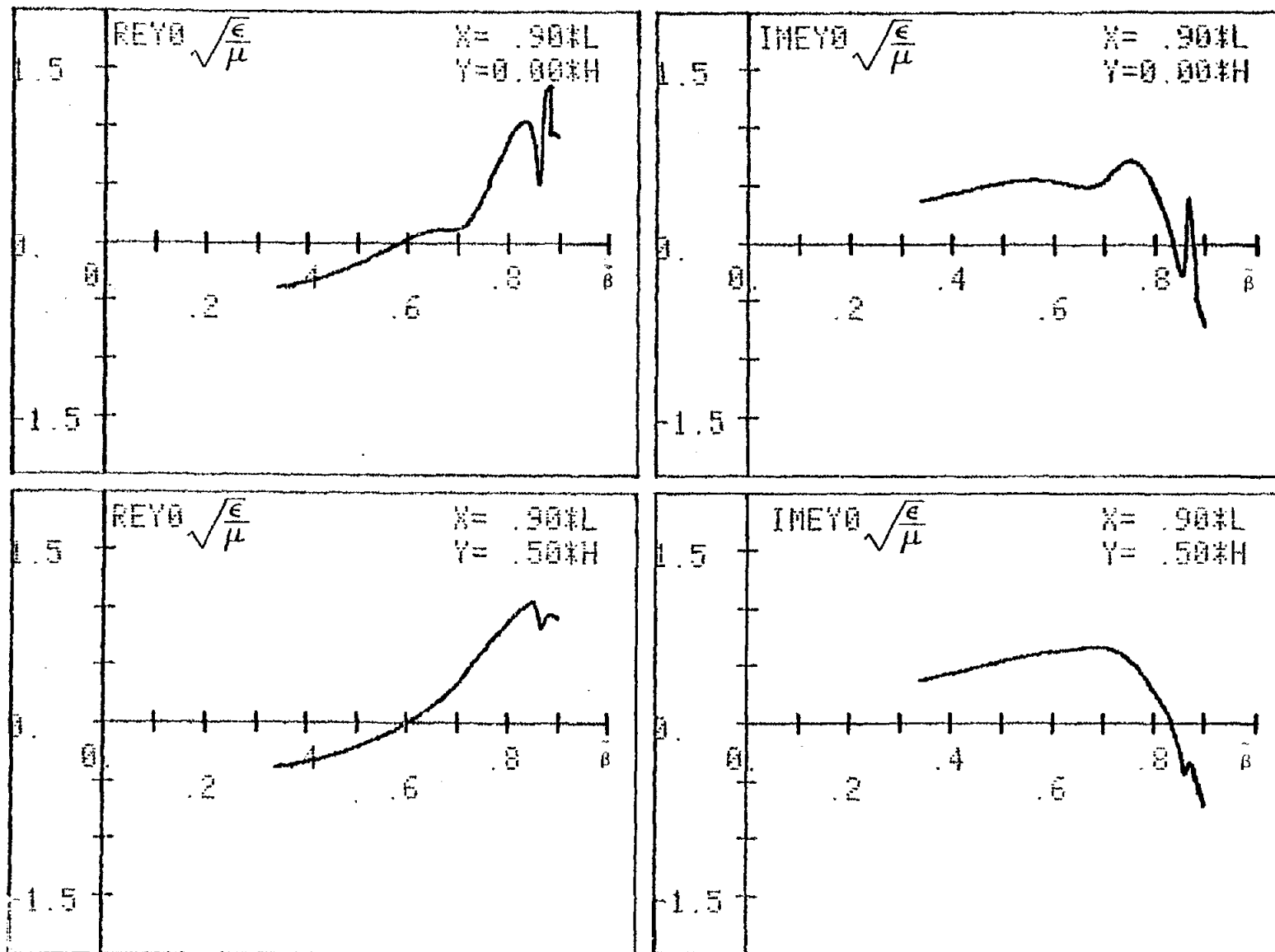
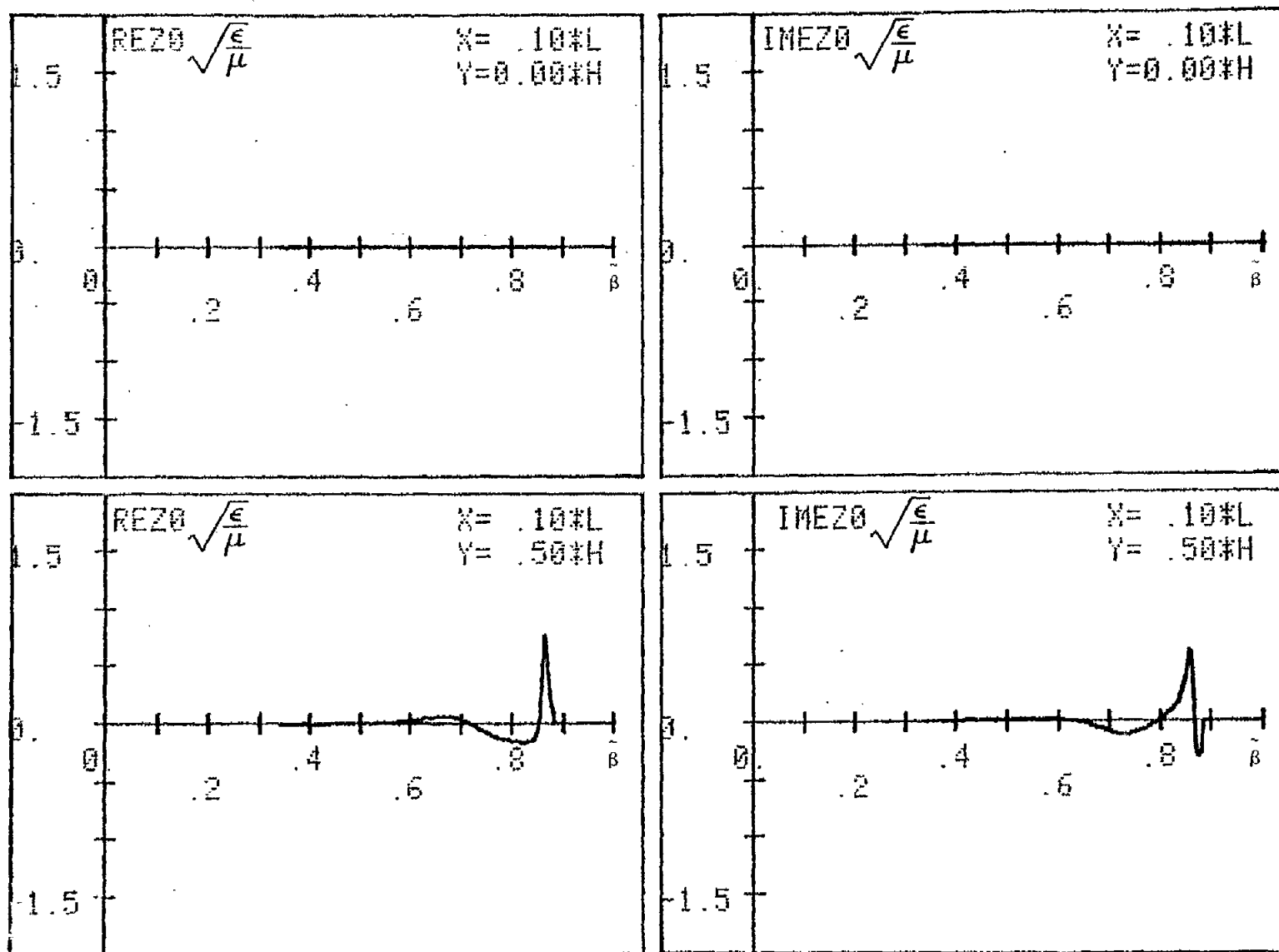


Figure 8. Real and imaginary parts of  $E_x$  as functions of  $\beta$  for parameters given in the lower half of Page 1. The  $x, y$  values of the observation point are shown in the inset.



438

Figure 9. Real and imaginary parts of  $E_x$  as functions of  $\beta$  for parameters given in the lower half of Page 1. The  $x, y$  values of the observation point are shown in the inset.

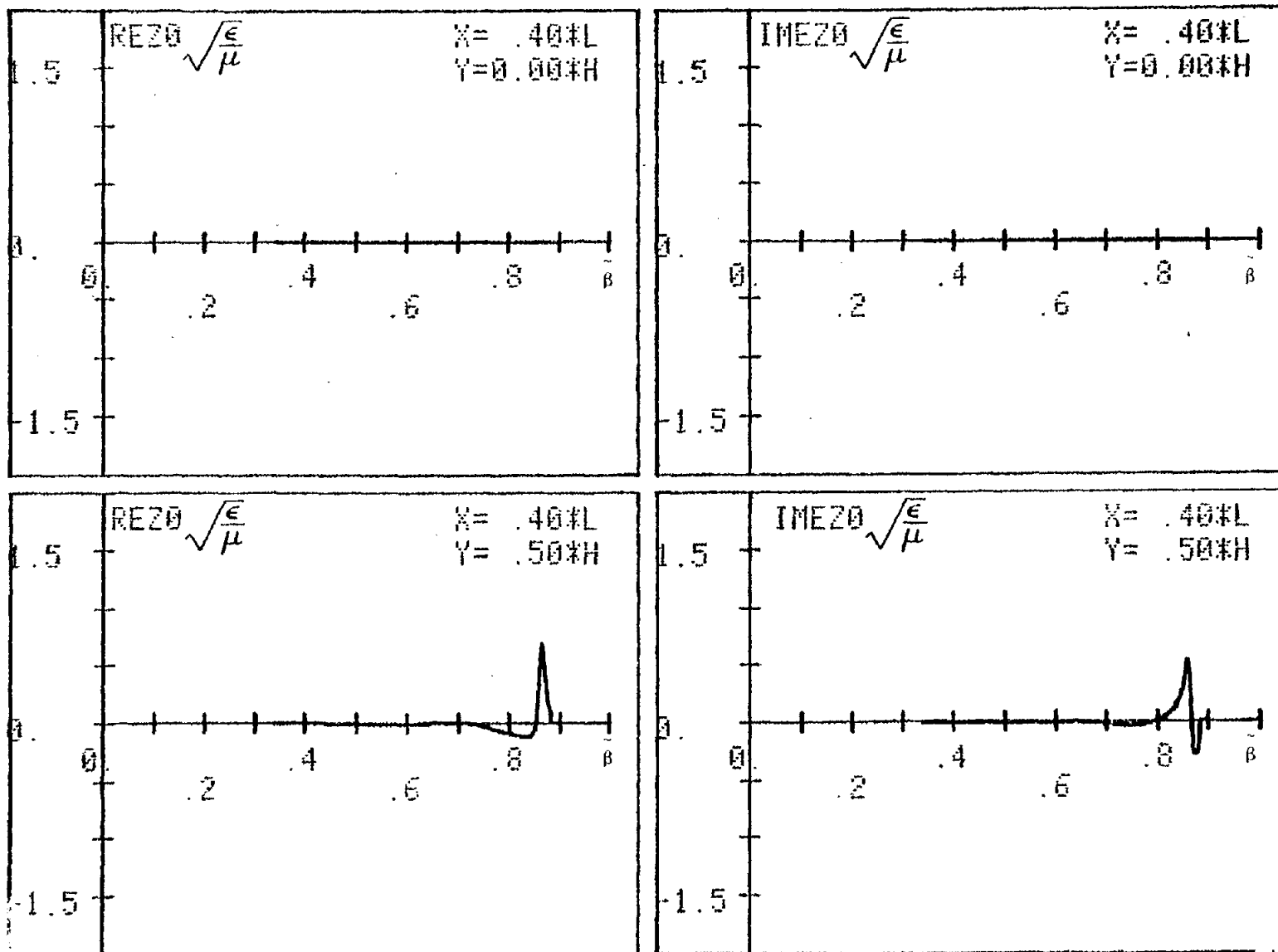


Figure 10. Real and imaginary parts of  $E_x$  as functions of  $\beta$  for parameters given in the lower half of Page 1. The  $x, y$  values of the observation point are shown in the inset.

440

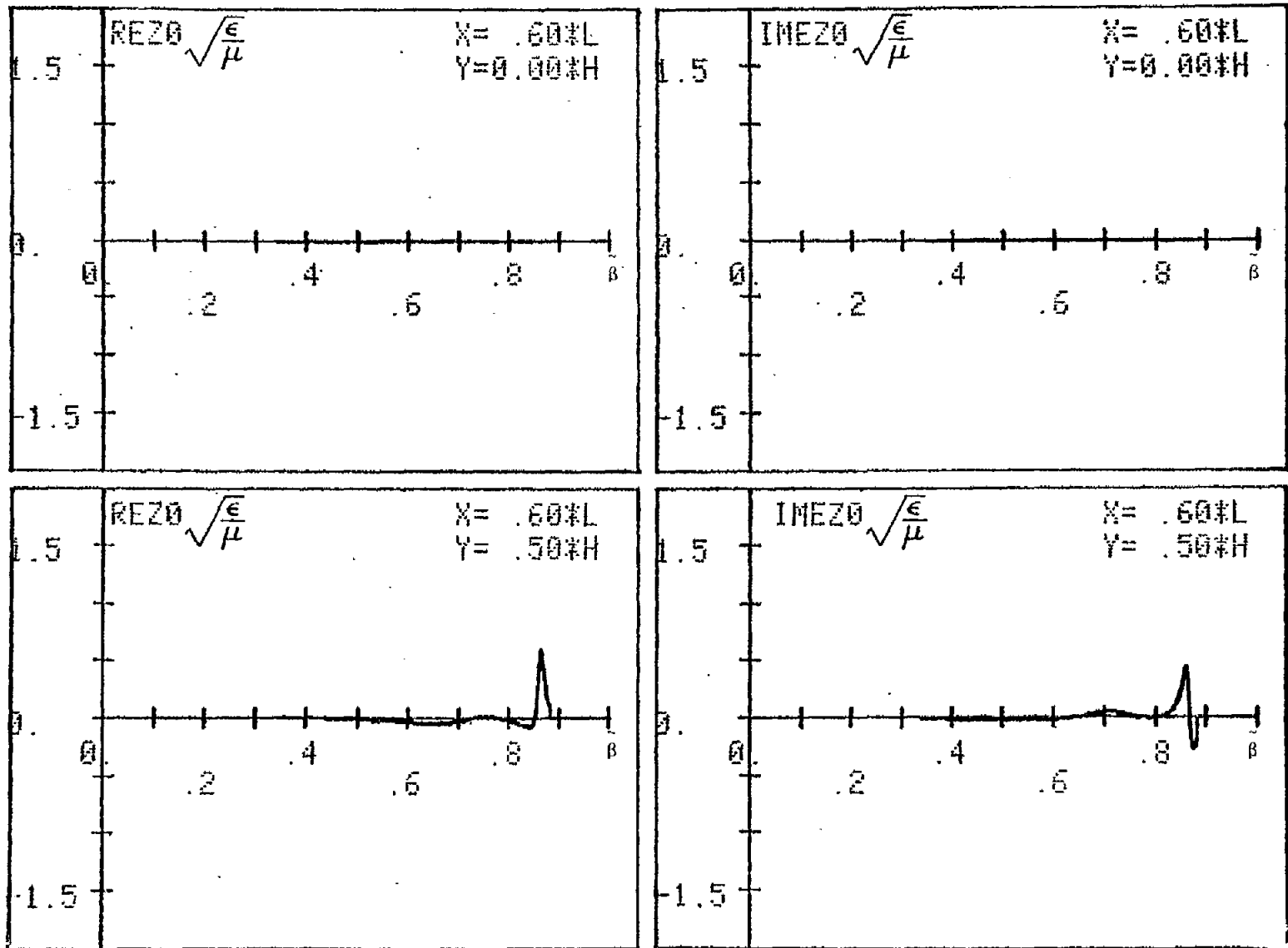


Figure 11. Real and imaginary parts of  $E_x$  as functions of  $\beta$  for parameters given in the lower half of Page 1. The  $x, y$  values of the observation point are shown in the inset.

441

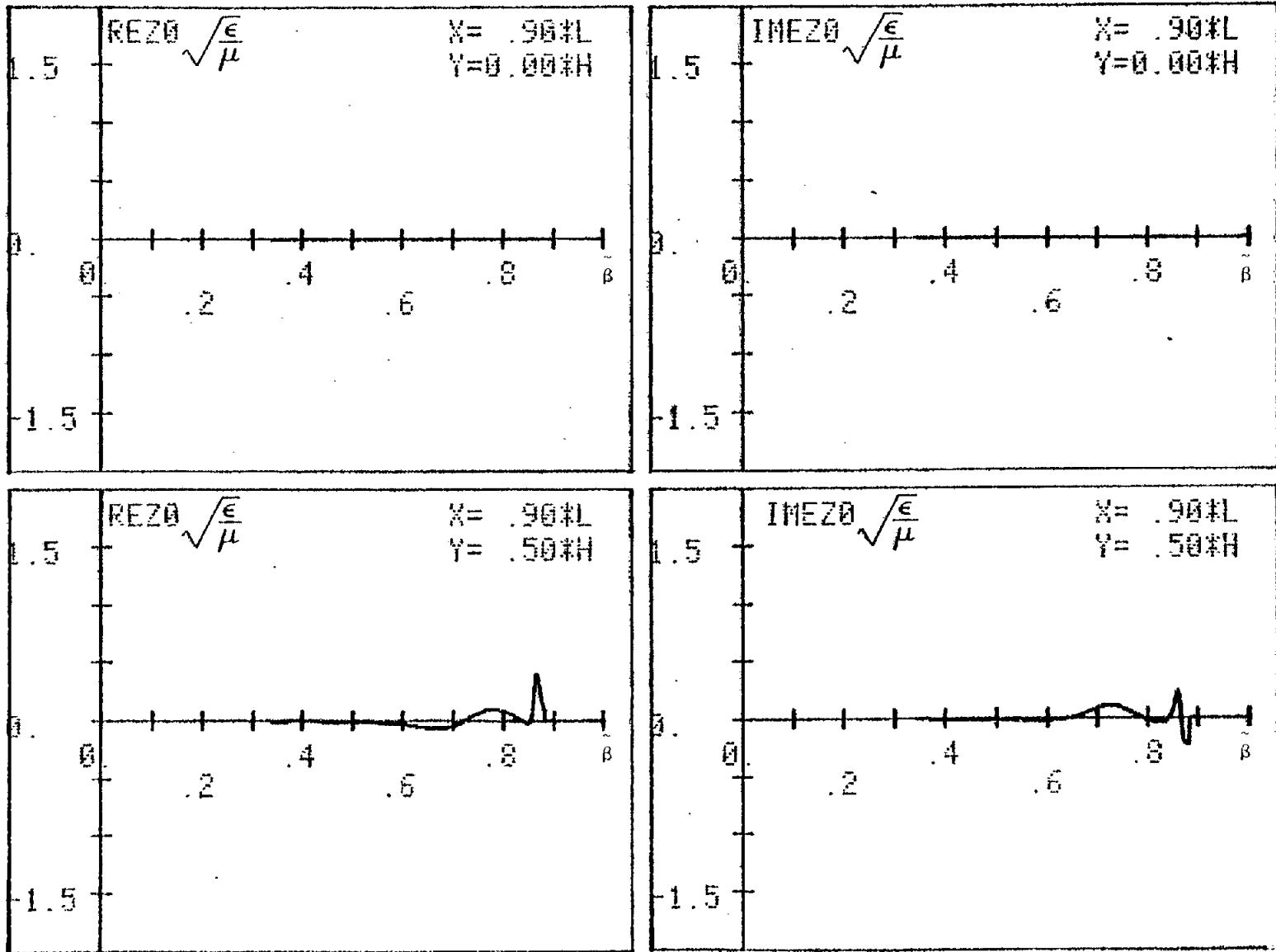


Figure 12. Real and Imaginary parts of  $E_x$  as functions of  $\beta$  for parameters given in the lower half of Page 1. The  $x, y$  values of the observation point are shown in the inset.

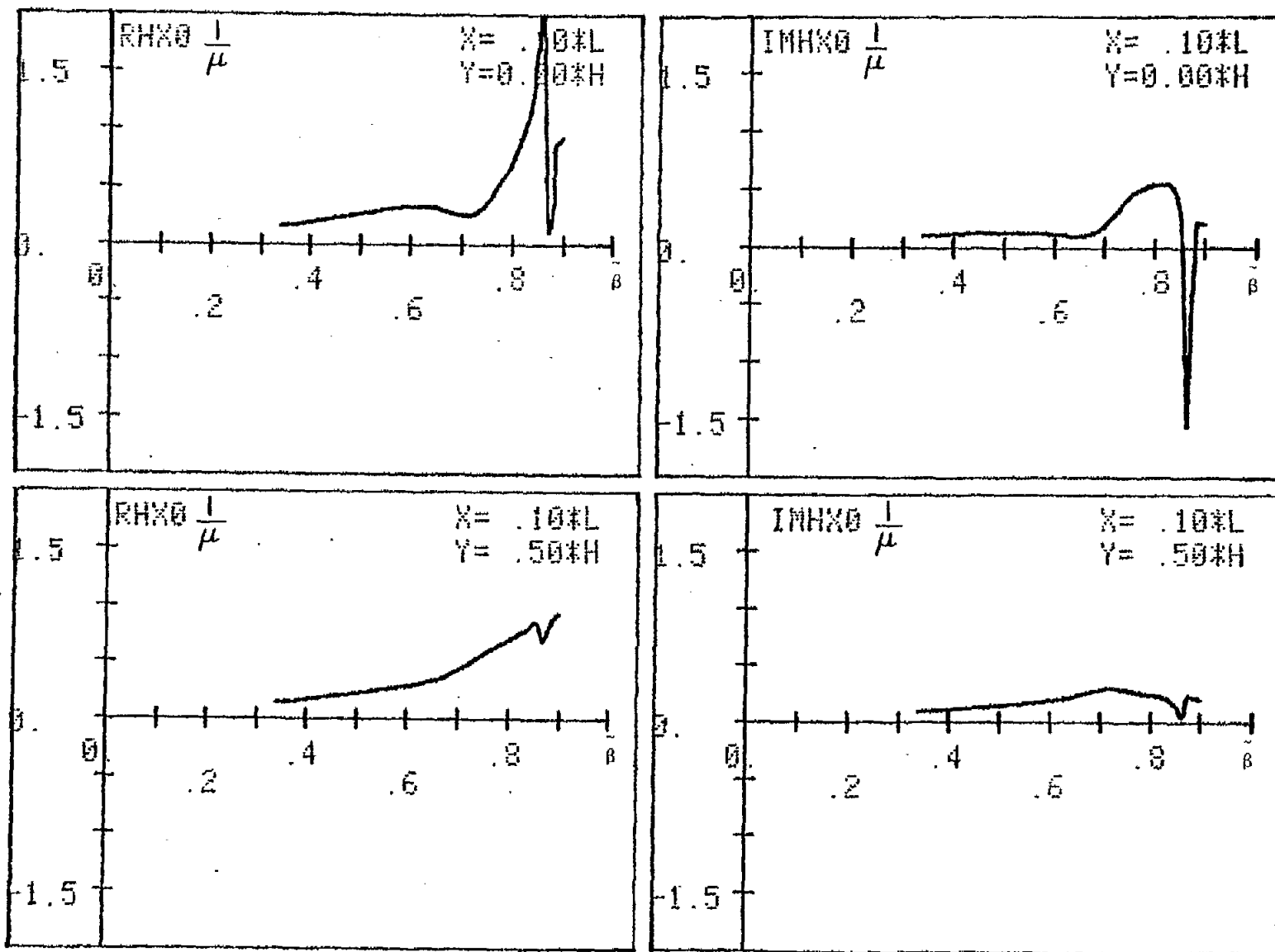


Figure 13. Real and imaginary parts of  $E$  as functions of  $\beta$  for parameters given in the lower half of Page 1. The  $x, y$  values of the observation point are shown in the inset.

443

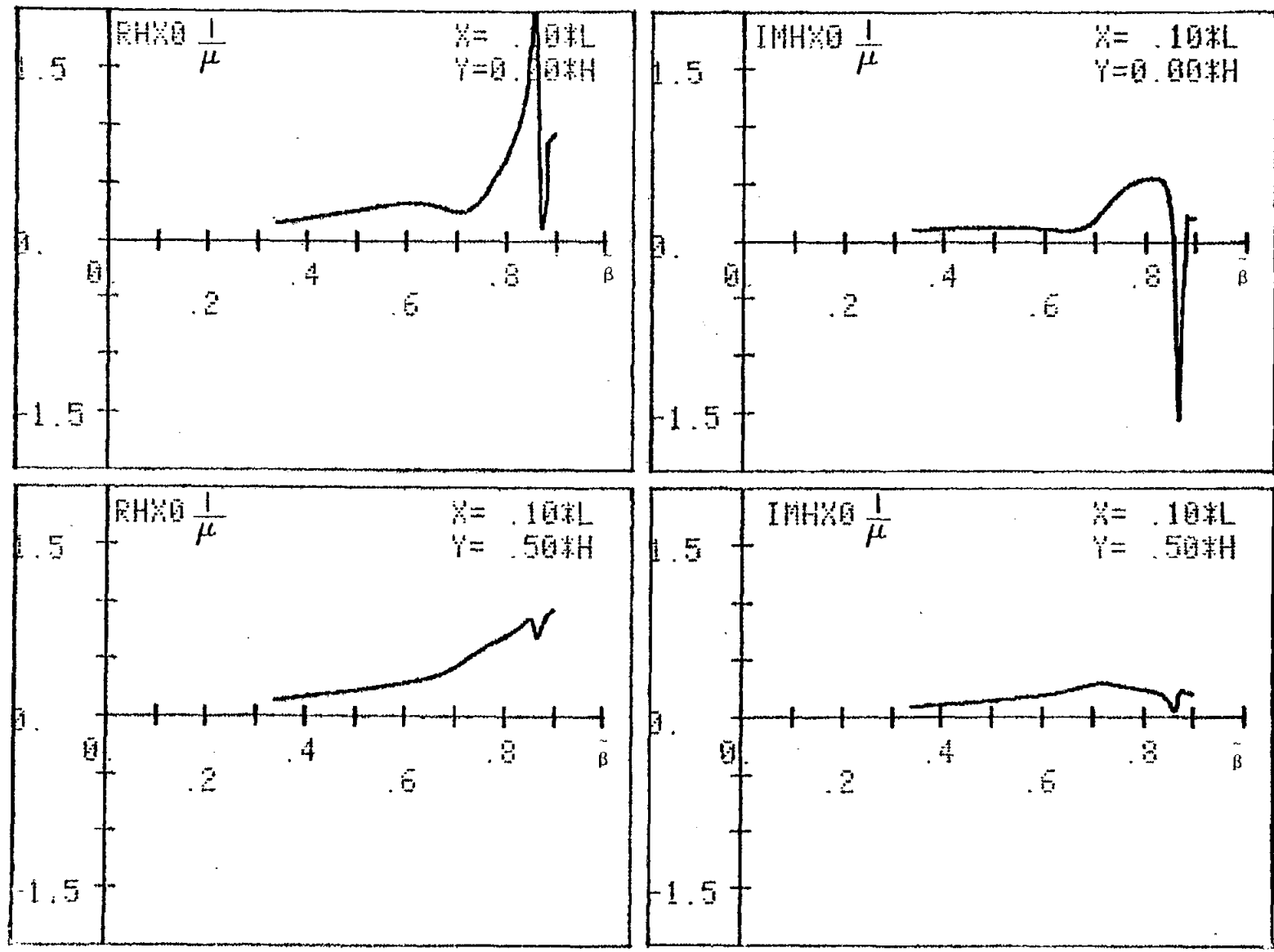


Figure 14. Real and imaginary parts of  $E_x$  as functions of  $\beta$  for parameters given in the lower half of Page 1. The  $x, y$  values of the observation point are shown in the inset.

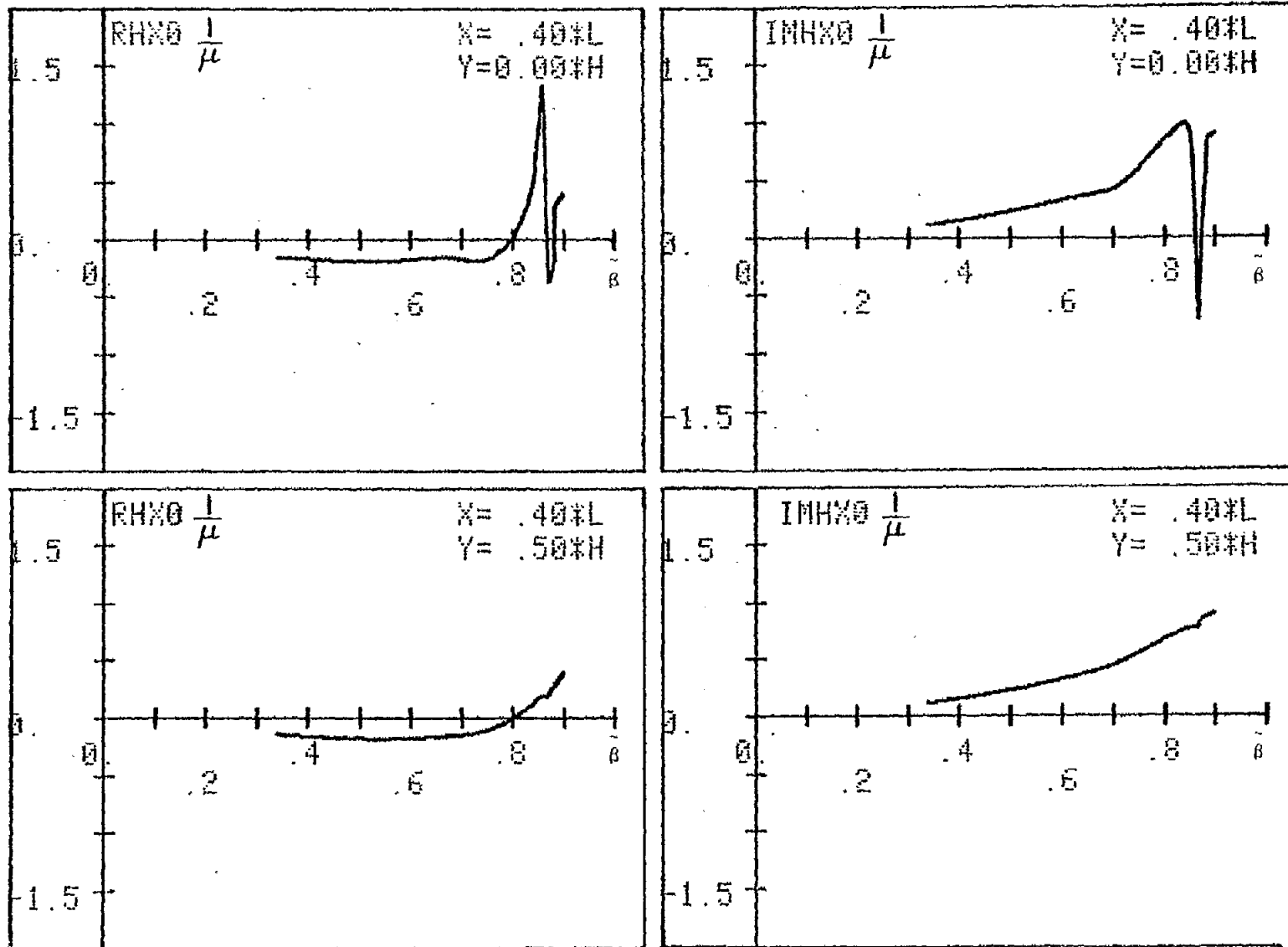


Figure 15. Real and imaginary parts of  $E_x$  as functions of  $\beta$  for parameters given in the lower half of Page 1. The  $x, y$  values of the observation point are shown in the inset.

445

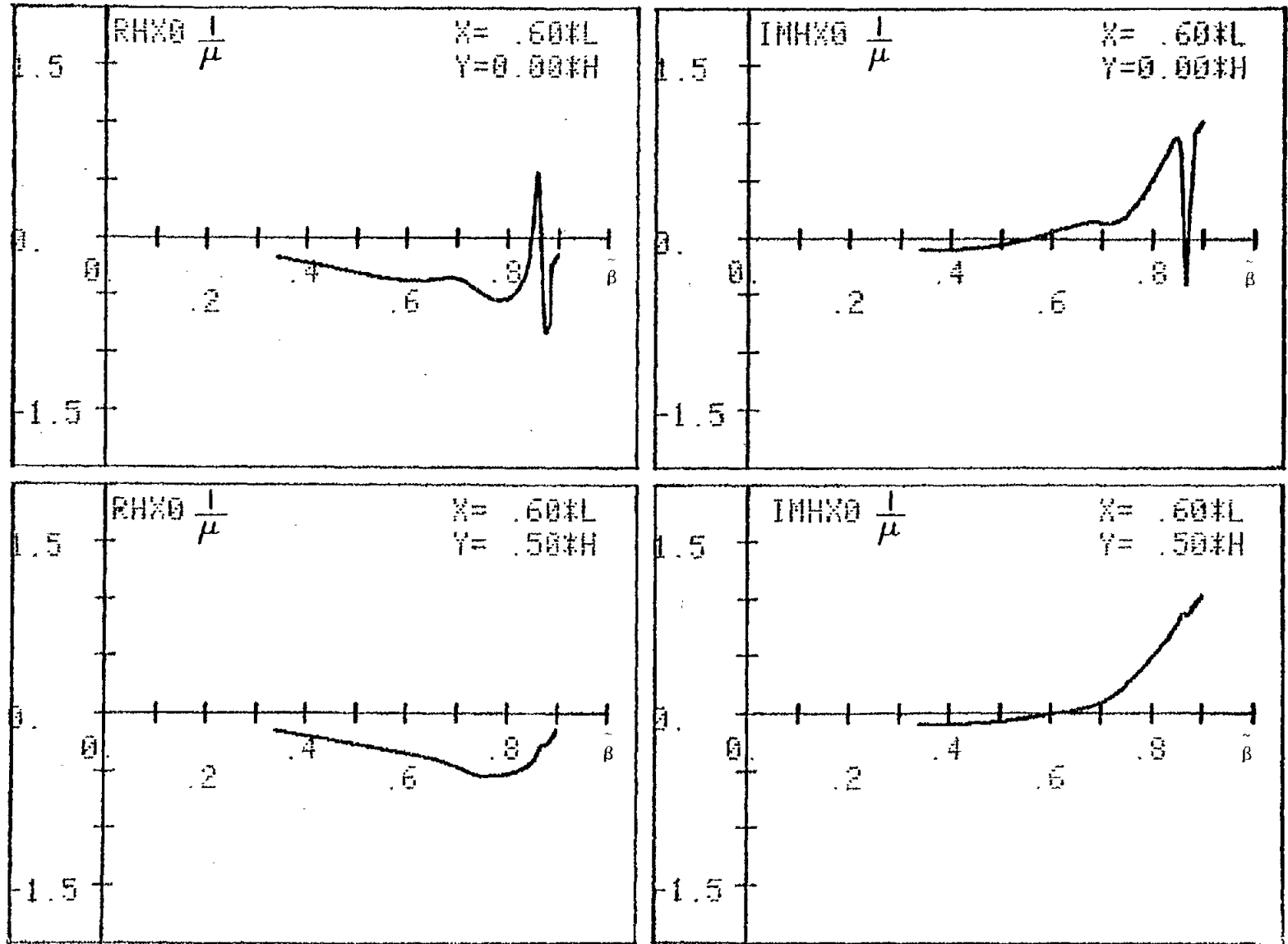


Figure 16. Real and imaginary parts of  $E_x$  as functions of  $\beta$  for parameters given in the lower half of Page 1. The  $x,y$  values of the observation point are shown in the inset.

446

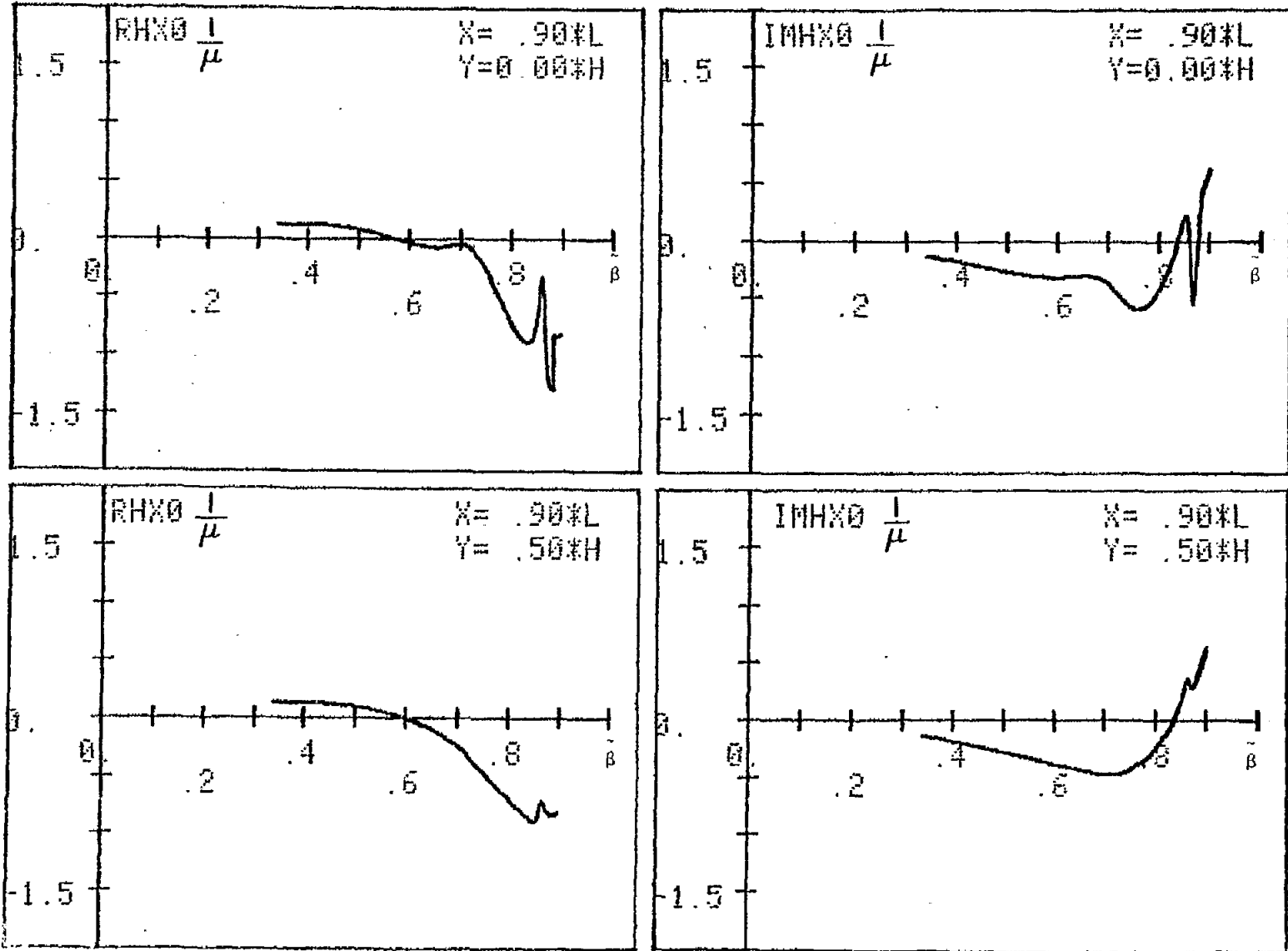


Figure 17. Real and imaginary parts of  $E$  as functions of  $\beta$  for parameters given in the lower half of Page 1. The  $x, y$  values of the observation point are shown in the inset.

447

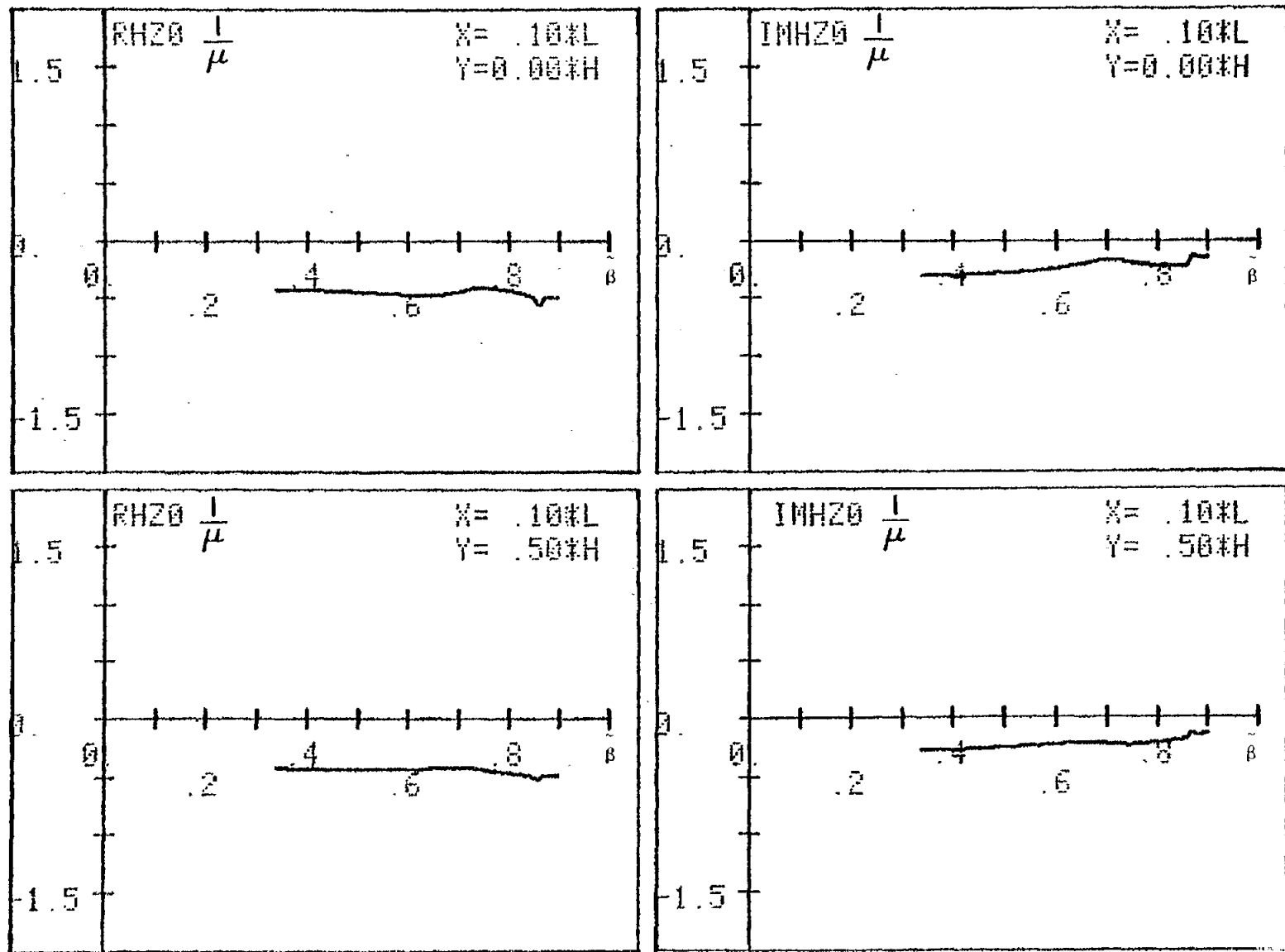


Figure 18. Real and imaginary parts of  $E_x$  as functions of  $\beta$  for parameters given in the lower half of Page 1. The  $x, y$  values of the observation point are shown in the inset.

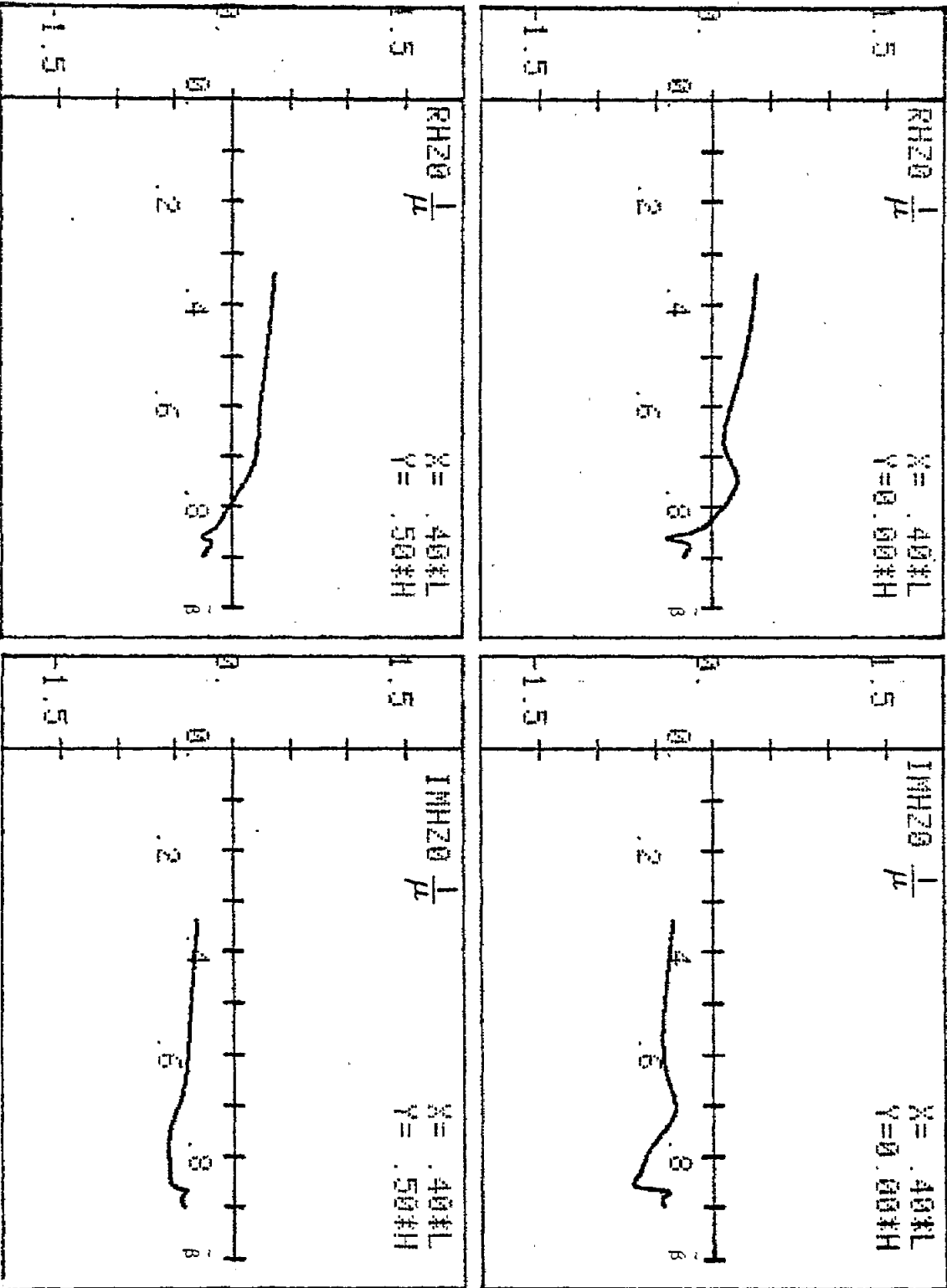
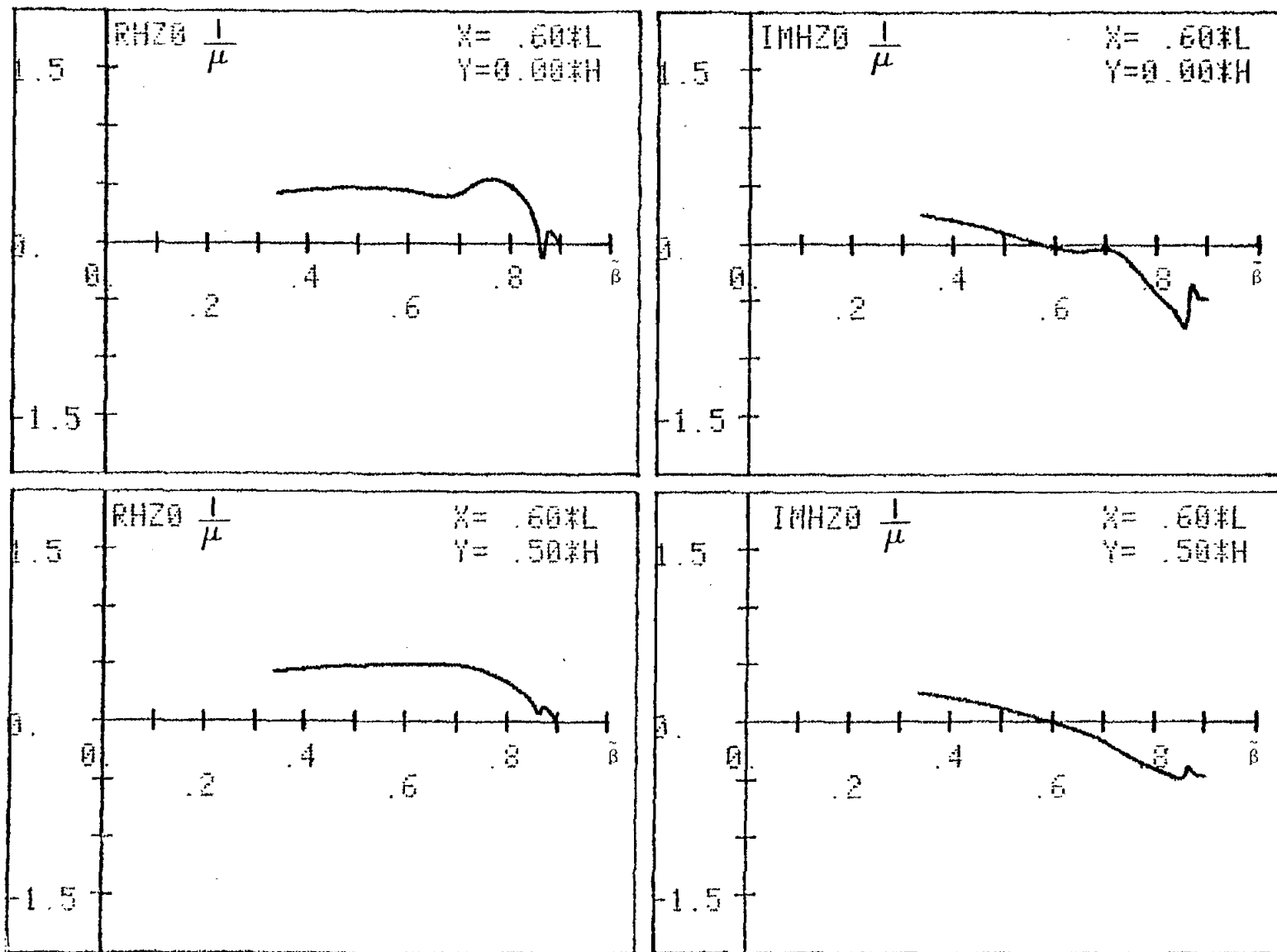


Figure 19. Real and imaginary parts of  $E_x$  as functions of  $B$  for parameters given in the lower half of Page 1. The  $x, y$  values of the observation point are shown in the inset.



449

Figure 20. Real and imaginary parts of  $E_x$  as functions of  $\beta$  for parameters given in the lower half of Page 1. The  $x, y$  values of the observation point are shown in the inset.

450

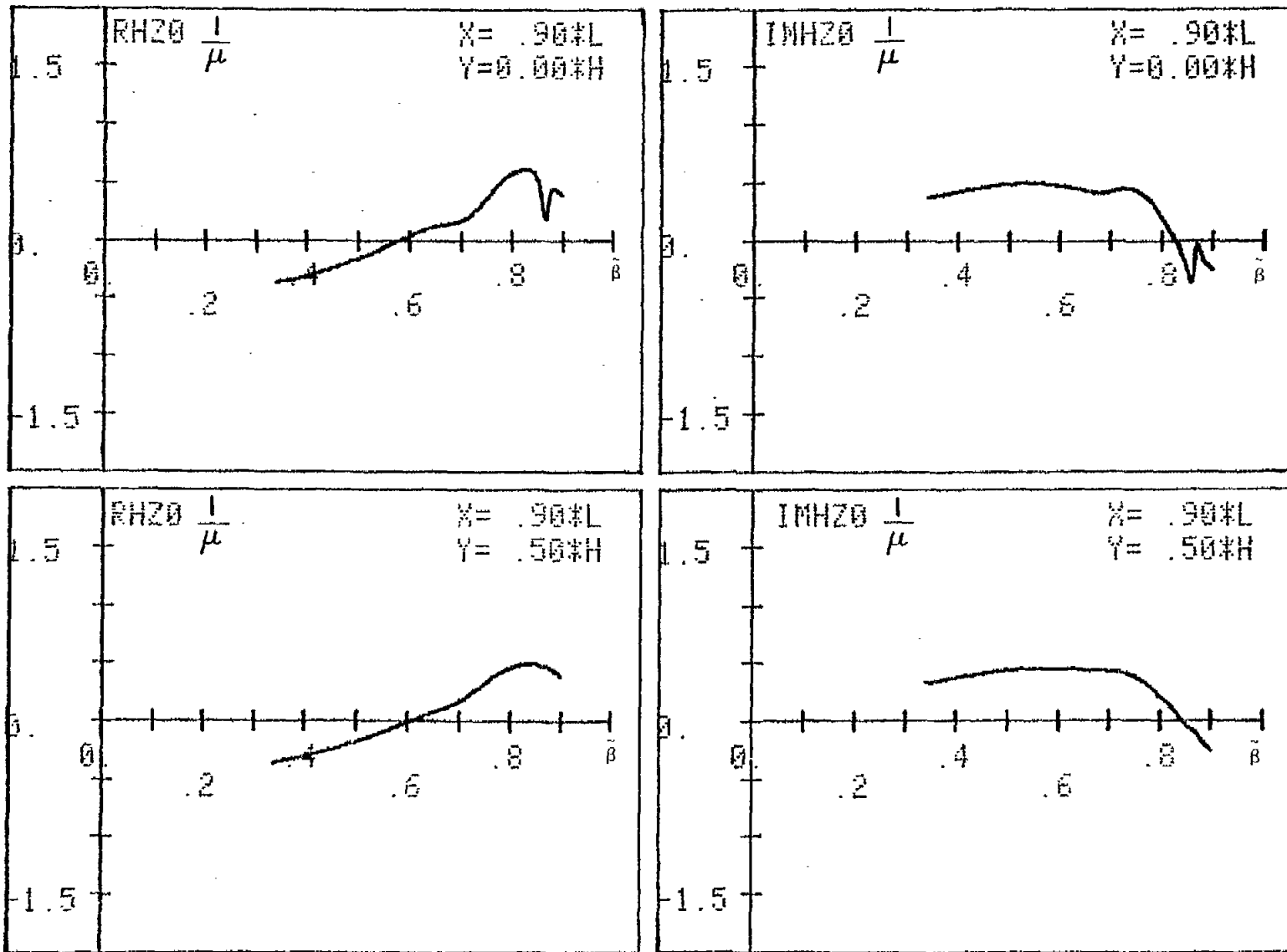


Figure 21. Real and imaginary parts of  $E_x$  as functions of  $\beta$  for parameters given in the lower half of Page 1. The  $x,y$  values of the  $x$  observation point are shown in the inset.

DISTRIBUTION

AUL/LDE/Maxwell AFB

DTIC/DDA/Alexandria

AFSC/DLW/Andrews

AFWL, Kirtland AFB

(SUL)

(HO)

Official Record Copy (AFWL/NTMT/Dr Baum)